METHANE OUTPUT FROM COLD SEEP STRUCTURES ALONG THE CENTRAL AMERICAN CONTINENTAL MARGIN

Dissertation
zur Erlangung des Doktorgrades
der Mathematisch-Naturwissenschaftlichen Fakultät
der Christian-Albrechts-Universität
zu Kiel

vorgelegt von

Susan Mau

Kiel 2004

Referent/in: ...Prof. Erwin Suess.....

Korreferent/in: ...PD. Dr. Klaus Wallmann .....

Tag der mündlichen Prüfung: ...7. Dezember 2004.....

Zum Druck genehmigt: ...Kiel, den 15. Dezember 2004.....

Der Dekan

Hiermit erkläre ich, daß ich die vorliegende Doktorarbeit selbständig und ohne unerlaubte Hilfen erstellt habe. Ferner habe ich weder diese noch eine ähnliche Arbeit an einer anderen Abteilung oder Hochschule im Rahmen eines Prüfungsverfahrens vorgelegt, veröffentlicht oder zur Veröffentlichung vorgelegt.

Susan Mau

Preface

This study comprises a general introduction presented in Chapter I, three stand-alone publishable papers – Chapter II to IV and an overall summary and conclusion – Chapter V. Each of the Chapters II, III and IV contains a separate introduction, description of methods, presentation of data and discussion as well as a separate reference list. Chapter II has already been submitted for publication in Marine Geology; Chapters III and IV are to be submitted to Global Biochemical Cycles and Geo-Marine Letters, respectively and might be subject to revisions.

The titles and authors of the papers (Chapters II, III and IV) are briefly listed below:

Chapter II	**Estimates of methane output from mud extrusions at the erosive convergent margin off Costa Rica**
Authors	S. Mau, H. Sahling, G. Rehder, E. Suess, P. Linke and E. Soeding
Status	submitted to *Marine Geology*
Chapter III	**Sources, fate and output of methane from cold seeps in Jaco Scarp, an embayment caused by seamount subduction offshore Costa Rica**
Authors	S. Mau, G. Rehder, E. Soeding, H. Sahling, E. Suess and K. Stange
Status	to be submitted to *Global Biogeochemical Cycles*
Chapter IV	**Variations in CH_4 seepage from mud extrusions and landslides offshore Costa Rica affected by seismo-tectonics**
Authors	S. Mau, G. Rehder, I. G. Arroyo, J. Gossler and E. Suess
Status	to be submitted to *Geo-Marine Letters*

I contributed to these papers by: work at sea, acquisition and processing of all methane data and current velocity data, interpretation of the data and calculation of methane output (Chapter II and III), correlation of methane data to oceanographic data and earthquake data (Chapter IV), graphical presentation of methane data, writing and preparation of manuscript.

Abstract

Methane seepage from different geological structures was investigated along the convergent margin off the Pacific coast of Costa Rica. This segment of subduction zone is dominated by tectonic erosion rather than sediment accretion. Thus, in contrast to accretionary margins, where sediments accumulate and fluids derive mainly from compaction and diagenesis of these sediments, the sediment load at an erosive margin is much less and fluids derive predominantly from the subducted sediments from greater depths. These fluids ascend through high-permeability conduits to the seafloor and discharge into the ocean at various vent sites. Mud extrusions were found to be the most abundant fluid expelling structures along the Costa Rican margin. Therefore, four mud extrusions were investigated in detail to identify the fate and the amount of CH_4 discharging into the ocean. Similarly, one of the several embayments caused by the subduction of seamounts (scarps) was investigated, because hardly anything is known of their seeping potential. In addition, several of these structures were repeatedly sampled over the course of four years to study long-term variations in CH_4 seepage.

All investigated sites show active fluid seepage indicated by chemosynthetic communities, authigenic carbonates and CH_4 plumes in the water column. The vent derived CH_4 is mainly dispersed and diluted by mixing with background water. Only a part of the CH_4 is oxidized in the center of the plume in Jaco Scarp where concentrations of CH_4 are high, and close to the scarp's slopes. This results probably from diminished current flow and/or other components influencing the pathway of oxidation. However, the fate of the emitted CH_4 is rather dilution than oxidation.

The CH_4 outputs were estimated based on measurements of near-bottom CH_4 concentrations and current velocities. This approach comprises transient, fast and slow CH_4 seepage. The estimates per mud extrusion range between 1 – 10 Mg yr^{-1} (1 Mg = 10^6 g) and are lower than those reported from other mud extrusions at accretionary and passive margins which may be due to the erosive nature of the subduction. Assuming a similar vent activity at all 48 mounds discovered offshore Costa Rica and constant seepage over time, 307 Mg yr^{-1} of CH_4 are emitted from mud extrusions along this segment of the subduction zone. The CH_4 output from Jaco Scarp yields a value of 61 Mg yr^{-1}. This amount equals the CH_4 emission of ~10 mud extrusions, but other scarps in the area seem to be less active. Assuming a vent activity of 5%,

which is deduced from data at Parrita Scarp, at each of the other three scarps compared to Jaco Scarp, 70 Mg yr^{-1} would be emitted from all four scarps. In total, 377 Mg yr^{-1} of CH_4 is discharged into the ocean. However, repeated measurements at these geological structures indicate long-term variations in methane seepage. These changes appear to be related to earthquake activity. Higher CH_4 concentrations in 1999 and 2002 correlate with major earthquakes occurring in these years whereas CH_4 content was less in 2003 – a year of lowered seismic activity. The temporal changes of CH_4 emission emphasize that estimates of CH_4 output cannot be simply extrapolated.

The amount of CH_4 released from mud extrusions and scarps offshore Costa Rica adds up to ~0.2‰ of the global CH_4 output from the seafloor, which was estimated to be in the order of 20 Tg yr^{-1} (1 Tg = 10^{12} g). The total amount emitted from the margin is most likely higher, because the estimated value does not include CH_4 seepage from other vent sites e.g. small landslides and enhanced CH_4 output from sites, that have not been investigated in detail. However, the estimated CH_4 outputs present the first ones from an erosive margin and are, thus, of great significance for assessments of the global methane output in general and of specific geological structures, e.g. mud extrusions, in particular.

Zusammenfassung

Das Ausströmen methanreicher Fluide von unterschiedlichen geologischen Strukturen wurde entlang des aktiven Kontinentalrandes der pazifischen Küste Costa Ricas untersucht. Dieser Abschnitt der Subduktionszone ist von tektonischer Erosion anstatt von Sedimentakkretion geprägt. Im Unterschied zu einem akkretionären Kontinentalrand, an dem Sedimente akkumuliert werden und Fluide vor allem aus diesen durch Kompaktion und Diagenese beeinflußten Sedimenten stammen, sind an erosiven Kontinentalrändern bedeutend weniger Sedimente zu finden. Fluide, die an diesen Kontinentalrändern austreten, stammen größtenteils aus den subduzierten Sedimenten und somit aus größerer Tiefe. Sie steigen entlang hoch permeabler Zonen bis zum Meeresboden auf, wo sie an verschiedenartigen Austrittsstellen in den Ozean strömen. Schlammextrusionen sind die am häufigsten auftretenden Fluidquellen am Kontinentalrand von Costa Rica. Aufgrund dessen wurden vier Schlammextrusionen im Detail untersucht. Insbesondere galten die Untersuchungen den Reaktionen von CH_4 in der Wassersäule und dienten dazu, die Menge von austretendem CH_4 abzuschätzen. Eine Hangabrutschung, die durch die Subduktion von Seamounts verursacht wurde, wurde ebenfalls untersucht. Über Methanaustritte an diesen Strukturen ist bis heute kaum etwas bekannt. Zusätzlich wurden einige Schlammextrusionen und Hangabrutschungen über einen Zeitraum von vier Jahren mehrfach beprobt, um zeitliche Veränderungen der Methanausflüsse festzustellen.

Chemoautotrophe Organismen, authigene Karbonate und Methananreicherungen in der Wassersäule wurden an all diesen geologischen Strukturen gefunden. Diese Merkmale deuten auf ein aktives Austreten von Fluiden hin. Das in den Ozean strömende CH_4 wird hauptsächlich durch Vermischung mit Meerwasser verteilt und verdünnt. Dagegen wurde Oxidation von CH_4 nur im Zentrum der „Methanwolke“ im Jaco Scarp – wahrscheinlich aufgrund stark erhöhter Methankonzentrationen – und entlang der Ränder dieser Hangabrutschung festgestellt. Letzteres ist vermutlich zurückzuführen auf geringere Strömungsgeschwindigkeiten und/oder zusätzlicher Komponenten, die den Ablauf der Oxidation beeinflussen.

Die Methanemissionen wurden basierend auf gemessenen bodennahen CH_4-Konzentrationen und Strömungsgeschwindigkeiten abgeschätzt. Diese Abschätzung beinhaltet kurzzeitiges, schnelles und langsames Ausströmen von CH_4. Die abgeschätzten Methanflüsse pro

Schlammextrusion von 1 – 10 Mg a^{-1} (1 Mg = 10^6 g) sind gering im Vergleich zu anderen Extrusionen, die an akkretionären und passiven Kontinentalrändern vorkommen. Das hängt wahrscheinlich mit dem erosiven Charakter der Subduktion vor Costa Rica zusammen. Unter der Annahme, daß alle 48 vor Costa Rica entdeckten Schlammextrusionen gleich aktiv sind und der Ausfluß über die Zeit konstant ist, würden 307 Mg a^{-1} CH_4 entlang dieses Teiles des Kontinentalrandes aus Schlammextrusionen ausströmen. Der Methanfluß von Jaco Scarp beträgt 61 Mg a^{-1}. Diese Menge entspricht einer Methanemission von etwa 10 Schlammextrusionen. Die anderen Hangabrutschungen scheinen allerdings weniger aktiv zu sein. Ausgehend von den Daten, die im Parrita Scarp erfaßt wurden, wird angenommen, daß nur ca. 5% der CH_4-Menge, die an Jaco Scarp austritt, jeweils an den anderen drei Hangabrutschungen in den Ozean entweicht. Das wären folglich 70 Mg a^{-1} CH_4 von allen vier Strukturen zusammen genommen. Insgesamt würden somit 377 Mg a^{-1} CH_4 in den Ozean fließen. Wiederholte Beprobungen an diesen geologischen Strukturen zeigten jedoch einen sich über die Zeit verändernden Methanausfluß, der korreliert werden kann mit der seismischen Aktivität dieser Region. 1999 und 2002 erschütterten schwere Erdbeben die Region. In diesen Jahren wurden auch höhere CH_4-Konzentrationen gemessen. Hingegen wurden 2003 – einem Jahr, in dem weniger Erdbeben auftraten – geringere CH_4-Konzentrationen gemessen. Diese zeitliche Variabilität der Methanemissionen zeigt deutlich, daß die Abschätzungen der Methanflüsse nicht einfach extrapoliert werden können.

Die CH_4-Menge, die an den Schlammextrusionen und den Hangabrutschungen vor Costa Rica austritt, beträgt ~0.2‰ des globalen Methanflußes vom Meeresboden, der eine Größenordnung von ca. 20 Tg a^{-1} (1 Tg = 10^{12} g) hat. Die Gesamtmenge von CH_4, die entlang dieses Teils des Kontinentalrandes austritt, ist wahrscheinlich höher, da der errechnete Betrag nicht den Methanfluß von weiteren potentiellen Strukturen einbezieht. Mehrere kleinere Hangabrutschungen und die Methanemissionen von Strukturen, die nicht oder nur oberflächlich untersucht wurden, fehlen bei dieser Abschätzung. Die berechneten Methanflüsse stellen die ersten Ergebnisse von einem erosiven Kontinentalhang dar und sind infolgedessen wichtig für generelle Berechnungen globaler Methanflüsse vom Meeresboden als auch für spezielle Berechnungen spezifischer Methanflüsse z.B. von Schlammextrusionen.

Contents

General Introduction

Objectives

Methane is the most common 'geological gas' and attempts of quantification (Cranston et al., 1994; Hovland et al., 1997; Judd et al., 1997; Hornafius et al., 1999; Judd et al., 2002) have illustrated its significance to the global carbon budget (Judd et al., 2002). It is generated in sediments by the destruction of organic matter buried when the sediments were deposited. Microbial or biogenic methane is produced by methanogenesis at relatively shallow depths whereas thermogenic methane is formed at high temperature and pressure conditions in depths greater than 1 km (Tissot and Welte, 1984). As soon as it is generated it starts to migrate towards the earth surface. Even though this is an ongoing process, its importance in the global carbon budget and its role in the change of global climate is still not entirely recognized. Often, it is not even considered in the global carbon cycle (Judd et al., 2002) and in estimates of the annual source of methane to the atmosphere (Kvenvolden et al., 2001).

Geological sourced methane contributes with about 20 Tg yr^{-1} (Kvenvolden et al., 2001) or with 2.4 – 6.7 % (Judd et al., 2002) to the annual methane release to the atmosphere (535 Tg yr^{-1}) (Houghton, 1997). The contribution of methane from continental margins to the total atmospheric methane budget is approximately 1.2 – 3.6 % (Judd et al., 2002). Even though this is a minor source, the continental margins have gained in significance to global climate, because vast amounts of methane are stored in form of gas hydrates in margin sediments. Gas hydrates are ice-like mixtures of water and gas forming under special temperature and pressure conditions (Kvenvolden, 1993; Sloan, 1998). If an adequate supply of gas is given, gas hydrates form within seabed sediments in water depth exceeding 300 – 500 m and at bottom water temperatures below 5 °C (Ginsburg and Soloviev, 1998). Dickens (1995) initially proposed that these gas hydrates influenced the global climate in the past.

Massive releases of methane from the seafloor are discussed as one of the most likely scenarios explaining large deviations in the carbon isotopic record (Fig. 1), e.g. at the Late Paleocene Thermal Maximum (LPTM), 55.5 Ma ago (Dickens et al., 1995). The 'LPTM hydrate dissociation hypothesis' suggests that a long-term global warming during the late Paleocene caused a rise in deep ocean temperatures (Kennett and Stott, 1991) which in turn has led to the dissociation of CH_4 hydrates. Assuming that most CH_4 stored in gas hydrates is

enriched in ^{12}C, an amount of 1 x 10^{18} – 2 x 10^{18} g escaped rapidly into the ocean. The flux of CH_4 invoked during the ~10^4 yr period is comparable to the present-day anthropogenic methane release (Dickens et al., 1997). The methane release would have occurred on continental slopes between 900 and 2000 m water depth, because hydrates in these sediments would have dissociated with a 4 – 8 °C rise in bottom water temperatures (Dickens et al., 1995). This event coincides with mass extinction of marine and terrestrial fauna (Katz et al., 1999).

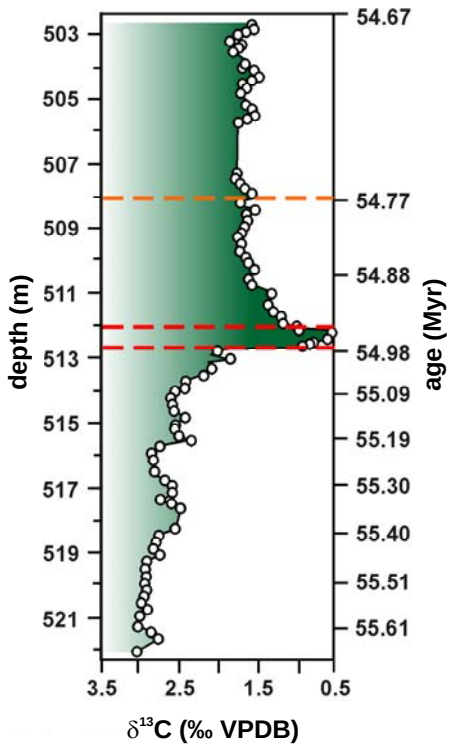

Fig. 1 $\delta^{13}C$ anomaly ~55 Ma ago (Norris and Röhl, 1999). $\delta^{13}C$ values of bulk carbonate in a sediment core (ODP Site 1051) from the western North Atlantic Ocean show a large shift near the Palaeocene-Eocene boundary. The lower two dashed lines indicate the sharp initial drop associated with extinction of up to 50% of benthic foraminifera and the upper one the termination of the $\delta^{13}C$ anomaly.

Recently, Svensen et al. (2004) reported another explanation for the negative carbon isotope excursion. They presented evidence of thousands of hydrothermal vents deposited in the Voring and More basin in the Norwegian Sea about 55 Ma ago observed on seismic reflection profiles. They propose the intrusion of mantle derived melts into carbon-rich sediments, producing thermogenic methane in the contact aureols. The estimated amount of methane generated would be sufficient to cause the carbon isotopic excursion. Fluids and methane escape through conduits which outcrop closely resemble the structures observed nowadays at the seafloor. Dickens (2004) stated that a greater amount of CH_4 than the one proposed from the dissociation of gas hydrates must have escaped, because thermogenic CH_4 contains a greater portion of ^{13}C than biogenic CH_4. Alternatively, the methane could originate from gas hydrates which would have dissociated as a consequence of the temperature increase from below.

The example of the LPTM shows the relevance of CH_4 emitted at continental margins on earth climate (Dickens, 2004). Moreover, Judd et al. (2002) suggest that not only methane from gas hydrates but also CH_4 escaping at natural seeps and mud volcanoes influences the

direction and speed of global climate change. This illustrates that the interest in methane seepage is growing and the role of methane from natural vent sites is of enormous importance. More estimates of methane outputs from various sources are needed to determine the contribution of seafloor-methane to the global carbon budget.

Another important question is: What is the fate of methane once it resides in the water column? The atmospheric response of additional carbon is strongly dependent on the gas species that reach the atmosphere. CH_4 has on a mole-for-mole basis a stronger greenhouse potential than CO_2 and intensely affects atmospheric chemistry leading to increases of other greenhouse gases (O_3, H_2O, CO_2) (Lelieveld and Crutzen, 1992). Several processes affect the fate of methane in the water. CH_4 can either be released as free gas or dissolved in fluids. Bubbles rising from the seabed loose a portion of CH_4 to the hydrosphere by solution. Dissolved methane is diluted and transported by ocean currents. CH_4 is also lost to the hydrosphere by microbial oxidation generating CO_2. Depending on the mode of release and the dominant process, CH_4 contributes either to the CH_4 budget of the ocean or to the CH_4 budget of the atmosphere.

Outline of thesis

In order to quantify the methane output from various geological structures and to better understand the fate of methane in the water column, several vent sites, so called ‘cold seeps’, have been investigated at the continental slope offshore Costa Rica. A description of the geological setting of the research area and a summary of the water masses and circulation pattern follows below. Apart from the results described in Chapters II – IV, additional data is presented in the sections covering the water column work in the GEOMAR Reports 106, 111 and 115 (Weinrebe and Flueh, 2002; Soeding et al., 2003; Flueh et al., 2004).

Role of mud extrusions

Numerous mud extrusions were discovered offshore Costa Rica and Nicaragua in the course of work of the SFB 574. Similar structures - conduits piercing the seafloor - have been proposed by Svensen (2004) as main transport mechanism for rapid CH_4 emission into the ocean 55 Ma ago. Mud volcanoes have been described from many parts of the world, e.g. the southern Caspian Sea (Guliyiev and Feizullayev, 1996), the Black Sea (Ivanov et al., 1996), Taiwan (Shih, 1967), Indonesia (Barber et al., 1986), the West Indies (Brown and Westbrook,

1988) and the Mediterranean Ridge (Ivanov et al., 1996). Mainly due to their widespread occurrence, the magnitude and timing of methane seepage from mud extrusions should be investigated in order to evaluate their role in the global carbon cycle as argued by Judd et al. (2002). Therefore, the main subject of Chapter II is the determination of the amount of methane discharging from four different mud extrusions. The fate of methane injected into the water column from these mud extrusions is also discussed comparing the time frame of oxidation and dilution. The CH_4 output was estimated using two different approaches. One approach is based on the area covered by the dominant chemosynthetic communities and CH_4-emission rates of the specific fauna. The other estimate of the annual release of CH_4 is derived from CH_4-analysis in the water column and current measurements. The results of the two approaches are discussed and compared with published CH_4 outputs of other mud extrusions worldwide. Besides, the average of the estimated CH_4 outputs discharging was extrapolated for the number of mud extrusions discovered along the continental margin off Costa Rica.

Role of scarps

Chapter III addresses the fate and the output of methane at Jaco Scarp, one of the scarps located offshore Costa Rica. Scarps are created by the subduction of seamounts which uplift the continental plate and cause failure of oversteepend slope sediments. In principle, scarps are landslides, but we termed them differently because of their exclusive origin which is entirely due to the erosive nature of the margin (Chapter I). Methane seeping from them has not been reported yet, thus, one scarp, Jaco Scarp, was investigated in detail. Source areas, the distribution of methane in the scarp and temporal changes of methane concentrations are described and discussed. In contrast to Chapter II the fate of methane emitted from Jaco Scarp was derived from the stable carbon isotopic composition of CH_4, with which several mixing processes in addition to aerobe oxidation were identified. The calculation of the CH_4-output was adjusted to the special morphology of the scarp and its result compared with other vent sites including the estimates of the four mud extrusions.

Temporal variability

In addition to the estimates of methane output from these various settings, temporal changes of vent activity were investigated and are presented in Chapter IV. Some sampling stations

were revisited over a time span of four years (including measurements of a pre-site survey in this area in 1999) (Bohrmann et al., 2002; Heeschen, 2002) to identify long-term changes and their possible causes. The variations in CH_4 concentrations found are illustrated and discussed in reference to current measurements collected during the cruises in 2002 and 2003 and earthquake data provided by Red Sismologica Nacional (RSN:ICE-UCR).

A summary of the main results of Chapters II – IV together with overall conclusions are given in Chapter V.

Geological Setting

Along the Pacific coast of Nicaragua and Costa Rica the Cocos Plate is subducted beneath the Caribbean Plate at a rate of nearly 88 mm yr^{-1} since late Oligocene/early Miocene (Kimura et al., 1997). The subducting Cocos Plate is divided into three morphological segments (Fig. 2): (1) a smooth seafloor facing Nicaragua and Nicoya Peninsula, (2) a rough segment with abundant (40%) seamounts to the southeast and (3) the Cocos Ridge segment which is subducted off Osa Peninsula (von Huene et al., 2000). The boundary between the smooth seafloor and the seamount covered segment is marked by the Fisher Seamount and the Fisher Ridge. The seamount-segment extents southeast to Quepos Ridge, which is the outermost part of the Cocos Ridge-segment. The smooth seafloor segment is mainly generated at the East Pacific Rise spreading centre (EPR) for ~24 Ma, but a small segment situated between the EPR-crust and the rough-smooth boundary formed ~22 Ma ago along the Cocos-Nazca Spreading centre (CNS) (von Huene et al., 2000; Barckhausen et al., 2001). The rough seafloor, which has an age of 18 – 19 Ma, also originates at the CNS, but shows more influence by the Galapagos Hot Spot volcanism (von Huene et al., 2000). The seamounts of this segment have also a Galapagos geochemistry (Werner et al., 1999). The Cocos Ridge extends from the crestal area off Osa Peninsula to the Quepos Plateau. It is a classical hot spot trace with a crustal thickness of 12 km midway between Quepos Plateau and the crest (Werner et al., 1999; von Huene et al., 2000; Hoernle et al., 2002).

The entire oceanic crust is covered by a ~380 m thick sedimentary sequence consisting of ~220 m pelagic carbonates overlain by ~160 m siliceous hemipelagic sediments. The pelagic sediments mainly consist of siliceous and calcareous ooze whereas the hemipelagic sediments comprise diatomaceous ooze interbedded with thin ash layers and pods filled with upward grading sediments – from sand-sized clasts to diatomaceous ooze (Saffer et al., 2000). This

general stratigraphy extends from offshore Costa Rica to offshore Guatemala (Coulbourn, 1982; Aubouin and von Huene, 1985).

Results of ODP Leg 170 offshore Costa Rica suggest that not only the oceanic crust but also the entire incoming sedimentary section is subducted. Chrono-stratigraphic studies indicate a nearly identical age-depth relationship for the incoming and for the subducted sediments (Saffer et al., 2000). In addition, the small deformed frontal prism is lithologically and chemically similar to the continental margin sediments (Silver et al., 2000). This points to the fact that the Middle American subduction zone is an erosive convergent margin instead of an accretionary margin as was earlier assumed (e.g. Shipley et al., 1992). On global scale, about 24500 km of the total length of convergent margins are accretionary prism and ~19000 km are non-accretionary (von Huene and Scholl, 1991). However, Ranero and von Huene (2000)

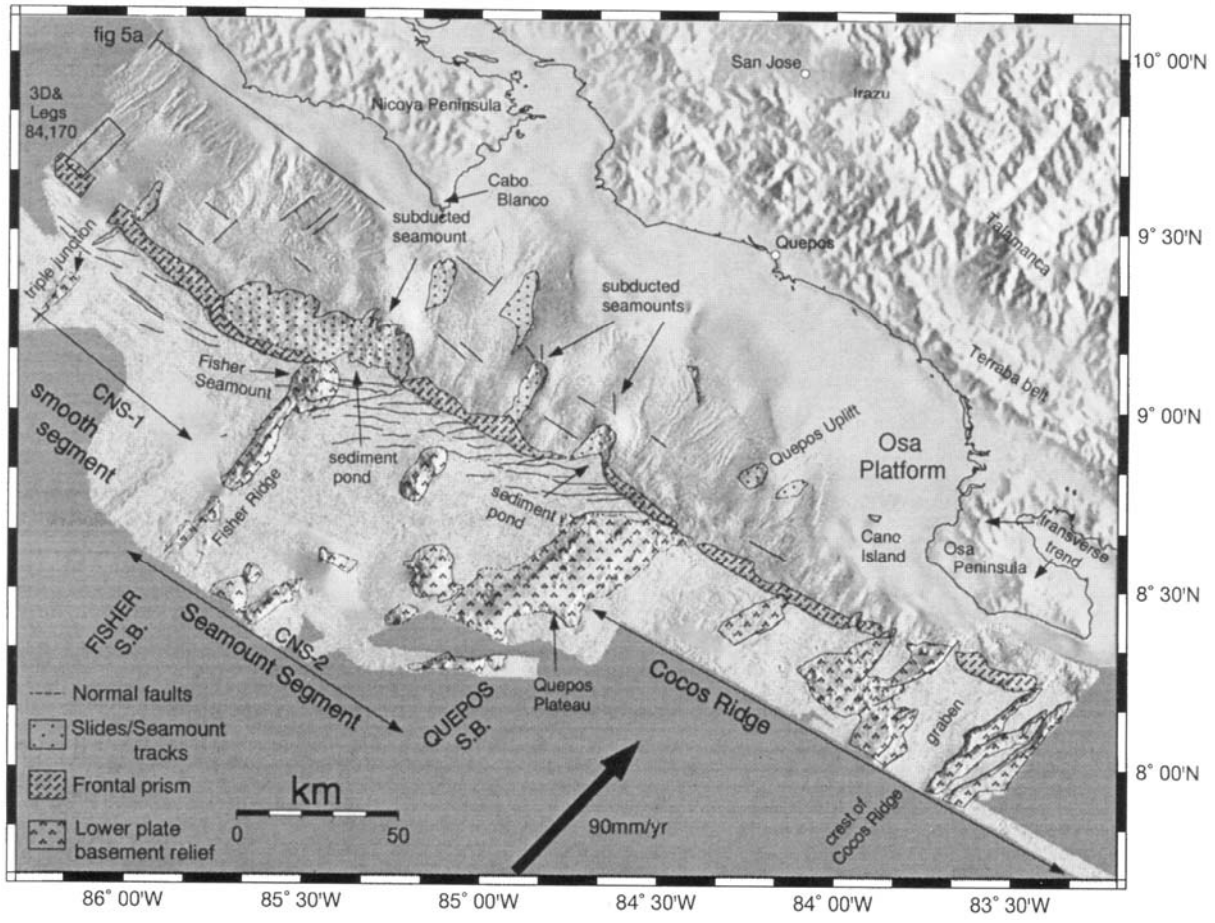

Fig. 2 Tectonic map of the continental margin off Costa Rica (von Huene, 2000) showing the different segments of oceanic crust and the respective continental margin. SB: segment boundary, CNS: Cocos-Nazca spreading center crust.

could illustrate removal of material from the upper continental plate by interpreting seismic records from the convergent margin of Costa Rica and Nicaragua. Two mechanisms of basal erosion are proposed. One mechanism is due to seamounts which scrape off continental material from the underside of the upper plate (Ranero and von Huene, 2000), and the other is a consequence of overpressured fluids invading fractures in the upper plate and separating fragments that are subducted (von Huene et al., 2004). The removal of material from underneath the continental margin leads to margin subsidence and the landward migration of the coastline (Meschede et al., 1999).

Subduction erosion in general and the erosional mechanism induced by the different segments of the oceanic crust affect greatly the structure and morphology of the continental margin (Fig. 2). The continental margin consists of igneous rock covered by 1 – 2 km of slope sediment, and is fronted by a small sedimentary prism (Ranero and von Huene, 2000). The prism (outermost 10 – 20 km) is characterized by compressive structures (Shipley et al., 1992) at which material from the frontal part is thrust underneath the igneous basement (Meschede et al., 1999). The main part of the continental margin is dominated by extension that is oriented parallel to the convergence direction. Evidence for extensional motion is provided by the observation of listric faults which lead to a landward tilt of blocks of the basement (Meschede et al., 1999). Some of the listric faults may penetrate the whole overriding plate down to the decollement (von Huene et al., 2004). The coastal region is uplifted possibly as a consequence of serpentinization of the igneous material in the deeper part of the continental wedge and/or due to underplating in this rearward part of the margin (Meschede et al., 1999). The effect of the subduction of different oceanic segments is pronounced at the extensional part, mainly at the middle and upper slope of the margin (Fig. 2) (von Huene et al., 2000). The continental margin opposite the smooth oceanic crust is characterized by an upper slope with many canyons and a gentler middle slope with shallower canyons. In contrast, trails from subducted seamount mark the continental slope opposite the rough oceanic crust. Above the crest of Cocos Ridge the continental slope is short, steep and without canyons.

On regional scale, the ocean crust thins and deepens (Ranero and von Huene, 2000) as well as the Middle American Trench axis deepens towards Nicaragua. The trench reaches 1 km depth at the crest of Cocos Ridge, 3.5 km through the seamount province, 4 km opposite the smooth segment and 5 km off Nicaragua (von Huene et al., 2000). In contrast, the continental margin thickens towards Nicaragua. It is thinner where the rough oceanic crust is subducted than

where the smooth oceanic crust is subducted. This illustrates the pronounced erosional effect where the seamounts and the Cocos Ridge is subducted compared to the relatively stable slope where smooth lower plate is subducted.

Significant fluid volumes are expelled from continental margins during this subduction process, which differ in geochemical and isotopic character from present-day sea water (Kahn et al., 1996). The fluids transport heat and dissolved chemical elements (e.g. CH_4) from varying depths within the lithosphere into the hydrosphere (Saffer et al., 2000). Fluids can originate from the interior of the continental margin and/or from the subducted sediments as the results of compaction of sediments and from dissociation of gas hydrate. Water loss and densification of the subducted sediments is indicated by the thinning of the underthrust sediments as drilling and seismic reflection surveys of the Costa Rica margin show (Saffer et al., 2000). The occurrence of gas hydrates in the slope sediments was proven by their recovery (Kimura et al., 1997; Schmidt et al., subm.) and by resistivity and velocity logs (Bohrmann et al., 2002). Dewatering occurs along faults, stratigraphic layers of high permeability e.g. sand rich layers or ash layers and along bedding planes (Saffer et al., 2000). One additional major fluid pathway for the water/chemicals lost by the subducted sediments is the decollement (Silver et al., 2000). The upward moving fluids can mix with seawater and/or fluids generated in shallower depths (Zuleger et al., 1996).

Numerous sites of fluid expulsion and their characteristic surface manifestations like authigenic carbonates, vent fauna, geochemical and geothermal anomalies in near surface sediments have been reported from the Costa Rican margin and are the subject of intense work by the SFB 574. However, the frontal prism revealed no evidence for fluid flow. The absence of vent communities on the lower 3 km of the prism and the elevated heat flow compared to the adjacent incoming Cocos plate suggests diffuse outflow through the toe of the prism (Kahn et al., 1996). Apart from the prism, biological evidence was observed in water depth between 3800 – 3480 m along thrust faults (Kahn et al., 1996), at mud extrusions in 3140 – 2400 m water depth (Kahn et al., 1996; McAdoo et al., 1996; Bohrmann et al., 2002), next to the headwall of landslides and scarps in 2600 – 300 m water depth (Bohrmann et al., 2002) and at one wall of a canyon in ~1600 m water depth (Kahn et al., 1996). Some of these vent sites and more recently discovered ones are the subject of the following Chapters II, III and IV.

Oceanography

The hydrography of the research area is controlled by the circulation system of the Eastern Equatorial Pacific Ocean. A detailed descriptions of the coastal circulation pattern from the Galapagos Islands to the Gulf of California is given by Badan-Dangon (1998) and an overview of the hydrology of the Pacific Ocean is given in Tomczak and Godfrey (1994). The characteristic water masses and circulation patterns off Central America are summarized below.

In general, this part of the Pacific Ocean contains four water masses. These have been identified in the T-S properties from CTD-profiles obtained during RV SONNE and RV METEOR cruises in 2002 and 2003 (Fig. 3). The uppermost 20 – 50 m of the surface water consist of Tropical Surface Water (TSW, T > 25 °C, S < 34) which spreads latitudinally near the coast from the equatorial front off Ecuador to the entrance of the Gulf of California. The low salinity is due to the excess of rainfall over evaporation (Wyrtki, 1966). The salinity maximum beneath the surface layer is caused by the discharge of high-salinity water of the Equatorial Undercurrent that forms together with the lower salinity water of the Subarctic Intermediate Water (SIW) the Subtropical Subsurface Water mass (StSsW). This water mass fills the eastern tropical Pacific Ocean to a depth of 600 m. Its cyclonic spreading starts at the Galapagos Island continues towards the northeast around the Costa Rica Dome and spreads farther to the northwest in the lower portion of the Costa Rica Coastal Current to finally merge in the North Equatorial Current flowing to the west. On its way it loses salt to the fresher upper layer. The deeper water masses are formed outside of the region (Wyrtki, 1966). At depths of 600 to 900 m the salinity decreases to ~34.5 presenting the Subarctic Intermediate Water (SIW). The SIW originates from the Polar Front in the western North Pacific Ocean and is subducted into the subtropical gyre, filling the northern hemisphere south of 40°N from the east. At this depth the movement of the water is still a part of the upper layer circulation, below 1000 m the water follows the deep circulation, i.e. northward movement in western boundary currents with slow return circulation through the eastern basins. Beneath the SIW the Pacific Deep Water (PDW) fills the entire basin at 1000 – 3000 m depth. It is formed almost entirely through slow mixing processes of Antarctic Bottom Water, North Atlantic Deep Water and Antarctic Intermediate Water. All of these water masses form a well-stratified water body, because the T-S curve crosses the density contours in such a way that density increases (Fig. 3). Therefore, horizontal mixing dominates, but

vertical mixing is enhanced in certain areas where upwelling of deeper water occurs, as discussed below.

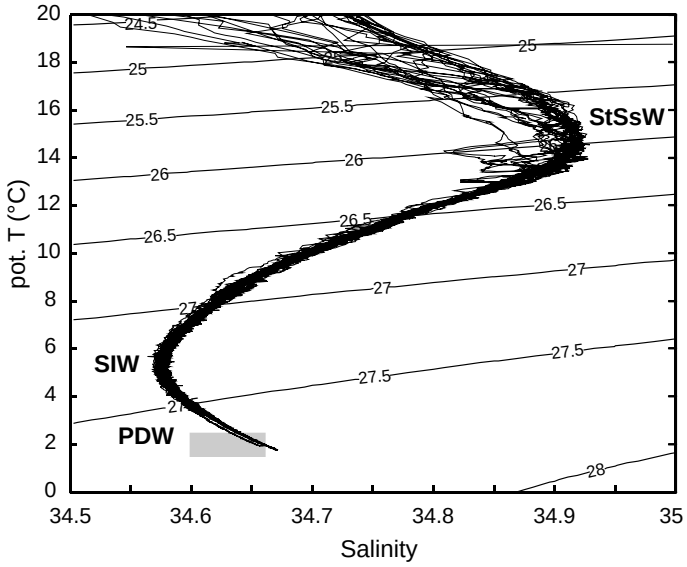

Fig. 3 T-S diagram of exemplary CTD profiles collected during SO 163 offshore Costa Rica. Isopycnals refer to surface pressure. The major Pacific water masses in this region are included, StSsW - Subtropical Subsurface Water, SIW - Subarctic Intermediate Water and PDW - Pacific Deep Water.

The oxygen minimum layer, which is present everywhere in the eastern tropical Pacific Ocean can be considered as a water mass in its own right, even though it overlaps with other T-S defined water masses. It is defined by an O_2 content of less than 1 ml L^{-1} as a result of high input of oxidizable organic matter from surface layers and sluggish circulation (Badan-Dagon, 1998). The eastern tropical Pacific Ocean is a region into which the ocean-wide circulation does not penetrate. The absence of a strong circulation reduces the supply of oxygen (Wyrtki, 1966). Additionally, the consumption of oxygen is increased due to the high surface ocean productivity fueled by upwelling of nutrient rich deep waters (e.g. Sansone et al., 2001). These factors combined lead to the formation of a large area in the upper ocean with depleted levels of oxygen; in fact the region of oxygen-depleted water in the subsurface of the eastern tropical Pacific Ocean is the largest one in the world's ocean. The 'oxygen minimum layer' is more than 1200 m thick off the coast of Mexico and 800 m thick off Peru (Wyrtki, 1966). The actual minimum with concentrations < 0.25 ml/L lies between 300 – 500 m. The upper boundary comes to within 50 m of the sea surface off Central America and Peru. This corresponds with our data which shows the upper boundary at ~50 m and the lower one at ~1200 m (Fig. 4). The oxygen-depleted condition extend beyond 5700 km off the coast where it was observed at 650 – 1200 m depth (Sansone et al., 2001).

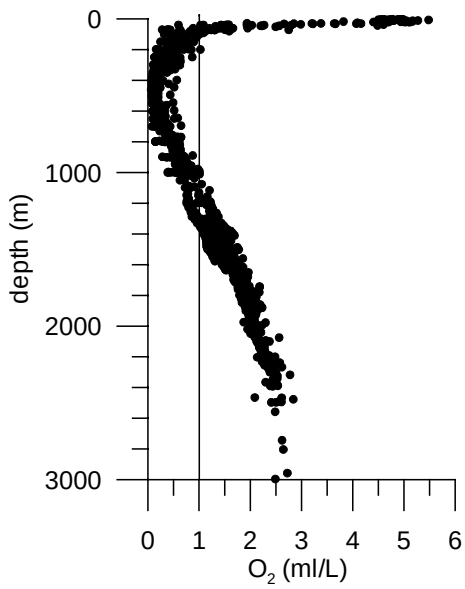

Fig. 4 Concentration of O_2 versus depth. Discrete water samples collected during SO 163-2, M54-2/3a, and SO 173-3/4 are shown in which oxygen was measured by Winkler Titration. The oxygen minimum layer is defined by an O_2 content below 1 ml L^{-1} (Badan-Dagon, 1998).

The northward flowing Costa Rica Coastal Current (CRCC) dominates the current system in the study area offshore Costa Rica. Its northern portion is also known as Mexican Current. It is one of the least explored coastal currents of the world; its presence is only inferred from large scale hydrography, because no direct measurements exist. Like the other currents in the eastern tropical Pacific Ocean it varies seasonally due to changes in strength and position of the large wind systems. A detailed description of the current system is given in Wyrtki (1966) which is summarized as follows: From August to December the North Equatorial Counter Current (NECC) is fully developed flowing around the Costa Rica Dome into the CRCC. The CRCC carries probably subtropical subsurface water (StSsW) to the North starting from Panama Bight and flowing along the coast of Central America (Badan-Dagon, 1998). It ends at the mouth of Gulf of California where it meets the southward flowing California Current (CC). Finally it turns towards the west streaming in the North Equatorial Current (NEC). The CRCC constitutes a major portion to the water in the Gulf of California, but a fraction feeds also the northward flowing California Undercurrent or Davidson Current. In January the NECC becomes weaker and the CC stronger extending farther to the south. In February to April the CC penetrates far south, the NECC is absent and eddies develop offshore Central America, which result from strong wind jets crossing Central America through several isthmuses. The constant northward flow of the CRCC is disrupted during this time. In May to July the NECC becomes stronger and most of its water turns into the CRCC again flowing north. The CC is still strong, but does not penetrate much into the eastern tropical Pacific. In July to August the CC becomes progressively weaker and the NEC gains more and more water from the CRCC.

Both, coastal upwelling along eastern boundaries and oceanic upwelling along offshore divergence occur off Central America (Fiedler et al., 1991). The thermocline is shallow (40 – 50 m) in this region, so that vertical advection and mixing brings cold, nutrient-rich water

from below the thermocline into the surface layer (Fiedler et al., 1991). A detailed description of the mechanism of coastal upwelling is given in Tomczak and Godfrey (1994). They stated among other things that the onshore movement of subsurface water which feeds water into the upwelling region does not extend below 400 m. The coastal upwelling off Central America is induced by wind jets crossing the continent at mountain passes near the isthmuses of Tehuantepec, Papagayo and Panama (e.g. Fiedler et al., 1991). The wind jets cross the shelf and cause intense vertical mixing and entrainment of subsurface water (Badan-Dagon, 1998). The Papagayo wind jet affects strongly the location and magnitude of the Costa Rica Dome. A detailed description of the annual cycle caused by the wind jet can be found in Fiedler (2002). The CRD is the eastern end of a thermocline ridge. The thermocline ridge itself results from the offshore divergence found between the NECC and the NEC at 10°N. Even though the thermocline is shallow along the ridge, the nutrient-rich deep waters do not reach the surface except at the eastern end of the thermocline ridge, i.e. in the Costa Rica Dome (CRD) (Fiedler et al., 1991; Badan-Dagon, 1998). The CRD is similar to other tropical thermocline domes in analogous locations of the Atlantic and Pacific oceans e.g. off Peru, Guinea and Angola (Fiedler, 2002; Kessler, 2002). They all have in common that they are part of a thermocline ridge, surface currents flow cyclonically around them and their seasonality is affected by large-scale wind patterns. The occurrence of the CRD appears to be a general feature of global circulation, but the specific features of it are produced by the Papagayo wind jet (Kessler, 2002). Therefore, both upwelling mechanism (coastal and oceanic) apply to the CRD. The CRD is centered 300 km off the Gulf of Papagayo between Costa Rica and Nicaragua, extends to 300 m depth and reaches 300 – 500 km in diameter. About 3.5 Sv (Sv = 10^6 m^3/s) of intermediate-depth water rise through the base of thermocline under the CRD (Kessler, 2002).

Methods

CH_4-analysis

For CH_4-analyses aboard a ship a modification of the vacuum degassing method described by Lammers and Suess (1994) was used (Rehder et al., 1999). 1600 ml of water were injected into pre-evacuated 2200 ml glass bottles, which led to almost quantitative degassing. The gas phase was subsequently recompressed to atmospheric pressure and the CH_4 mole fraction of the extracted gas was determined by gas chromatography. A Shimadzu GC14A gas chromatograph equipped with a flame ionisation detector was used in connection with a

Shimadzu CR6A Integrator. Nitrogen was used as carrier gas. Separation was achieved using a 4 m 1/8' SS column packed with Porapack Q (50/80 mesh) run isothermally at 50°C. The total gas content of the sample was calculated from the measured dissolved oxygen concentration assuming that N_2 and Ar are 100% saturated relative to their atmospheric partial pressures (Weiss, 1970). In addition to the oxygen sensor of the CTD, the Winckler titration (Grasshoff et al., 1997) was used for the determination of the oxygen content. The data of the oxygen sensor was corrected by the difference of titration to sensor data. The dissolved methane concentration was estimated as the product of the mole fraction in the extracted gas phase and the amount of total gas (STP) in the sample. For calibration, mixtures of 1.936 ppm ±0.003 ppm and 9.854 ±0.006 ppm of synthetic air (Deuste Steininger, calibrated against NOAA/CMDL standards at the Institute for Environmental Physics, Heidelberg) were used. Replicate analysis of samples of a single hydrocast yield a precision of ± 10% for samples with methane concentration < 2 nmol/L and ± 5% for CH_4 concentration > 2 nmol/L.

The remainder of the extracted gas was transferred to an evacuated 20 ml vial for shore-based analysis of stable isotopes. The routine for preservation of the sample and analysis is described in Chapter III.

Current measurements

Moorings were deployed at sites of active seepage during SO173/3-4. Each mooring was equipped with an anchor, two Aanderaa-current meters (RCM 8), two acoustic releases and subsurface floating units (Fig. 5). Benthos spheres were attached above each instrument to keep the mooring vertical in the water column during deployment. At each location current meters were recording at about 10 m and 120 m above seafloor.

ADCPs (Acoustic Doppler Current Profiler) were deployed in addition to the moored current meters. The Long Ranger Lander (LORA) equipped with an upward-looking 75 kHz ADCP (RD Instruments) was used and a downward-looking 300 kHz ADCP attached to the rosette water sampler (Lowered ADCP = LADCP) recorded data while the water column was sampled in the vicinity of vent sites. The data of the LADCP was post-processed together with navigation data of the ship using software by M. Visbeck (IFM Kiel). Unfortunately, the precision of the LADCP-data was not good enough for publication. Therefore, an upward-looking ADCP should be used in addition to the downward-looking ADCP and if available data of a ship-board ADCP should be included in post-processing.

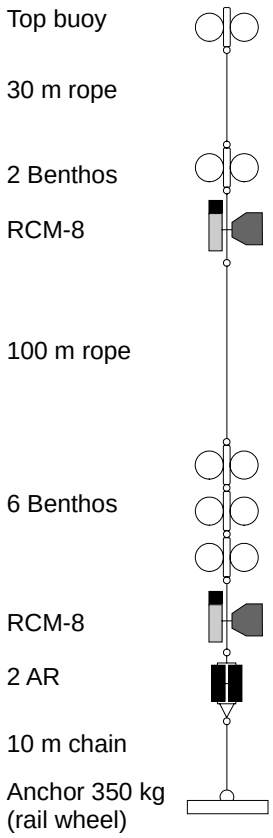

Fig. 5 Scheme of mooring used during SO 173-3/4 with its components (rope - METEOR nylon string, RCM-8 - Aanderaa Recording Current Meter, AR - Oceano Acoustic Releaser). The total length is about 140 m.

References

Aubouin, J. and von Huene, R., 1985. Summary; Leg 84, Middle American Trench transect off Guatemala and Costa Rica. Proc. DSDP Init. Rep., 84: 939-957.

Badan-Dagon, A., 1998. Coastal circulation from the Galapagos to the Gulf of California. In: A.R. Robinson and K.H. Brink (Editors), The Sea, Vol. 11: The Global Coastal Ocean - Regional Studies ans Syntheses. John Wiley & Sons, Inc., pp. 315-343.

Barber, A.J., Tjokrosapoetro, S. and Charlton, T.R., 1986. Mud volcanoes, shale diapirs, wrench faults and mélanges in accretionary complexes, eastern Indonesia. American Association of Petroleum Geologists, Bulletin, 70: 1729-1741.

Barckhausen, U., Ranero, C.R., von Huene, R., Cande, S.C. and Roeser, H.A., 2001. Revised tectonic boundaries in the Cocos Plate off Costa Rica: Implications for the segmentation of the convergent margin and for plate tectonic models. Journal of Geophysical Research, 106(No. B9): 19207-19220.

Bohrmann, G., Jung, C., Heeschen, K., Weinrebe, W., Baranov, B., Cailleau, B., Heath, R., Hühnerbach, V., Hort, M., Masson, D. and Schaffer, I., 2002. Widespread fluid expulsion along the seafloor of Costa Rica convergent margin. Terra Nova, 14: 69-79.

Brown, K.M. and Westbrook, G.K., 1988. Mud diapirism and subcretion in the Barbados ridge accretionary complex: the role of fluids in accretionary processes. Tectonics, 7(No. 3): 613-640.

Coulbourn, W.T., 1982. Stratigraphy and structure of the Middle American Trench; Deep Sea Drilling Project Leg 67 transect off Guatemala. Proc. DSDP Init. Rep., 67: 691-706.

Cranston, R.E., Ginsburg, G.D., Soloviev, V.A. and Lorenson, T.D., 1994. Gas venting and hydrate deposits in the Okhotsk Sea. Bulletin of the Geological Society of Denmark, 41: 80-85.

Dickens, G.R., 2004. Hydrocarbon-driven warming. Nature, 429: 513-515.

Dickens, G.R., Castillo, M.M. and Walker, J.C.G., 1997. A blast of gas in the latest Paleocene: Simulating first-order effects of massive dissociation of oceanic methane hydrate. Geology, 25(3): 259-262.

Dickens, G.R., O'Neil, J.R., Rea, D.K. and Owen, R.M., 1995. Dissociation of oceanic methane hydrate as a cause of the carbon isotope excursion at the end of the Paleocene. Paleoceanography, 10(6): 965-971.

Fiedler, P.C., 2002. The annual cycle and biological effects of the Costa Rica Dome. Deep-Sea Research I, 49: 321-338.

Fiedler, P.C., Philbrick, V. and Chavez, F.P., 1991. Ocean upwelling and productivity in the eastern tropical Pacific. Limnology and Oceanography, 36(8): 1834-1850.

Flueh, E., Soeding, E. and Suess, E., 2004. RV SONNE Cruise Report SO173/1, 3 & 4 Subduction II: The Central American Continental Margin. GEOMAR Report, 115, Kiel, 491 pp.

Ginsburg, G.D. and Soloviev, V.A., 1998. Submarine Gas Hydrates. Statoil, Norway.

Grasshoff, K., Ehrhardt, M. and Kremling, K., 1997. Methods of seawater analysis. Verlag Chemie, Gulf Publishing, Houston, 757-773 pp.

Guliyiev, I.S. and Feizullayev, A.A., 1996. Geochemistry of hydrocarbon seepages in Azerbaijan. In: D. Schumacher and M.A. Abrams (Editors), Hydrocarbon migration and its near-surface expression. American Association of Petroleum Geologists, Tulsa, pp. 63-70.

Heeschen, K., 2002. Processes and fluxes controlling methane in different marine settings: Continental margins of Cascadia and Costa Rica and the Weddell Basin, Christian-Albrechts-Universität, Kiel, 128 pp.

Hoernle, K., vd Bogaard, P., Werner, R., Lissinna, B., Hauff, F., Alvarado, G. and Grabe-Schoenberg, D., 2002. Missing history (16-71 Ma) of the Galapagos hotspot: Iplications for the tectonic and biological evolution of the Americas. Geology, 30(4): 795-798.

Hornafius, J.S., Quigley, D.C. and Luyendyk, B.P., 1999. The world's most spectacular marine hydrocarbon seeps (Coal Oil Point, Santa Barbara Channel, California): Quantification of emission. Journal of Geophysical Research, 104(C9): 20703-20711.

Houghton, J.T., 1997. Global Warming: the complete briefing. Cambridge University Press, Cambridge.

Hovland, M., Gallagher, J.W., Clennell, M.B. and Lekvam, K., 1997. Gas hydrate and free gas volumes in marine sediments: Example from the Niger Delta front. Marine and Petroleum Geology, 14(3): 245-255.

Ivanov, M.K., Limonov, A.F. and van Weering, T.C.E., 1996. Comparative characteristics of the Black Sea and Mediterranean Sea mud volcanoes. Marine Geology, 132: 253-271.

Judd, A.G., Davies, G., Wilson, J., Holmes, R., Baron, G. and Bryden, I., 1997. Contributions to atmospheric methane by natural seepages on the U.K. continental shelf. Marine Geology, 140: 427-455.

Judd, A.G., Hovland, M., Dimitrov, L.I., Garcia Gil, S. and Jukes, V., 2002. The geological methane budget at continental margins and its influence on climate change. Geofluids, 2: 109-126.

Kahn, L.M., Silver, E.A., Orange, D., Kochevar, R. and McAdoo, B., 1996. Surficial evidence of fluid expulsion from the Costa Rica accretionary prism. Geophysical Research Letters, 23(8): 887-890.

Katz, M.E., Pak, D.K., Dickens, G.R. and Miller, K.G., 1999. The source and fate of massive carbon input during the Latest Paleocene Thermal Maximum. Science, 286(19): 1531-1533.

Kennett, J.P. and Stott, L.D., 1991. Abrupt deep-sea warming, palaeoceanographic changes and benthic extinctions at the end of the Palaeocene. Nature, 353: 225-229.

Kessler, W.S., 2002. Mean and Annual Cycle of temperature and geostrophic currents in the east pacific warm pool.

Kimura, G., Silver, E., Blum, P. et al., 1997. Proceedings of the ocean drilling program, 170, 458 pp.

Kvenvolden, K.A., 1993. A Primer on Gas Hydrates. The Future of Energy Gases, U.S. Geological Survey Professional Paper 1570: 279 - 291.

Kvenvolden, K.A., Lorenson, T.D. and Reeburgh, W.S., 2001. Attention turns to naturally occuring methane seepage. EOS, 82: 457.

Lammers, S. and Suess, E., 1994. An improved head-space analysis method for methane in seawater. Mar. Chem., 47: 115-125.

Lelieveld, J. and Crutzen, P.J., 1992. Indirect chemical effects of methane on climate warming. Nature, 355: 339-342.

McAdoo, B.G., Orange, D.L., Silver, E.A., McIntosh, K., Abbott, L., Galewsky, J., Kahn, L. and Protti, M., 1996. Seafloor structural observations, Costa Rica accretionary prism. Geophysical Research Letters, 23(8): 883-886.

Meschede, M., Zweigel, P. and Kiefer, E., 1999. Subsidence and extension at a convergent plate margin: evidence for subduction erosion of Costa Rica. Terra Nova, 11: 112-117.

Ranero, C.R. and von Huene, R., 2000. Subduction erosion along the Middle America convergent margin. Nature, 404: 748-752.

Rehder, G., Keir, R.S., Suess, E. and Rhein, M., 1999. Methane in the Northern Atlantic controlled by microbial oxidation and atmospheric history. Geophysical Research Letters, 26(5): 587-590.

Saffer, D.M., Silver, E.A., Fisher, A.T., Tobin, H. and Moran, K., 2000. Inferred pore pressure at the Costa Rica subduction zone: implications for dewatering processes. Earth and Planetary Science Letters, 177: 193-207.

Sansone, F.J., Popp, B.N., Gasc, A., Rust, T.M. and Graham, A.W., 2001. Highly elevated methane in the eastern tropical North Pacific and associated isotpically enriched fluxes to the atmosphere. Geophysical Research Letters, 28: 4567-4570.

Schmidt, M., Hensen, C., Moerz, T., Mueller, C., Grevemeyer, I., Wallmann, K., Sahling, H., Mau, S. and Brueckmann, W., subm. Shallow surface methane hydrate accumulation related to mud diapirism at "Mound 11" (Costa Rica forearc). Marine Geology.

Shih, T.T., 1967. A survey of the active mud volcanoes in Taiwan and a study of their types and the character of mud. Petroleum Geology of Taiwan, 5: 259-311.

Shipley, T.H., McIntosh, K.D., Silver, E.A. and Stoffa, P.L., 1992. Three-dimensional imaging of the Costa Rica accretionary prism: structural diversity in a small Volume of the lower slope. Journal of Geophysical Research, 97: 4439-4459.

Silver, E., Kastner, M., Fisher, A., Morris, J., McIntosh, K. and Saffer, D., 2000. Fluid flow paths in the Middle America Trench and Costa Rica margin. Geology, 28(No. 8): 679-682.

Sloan, E.D., 1998. Clathrate Hydrates of Natural Gases. Marcel Dekker, New York, 705 pp.

Soeding, E., Wallmann, K., Suess, E. and Flueh, E., 2003. RV METEOR Cruise Report M54/2+3 Fluids and Subduction Costa Rica 2002. GEOMAR Report, 111, Kiel, 366 pp.

Svensen, H., Planke, S., Malthe-Sørenssen, A., Jamtveit, B., Myklebust, R., Eidem, T.R. and Rey, S.S., 2004. Release of methane from a volcanic basin as a mechanism for initial Eocene global warming. Nature, 429: 542-545.

Tissot, B.P. and Welte, D.H., 1984. Petroleum Formation and Occurrence. Springer Verlag, Heidelberg.

Tomczak, M. and Godfrey, J.S., 1994. Regional Oceanography: an Introduction. Pergamon Press, New York, 422 pp.

von Huene, R., Ranero, C.R. and Vannucchi, P., 2004. Generic model of subduction erosion. Geology, 32(10): 913-916.

von Huene, R., Ranero, C.R. and Weinrebe, W., 2000. Quaternary convergent margin tectonics of Costa Rica, segmentation of the Cocos Plate, and Central American volcanism. Tectonics, 19(2): 314-334.

von Huene, R. and Scholl, D.W., 1991. Observations at convergent margins concerning
sediment subduction, subduction erosion and the growth of continental crust. Reviews of Geophysics, 29: 279-316.

Weinrebe, W. and Flueh, E., 2002. RV Sonne, Cruise Report SO 163, Subduction I, Balboa-Caldera-Balboa (March 13 - May 21, 2002). GEOMAR Report, 106: 534.

Weiss, R.F., 1970. The solubility of nitrogen, oxygen and argon in water and seawater. Deep-Sea Research, 17: 721-735.

Werner, R., Hoernle, K., van de Bogaard, P., Ranero, C., von Huene, R. and Korich, D., 1999. Drowned 14 Ma old Galapagos archipelago off the coast of Costa Rica: Implications for tectonic and evolutionary models. Geology, 27: 499-502.

Wyrtki, K., 1966. Oceanography of the Eastern Equatorial Pacific Ocean. Oceanogr. Mar. Biol. Ann. Rev., 4: 33-68.

Zuleger, E., Gieskes, J.M. and You, C.-F., 1996. Interstitial water chemistry of sediments of the Costa Rica accretionary complex off the Nicoya Peninsula. Geophysical Research Letters, 23(No. 8): 899-902.

Estimates of methane output from mud extrusions at the erosive convergent margin off Costa Rica

S. Mau[a*], H. Sahling[a]1, G. Rehder[b,a], E. Suess[b,a], P. Linke[b,a] and E. Soeding[a]

[a] Sonderforschungsbereich 574, Kiel University, Wischhofstr. 1-3, 24148 Kiel, Germany

[b] IFM-GEOMAR, Leibniz-Institut für Meereswissenschaften, Wischhofstr. 1-3, 24148 Kiel, Germany

1 present address: DFG Forschungszentrum Ozeanränder, Bremen University, Am Fallturm 1, 28359 Bremen, Germany

* corresponding author: S. Mau, smau@ifm-geomar.de, phone: +49-431-600-2564 / fax: +49-431-600-2915

Abstract

Four mud extrusions were investigated along the erosive subduction zone off Costa Rica. The diapiric structures of Mound Culebra and Mound 10 are situated on the continental slope northwest of Nicoya Peninsula. Mound 12 and Mound 11, which are described as mud volcanoes, are found to the southeast of Nicoya Peninsula. All mounds show active fluid seepage, indicated by chemosynthetic communities, authigenic carbonates and methane plumes in the water column. Bacterial mats and mytilid mussels were observed at the mud volcanoes in contrast to dominantly vesicomyid clams at the mud diapirs, suggesting that a higher methane output might exist at the mud volcanoes. Two independent estimates of the methane output from the mud extrusions are presented. Output estimates based on areas covered by the prevailing chemosynthetic community and fauna-specific CH_4 emission rates range from 10^3 – 10^4 mol yr^{-1} per mud extrusion. These values include the fractions of methane becoming anaerobically oxidized in the sediment and the remaining portion which is released into the ocean. The amount of CH_4 exclusively discharging into the water column was estimated based on measurements of the near bottom methane distribution and current velocities. This approach yields estimates between 10^4 – 10^5 mol yr^{-1}. Both approaches indicate higher discharge of CH_4 at the mud volcano sites than at the diapiric sites. These estimates are lower than other reported CH_4 emissions from mud extrusion at accretionary and passive margins, probably as consequence of the erosional nature of the subduction zone. The methane plumes are locally bound to the mud extrusions and contribute to the ocean carbon budget. Assuming that the averaged methane output of the mud extrusions investigated is

representative for the 48 mounds discovered offshore Costa Rica and that seepage is constant over time, 307 Mg yr^{-1} (1 Mg = 10^6 g) of methane are emitted along this part of the subduction zone.

Keywords: methane plume; chemosynthetic species; mud extrusion; methane output; Costa Rica forearc

Introduction

Mud extrusions are commonly associated with compressional tectonics, thus occurring abundantly at convergent margins (Kopf, 2003). Predominantly methane seeps from mud extrusions, which generally exceeds 90 vol% of the gas phase (Brown, 1990; Dimitrov, 2002; Kopf, 2003). However, estimates of the amount of methane discharging from submarine mud extrusions worldwide are sparse (Judd et al., 2002) and, thus, the role of methane seepage from mud extrusions in the global methane budget is highly speculative (Kopf, 2003; Milkov et al., 2003). In order to better constrain these estimates and contribute data from an erosional subduction setting, we estimated the CH_4-output from four mud extrusions offshore Costa Rica based on measurements in the water column overlying these features and their chemosynthetic benthic communities.

Numerous circular elevations were mapped during detailed swath bathymetry surveys on the middle and upper slope of the convergent margin of Middle America, along the coast of Nicaragua and Costa Rica (Ranero and von Huene, 2000). These circular elevations have been described as mud extrusions (Shipley et al., 1992; Kimura et al., 1997). Surficial fluid venting was detected at these features during a pre-site survey for ODP-Leg 170 in 1994 (McAdoo et al., 1996) and during expedition SO144 in 1999 (Bialas et al., 1999; Bohrmann et al., 2002). Methane measurements in the water column above the central depression of a mud extrusion surveyed during SO144 revealed a near bottom plume reaching up to 94 nmol L^{-1}, which is two orders of magnitude above the regional background of 0.5 – 2 nmol L^{-1} (Bohrmann et al., 2002).

Here we present seafloor observations and extensive methane analyses of the water column above four such mud extrusions. All are located at the mid-slope of the margin wedge, about

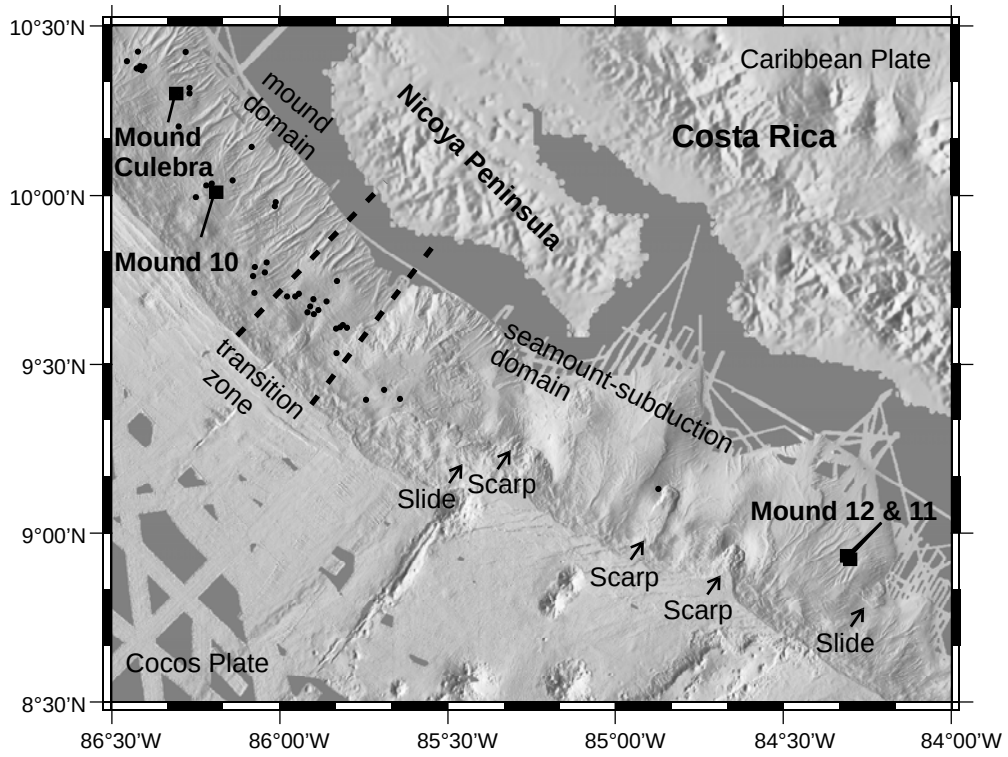

Fig. 1 Bathymetry of the continental margin off Costa Rica and locations of mud extrusions (filled circles). Mound Culebra and Mound 10 are located west of Nicoya Peninsula, at the mound segment where 27 mounds occur in the area shown. The southwestern continental margin is more strongly structured due to scarps created by the subduction of seamounts. At this margin segment, only few other mounds were observed beside Mound 11 & 12 (Sahling et al., in prep.).

25 – 40 km from the Middle American Trench in water depths from 1000 – 2300 m (Fig. 1). Based on the distribution of methane seeps along the slope and subsurface structures three domains were defined: (1) mound domain at the margin west off Nicoya Peninsula, (2) seamount-subduction domain east of Nicoya Penisula and (3) transitional domain in between (Sahling et al., in prep.). Mound Culebra and Mound 10 are located at the mound domain and Mound 12 and Mound 11 are located at the seamount-subduction domain (Fig. 1). About 27 mounds exist in the mound domain along the margin segment shown in Figure 1. They are typically cone-shaped with elevations of 100 m and more above the surrounding seafloor topography. The mounds are probably connected to extensional fault pattern caused by subduction erosion (Sahling et al., in prep). Von Huene et al. (2004) suggest that fluids from the subducted plate penetrate extensional fractures causing separation of pieces of the overriding continental plate that are subducted, hence, causing basal erosion of the upper plate and fluid migration along faults propagating partly to the seafloor. In the seamount-subduction domain the volcanic seamounts and ridges riding on the down-going

oceanic plate plow into the continental margin, causing severe deformation and opening up additional fluid pathways besides the ones along faults. Seven mounds were observed along this 180 km margin segment. In the transition zone fluid seepage appears to be related to numerous faults and 14 smaller mounds. This short margin segment is influenced by ridge subduction as well as the change in the oceanic plate origin (Sahling et al., in prep.).

This investigation supplements a suite of previous studies that focused on different aspects of mud diapirism and volcanism. Moerz et al. (in press) used sedimentological and structural data to reconstruct the evolution of Mound Culebra, Mound 12 and Mound 11. They showed that all three mounds are fault-controlled, but evolved differently. Mound Culebra developed by the diapiric rise of overcompacted silty clay that shows signs of intense brittle deformation, brecciation, hydrofracturing and secondary perforation by closely spaced conduits. In contrast, Mound 12 and Mound 11 are thought to be low relief mud volcanoes because of mud flows and vent debris found in sediment cores. At Mound Culebra fluid flow is indicated by an interrupted BSR and other reflectors underneath the mound and by heat-flow anomalies at certain areas of the mound (Grevemeyer et al., 2004). Schmidt et al. (subm.) reported the occurrence of near-surface gas hydrates at Mound 11. Hensen et al. (2004) showed that the source of one end-member of the fluids is clay-dehydration generated at temperature between 85 and 130 °C. These authors suggest that the fluids originate from subducted sediments on the down-going oceanic plate and are channeled upwards along deep-seated faults which cut through the basement and upper-plate sediments. Modeling of benthic chamber and porewater data at Mound 12 revealed high methane oxidation and seep rates at sediments with bacterial mats (Linke et al., subm.). Various fluid flow regimes at the different mounds were revealed by a comprehensive study on the fabric, mineralogy and isotope signature of authigenic carbonates that formed from anaerobic oxidation of methane (Han et al., 2004). For example, the range in the $\delta^{13}C$ values of methane-derived carbonates between -18.6 and -53.0 ‰ PDB indicate both, a deep thermogenic and a shallow biogenic origin of methane. Variations in the $\delta^{18}O$ values are attributed to the slow and rapid ascent of mixed fluids consisting of clay-dehydration water, gas hydrate water and normal pore water.

We complement these previous studies with our observations from the water column and the sediment-water interface above active emission sites and assess the fate of methane in the water column. Moreover, we derive estimates of the amount of CH_4 seepage at sites covered

by chemosynthetic communities and the total amount of methane escaping into the water column using two independent approaches.

Methods

The seafloor was surveyed with ocean floor observation systems (OFOS) during four cruises with the research vessels SONNE and METEOR: SO 144 (Sept. – Nov. 1999), SO 163 (Apr. – May 2002), M 54 (Aug. – Sept. 2002) and SO 173 (Sept. 2003). A super-short-baseline subpositioning system provided on RV SONNE was used during OFOS and CTD/rosette deployments. The OFOS is a towed camera sled equipped with video, still cameras and a CTD. Due to the considerable offset which exists between the CTD-derived depths and the depths of bathymetric charts based on hydroacoustic methods, we used data from the OFOS-mounted CTDs in order to better define the depths at which seafloor structures were observed and compared these with the depths of methane anomalies in the water column. Seafloor maps showing the distribution of geological and biological indications of fluid seepage were constructed based on the interpretation of available position and depth data as well as congruence of repeated observations, a method successfully used on many previous occasions (e.g. Wiedicke et al., 2002; Sahling et al., accepted).

During M 54, water column work was conducted with a standard CTD system (Mark III) and a 24 x 10-L-rosette water sampler as well as with a bottom water sampler (BWS), an instrument newly developed at the University of Bremen (Inthorn et al., subm.). The BWS consists of five 5-L-water bottles placed at different heights (0.14 – 1.2 m) in horizontal position on a frame with two fins to assure positioning in the direction of bottom current flow. After deployment of the BWS at the seafloor, the bottles were closed after 30 minutes to allow settling of the resuspension load. A total of 19 CTD-hydrocasts were taken and 3 times the BWS deployed in the area of mud extrusions. The positions were chosen to locate and track the extent of the methane plume based on OFOS-observations. The water samples for determination of methane and oxygen were taken with decreasing depth intervals towards the seafloor. For CH_4-analyses aboard a modification of the vacuum degassing method described by Lammers and Suess (1994) was used, modified by Rehder et al. (1999). In addition to the oxygen sensor of the CTD, Winckler titration (Grasshoff et al., 1997) was used for the determination of oxygen.

Current measurements were performed by upward looking ADCPs (Acoustic Doppler Current Profiler; RD Instruments) attached to lander devices during M 54. At Mound Culebra a 300 kHz ADCP was deployed for ~14 days and at Mound 12 and Mound 11 a 1200 kHz ADCP was deployed for 48 hours.

The amount of methane emitted from a mud extrusions was estimated using two independent approaches. The first one is based on the assessment of the total area covered by different chemosynthetic communities and methane flux rates presumed to be specific for the different habitats. To estimate the total area covered by dominant chemosynthetic species (vesicomyid clams, bacterial mats), a basal plane in which patches of clams or bacterial mats occur was defined based on the seafloor observations. The area that was observed by the camera sled within this basal plane was estimated by assuming a constant 2-m wide image of the seafloor along the length of the track. The area covered by clams or bacterial mats was estimated by classifying them as circular clusters with diameters of 0.5, 1 or 2 m. This could be done by scaling the images with the help of two parallel laser pointers mounted on the sled at 20 cm (RV SONNE) or 50 cm (RV METEOR) distance. The total area covered by clams and bacterial mats was calculated by assuming that the ratio of observed clams/bacterial mats in the area covered by video observation is the same as the ratio of total clams/bacterial mat-covered area to the basal plane. As this first-order approximation is rather crude we allow all parameters to vary by 20% and calculated minimum and maximum values. Then, we used outflow rates for methane that are specific for bacterial-mat or vesicomyid-clam habitats in addition to the areas that are covered by these communities to estimate a methane budget for each of the studied mounds.

In a second approach, the methane output per mud extrusion was calculated using measured methane concentrations in the water column and bottom-near current velocities. For that purpose the method described in Heeschen et al. (subm.) was slightly modified. These authors calculated the methane inventory as the product of methane concentration and a volume of a box defined by two CTD-transects perpendicular to the main current flow. The height of the box is given by the height of the methane plume. As our data lack such a defined base, we designated the base to be the area which is covered by water column measurements, leaving out the hydrocasts that showed no methane anomalies close to the seafloor. At Mound 11 we calculated the output from an area roughly encircling the main vent fields as examined by seafloor observations because of the poor coverage by hydrocasts. Both base areas at Mound

Culebra and Mound 12 are about the same. Methane concentrations were averaged over layers of 10 m in height. The upper and lower boundary of each layer is located at the same distance from the seafloor, e.g. one layer reaches from 10 – 20 m above ground. Background values of 0.5 – 2 nmol L^{-1} were subtracted from these averaged values. These vent-derived methane concentrations were then multiplied by the volume of the layers and the sum of all layers yields the inventory of the entire box above the mound. The 'clearing time', the time it takes to remove all methane from the volume inside the box, was calculated by dividing the length of the box by the current velocity. The flow data obtained by ADCP-measurements were processed over a time frame of one day and at different depth levels. Finally, the methane output is determined as the quotient of inventory and 'clearing time'.

Results

Mound Culebra

Mound Culebra is located at the continental slope west of Nicoya Peninsula (Fig. 1). Seafloor surveys and water column work were carried out throughout the mound (Fig. 2 & 3). The mound is elongated in southwest-northeast direction, with diameters of 1 to 1.6 km, and rises about 140 m above the surrounding slope at 1650 m water depth. A northwest-southeast trending fault system divides the summit region into a smaller western summit and a larger eastern summit. The central depression is 20 – 30 m deep with outcropping sediment layers containing authigenic carbonates. In the summit region the carbonates are exposed at the seafloor, in some areas forming nearly continuous pavements or free standing edifices (Fig. 4 C). The seafloor observations revealed an abundant but patchy occurrence of vesicomyid clams (Fig. 4 A, B) at the eastern summit, the northwestern flank and, to a minor extent, at the eastern flank. Typically, the clams were observed in 1-m size clusters in soft sediments between the massive carbonates at the summit region or between smaller-sized carbonates at the flanks. The clam-covered area at Mound Culebra is estimated to be much larger than the clam or bacterial mat-covered areas of the other mounds (Tab. 1). Apart from the predominat vesicomyid clams, a few small *Lamellibrachia* colonies were observed.

The concentration of methane in the water column above Mound Culebra was measured along a profile in direction of the current flow and perpendicular to it (Fig. 2). The prevailing current in the lower 30 m of the water column above the top of the mound was towards the northwest, with average flow velocities of 2.4 ± 1.4 cm s^{-1}. The distribution of methane can be explained mainly as a result of fluid venting from distinct source areas at the mound into the

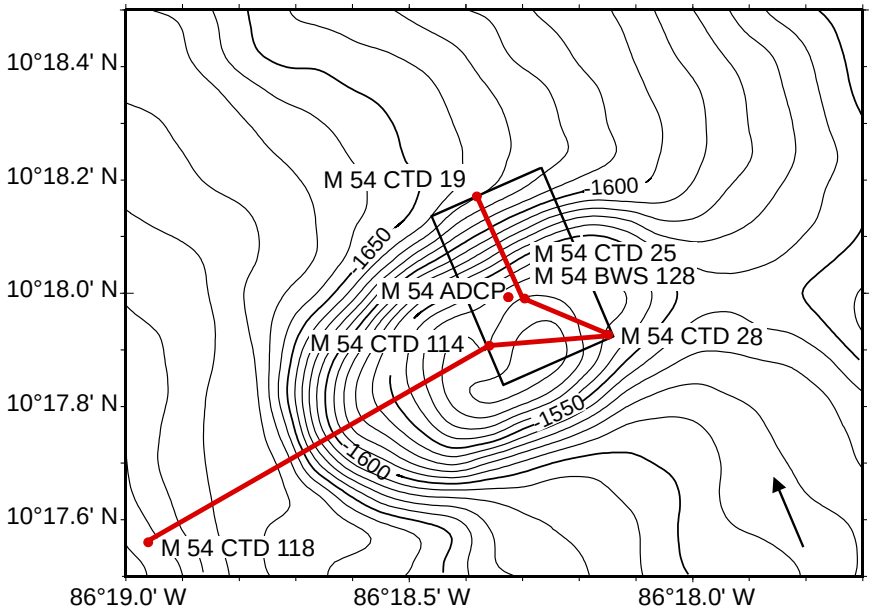

Fig. 2 Stations at Mound Culebra. Water for methane analysis was sampled by CTD and BWS along a profile in direction of current flow and perpendicular to it (thick line). Currents were recorded by ADCP: the main current direction is indicated by the arrow in the right, lower corner. The rectangle shows the base used for calculation of the methane output (see discussion).

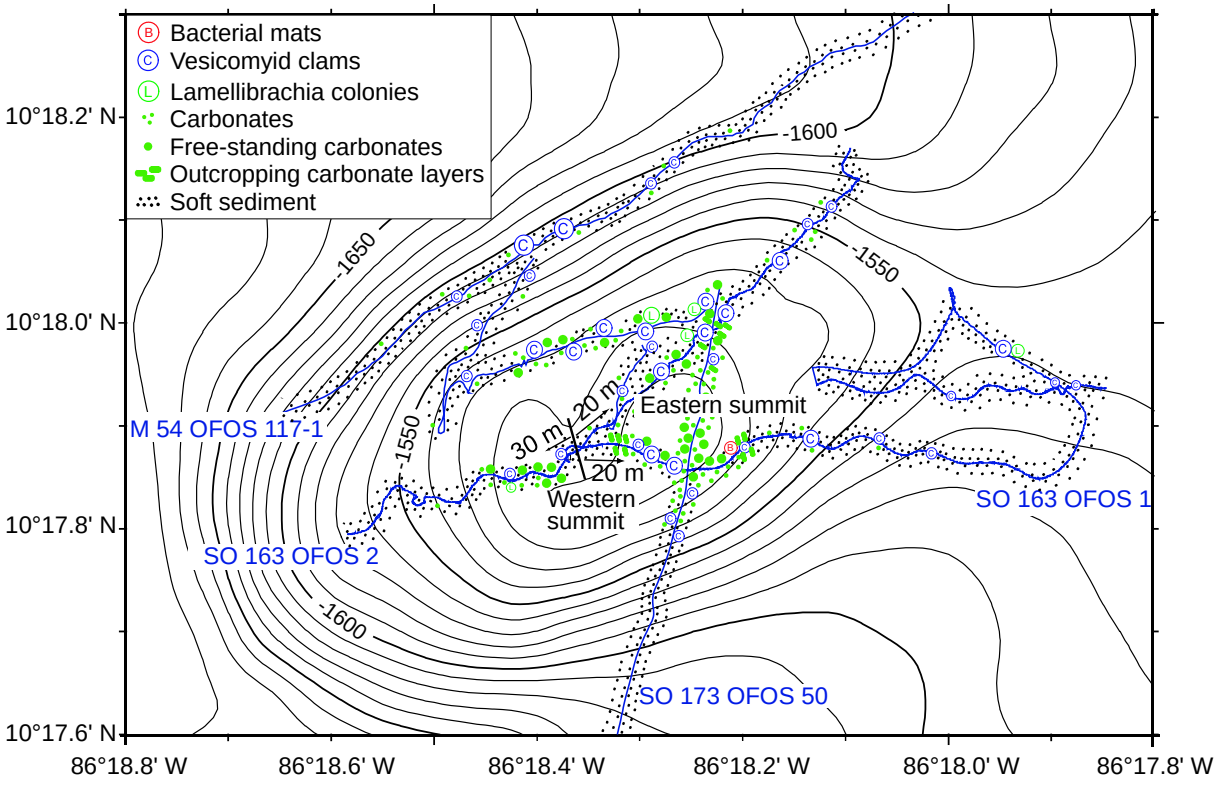

Fig. 3 Seafloor observations at Mound Culebra. Seafloor surveys were conducted with the camera sled OFOS and TV-guided multicorer (lines). Authigenic carbonate and vesicomyid clams are abundant but patchy distributed on the entire mound. Methane seepage is concentrated at the eastern summit and northwest of it as indicated by the densest occurrence of vesicomyid clam clusters.

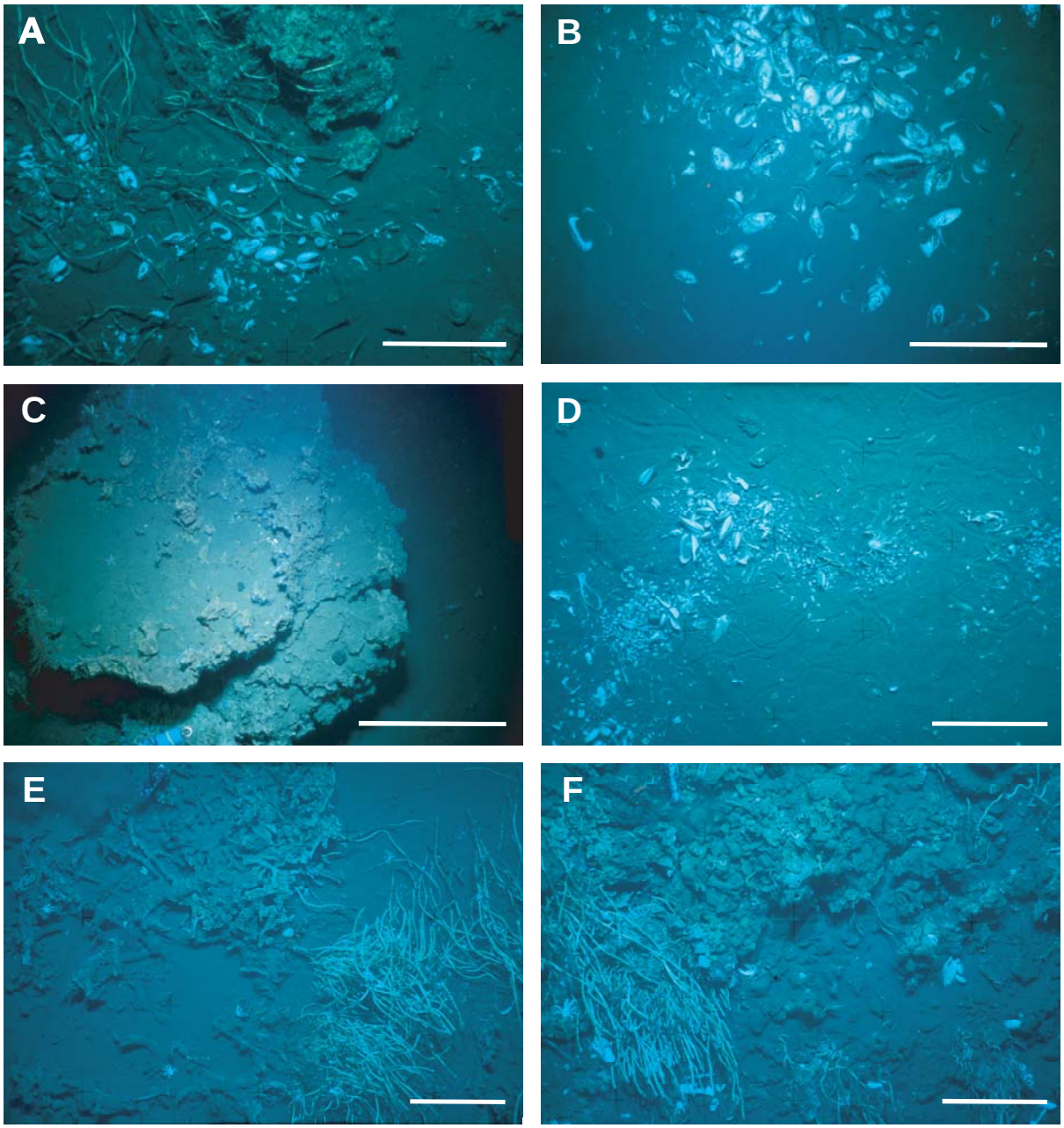

Fig. 4 Seafloor pictures taken by the video sled OFOS at Mound Culebra (A-C) and Mound 10 (D-F). (A) Authigenic carbonates, vesicomyid clam shells and *Lamellibrachia*-tubes at the eastern summit region (SO 163 OFOS 2, photo: 22:54:35). (B) Vesicomyid clam cluster consisting of living clams and shells (M 54 OFOS 117-1, photo: 3_5A). (C) Free-standing large carbonate on the northwestern flank (M 54 OFOS 117-1, photo: 2_7A). (D) Dense cluster of vesicomyid clams in soft sediment and tracks of crawling clams (SO 173 OFOS 80, photo: 08:50:40). (E) *Lamellibrachia*-colonies and tubular carbonates (SO 173 OFOS 80, photo: 08:41:03). (F) Exposed carbonates and Lamellibrachia-colonies (SO 173 OFOS 80, photo: 10:05:51). Scale bar 50 cm.

Tab. 1 First-order estimate of the total area occupied by chemosynthesis-based species and the resulting methane output. The calculation of output is based on flux rates for bacterial mat sites (Linke et al., subm.) and vesicomyid clams (see discussion).

Mound	**Dominant community**	**Area occupied by the dominant community in m^2**	**Calculation**	**CH_4-flux rates (including AOM)**	**CH_4-output**
		min - max		mol m^{-2} yr^{-1}	10^3 mol yr^{-1}
Mound Culebra	Vesicomyid clams	6 000 – 20 200	74 m^2 clamfields observed during 4 OFOS profiles, in area of 1 500 000 m^2 (SO 163 OFOS 1 and 2, M 54 OFOS 117-1, SO 173 OFOS 50)	2	12 – 40.4
Mound 10	Vesicomyid clams	600 – 2 100	19 m^2 clamfields observed during 5 OFOS profiles, in area of 230 000 m^2 (SO 173 OFOS 80)	2	1.2 – 4.2
Mound 12	Bacterial mats	1 500 – 5 000	60 m^2 bacterial mats observed during 3 OFOS profiles, in area of 100 000 m^2 (M 54 OFOS 161)	10.3	15.5 – 52.5
Mound 11	Bacterial mats	500 – 1 700	16 m^2 bacterial mats observed during 4 OFOS profiles, in area of 40 000 m^2 (SO 173 OFOS 107)	10.3	5.1 – 17.5

bottom water, where it is transported with the current and mixes. In general, all profiles show increased methane concentrations at a depth below ~1350 m compared to the background value of 0.5 – 2 nmol L^{-1} (Fig. 5). Sources of methane are located at the eastern summit region and on the northwestern flank of the mound. This is implied by the elevated methane concentrations towards the seafloor at the summit stations (M 54 CTD 25, 28) and the high concentrations around 1600 m depth northwest of the mound (M 54 CTD 19). The central depression between the western and eastern summit did not appear to be a major source for methane, the concentration in the water close to the seafloor is only slightly elevated (M 54 CTD 114).

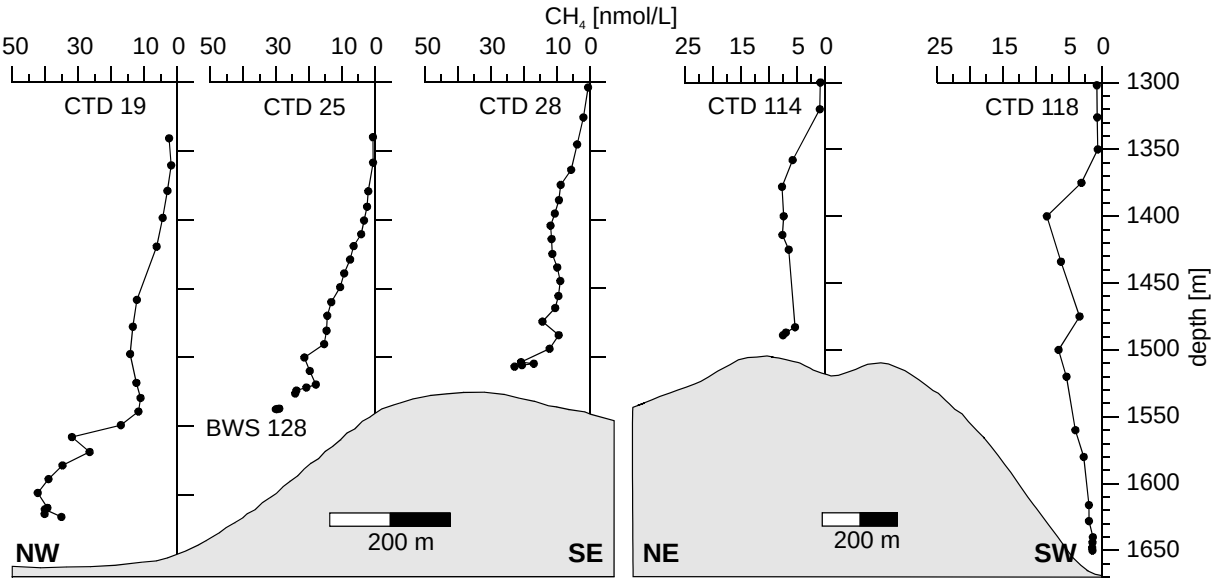

Fig. 5 CH_4 concentrations in the water column at Mound Culebra (for location of CTDs, see Fig. 2). Highest values were observed closest to the seafloor at the top of the mound (M 54 CTD 25, 28 and BWS 128) and at a depth of 1600 m on the northwest-flank of the mound (M 54 CTD 19). The methane concentrations are lower at the central depression (M 54 CTD 114) and no bottom near anomaly has been observed southwest of the mound (M 54 CTD 118).

The results of the seafloor observations and the water column work suggest that methane is seeping through the sediments in the area where vesicomyid clams are present. Vesicomyid clams were observed at depths between 1510 and 1570 m, but the highest abundance was found at distinct seafloor areas within two depth intervals. The injection of methane into the water column from the upper interval at 1510 m is clearly reflected in the increased methane concentrations at this depth in all CTD stations (Fig. 5). This injection causes elevated methane concentrations at stations close to the clam fields (M 54 CTD 25, 28, BWS 128) and lower values at stations farther away (M 54 CTD 114, 118), indicating rapid mixing of the

injected methane in the water column. At the northwestern flank of the mound the lower clam cluster aggregation falls below 1540 to 1570 m. Unfortunately, we can not give an exact lower depth limit as we did not search for seeps below that depth. However, the highest methane concentrations at depths around 1600 m (M 54 CTD 19) suggest that the clam areas at the northwestern flank are methane sources and might extend farther down-slope. In addition, CH_4 may accumulate in the sheltered zone behind the mound where reduced bottom water currents and turbulent mixing are expected.

Mound 10

Mound 10 is located southwest of Nicoya Peninsula at a water depth of 2400 m. It is an elongated structure with diameters between 0.7 and 1.8 km and an average height of about 80 m (Fig. 6). Seafloor observations revealed that authigenic carbonates and chemosynthetic communities occur in the summit area (Fig. 4 D-F). The area is bordered to the north by a

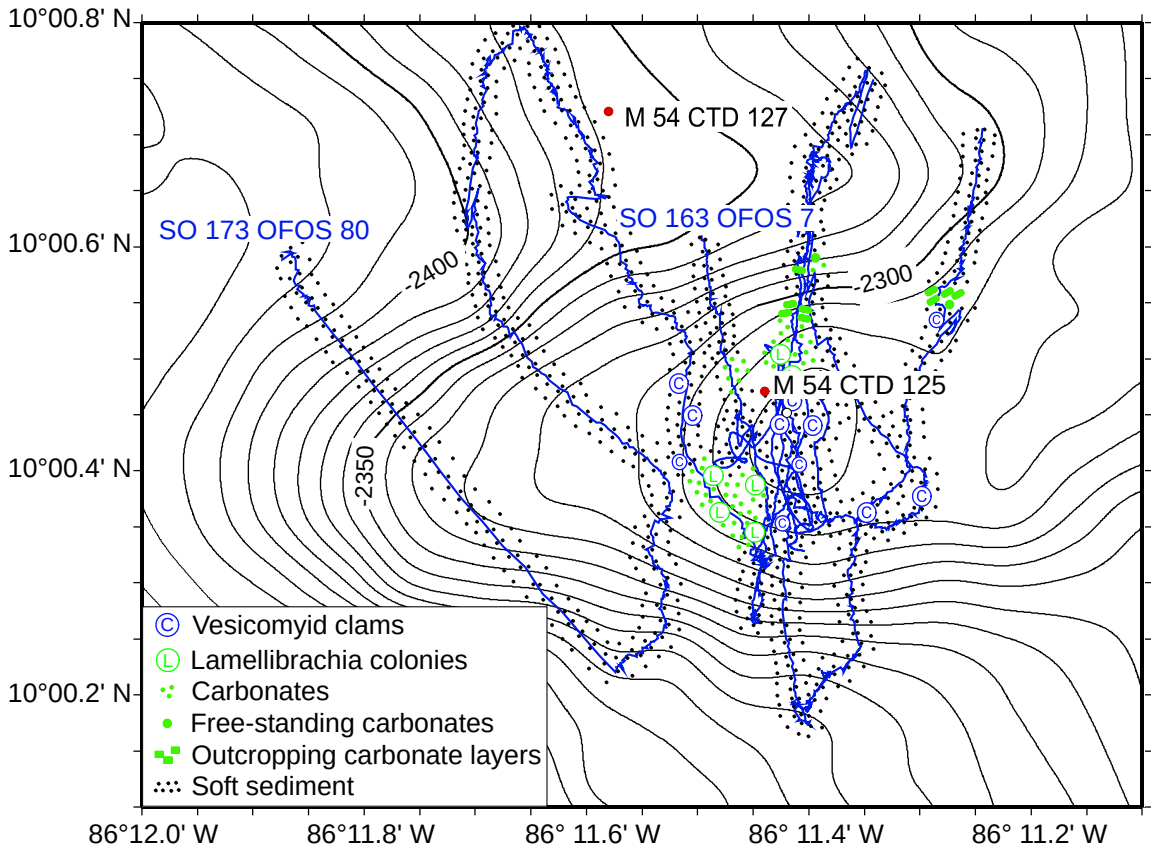

Fig. 6 Seafloor observations and CTD locations at Mound 10. Vesicomyid clams occur in the sediments at the summit. Tubular carbonates were found in association with *Lamellibrachia*-colonies (Fig. 4). Sediment layers and authigenic carbonates are exposed at a scarp north of the summit.

scarp where sediment layers and carbonates are exposed. Within the entire summit region clam clusters were found in soft sediments. Bushes of *Lamellibrachia*-colonies and associated tubular carbonates were observed (Fig. 4 E). These carbonates have probably been formed around the root system of the vestimentiferan tubeworms (Han et al., 2004). In general, less carbonates are exposed at Mound 10 compared to Mound Culebra. Furthermore, the area of active methane seepage as indicated by vesicomyid clams is smaller (Tab. 1).

Venting was confirmed by increased methane concentrations in water samples taken right above the summit area (M 54 CTD 125; Fig. 6). Methane is injected into the bottom water in dissolved form as indicated by the rapid decrease of its concentration with increasing distance from the seafloor (Fig. 7). Using the CTD/rosette equipment in the rough bathymetry, it was not possible to sample closer than 10 m to the seafloor. Thus, methane concentrations most likely rise to higher values than the maximum observed towards the seafloor. The methane plume spreads from Mound 10 to the northwest. Water samples at station M 54 CTD 127, about 500 m northwest of the summit, show a methane anomaly at the same depth range as in the hydrocast above the summit. Unfortunately, no current measurements were taken at this site, but similar densities of σ_Θ = 27.708 at M 54 CTD 125 and σ_Θ = 27.711 at M 54 CTD 127, which correspond to the maximum methane anomalies, support transport towards the northwest. This agrees well with the decrease in maximum methane concentration from the summit towards the northwest.

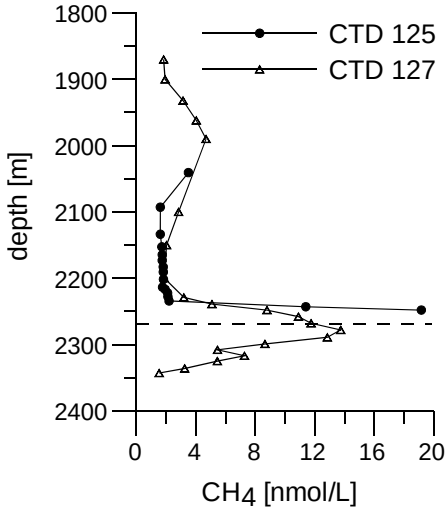

Fig. 7 CH_4 concentration versus depth at Mound 10 (for location, see Fig. 6). Methane is injected into the bottom water at the summit area of the mound (M 54 CTD 125). The dashed line marks the depth at the top of the mud extrusion. Methane is transported with the prevailing bottom currents to the northwest (Station M 54 CTD 127).

Mound 12

Mound 12 and Mound 11 are located farther to the southeast at the Costa Rican continental margin at water depths around 1000 m (Fig. 1). Mound 12 was extensively surveyed by OFOS, hydrocasts and BWS deployments (Fig. 8 & 9). The mound has a low morphological expression; it is only 30 m high and elongated in northeast-southwest direction with diameters

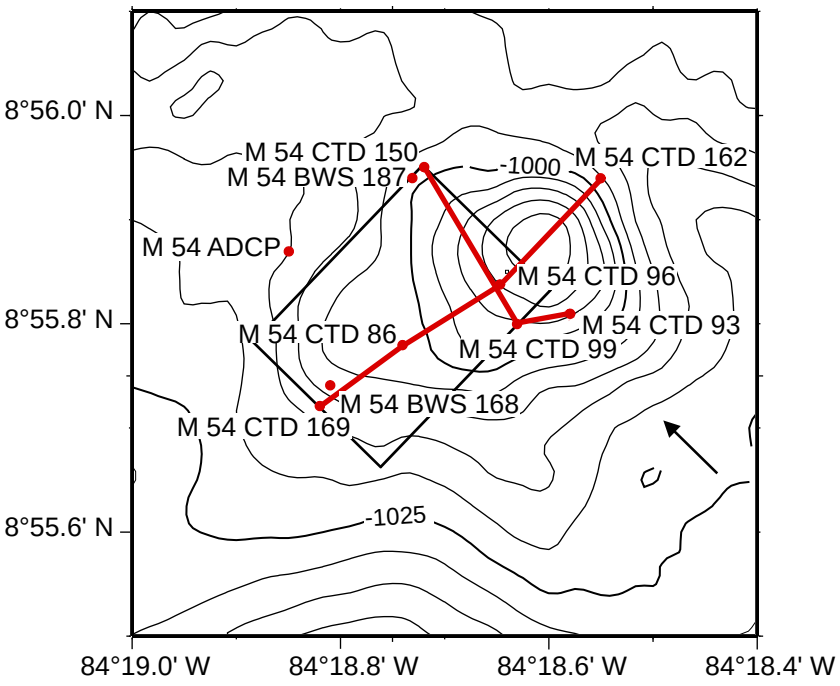

Fig. 8 Stations at Mound 12. Dots mark CTD and BWS water sampling positions and ADCP the location of current measurements. The main current direction is indicated by the arrow in the right, lower corner. The rectangle shows the base used for calculation of the methane output (see discussion).

of about 1 to 1.6 km. The seafloor observations revealed that authigenic carbonates and chemosynthetic communities occur along the central northeast-southwest trending axis (Fig. 9). In contrast to Mound Culebra and Mound 10, where mostly vesicomyid clams were encountered, bacterial mats and mytilid mussels were the dominant chemosynthetic communities at Mound 12 (Fig. 9 & 10 A, C).

The distribution pattern of authigenic carbonates and seep fauna reflect most likely different stages in the evolution of the mound. At the top massive fractured carbonates are exposed (Fig. 9 & 10 E) with individual blocks being several meters large. This area is possibly the oldest stage at which venting has ceased due to the sealing by carbonates. Towards the southwest, along the central axis the carbonates decrease in size and a mélange of carbonate pebbles, shells and sediments dominate the seafloor with occasional occurrence of bacterial mats. At a talus slope we observed scattered individuals of *Lamellibrachia*. The youngest stage of venting is probably represented farthest to the southwest: here bacterial mats occur in soft sediments, mostly as spotted mats in areas with exposed carbonate pebbles sometimes mixed with shell debris in soft sediments (Fig. 9 & 10 A). At the northern limit of this area mytilid bivalves live in fractures of massive carbonates (Fig. 10 C). Some of the massive carbonates and many mytilid shells were buried by a thin sediment cover indicating recent mud flows (Fig. 10 D). In summary, the seafloor observations revealed that the main active venting area is southwest of Mound 12 at water depths between 990 and 1015 m. Bacterial mats were much more common than mytilid mussels or *Lamellibrachia* colonies. Therefore, we estimated the active seepage area based on the occurrence of bacterial mats (Tab. 1).

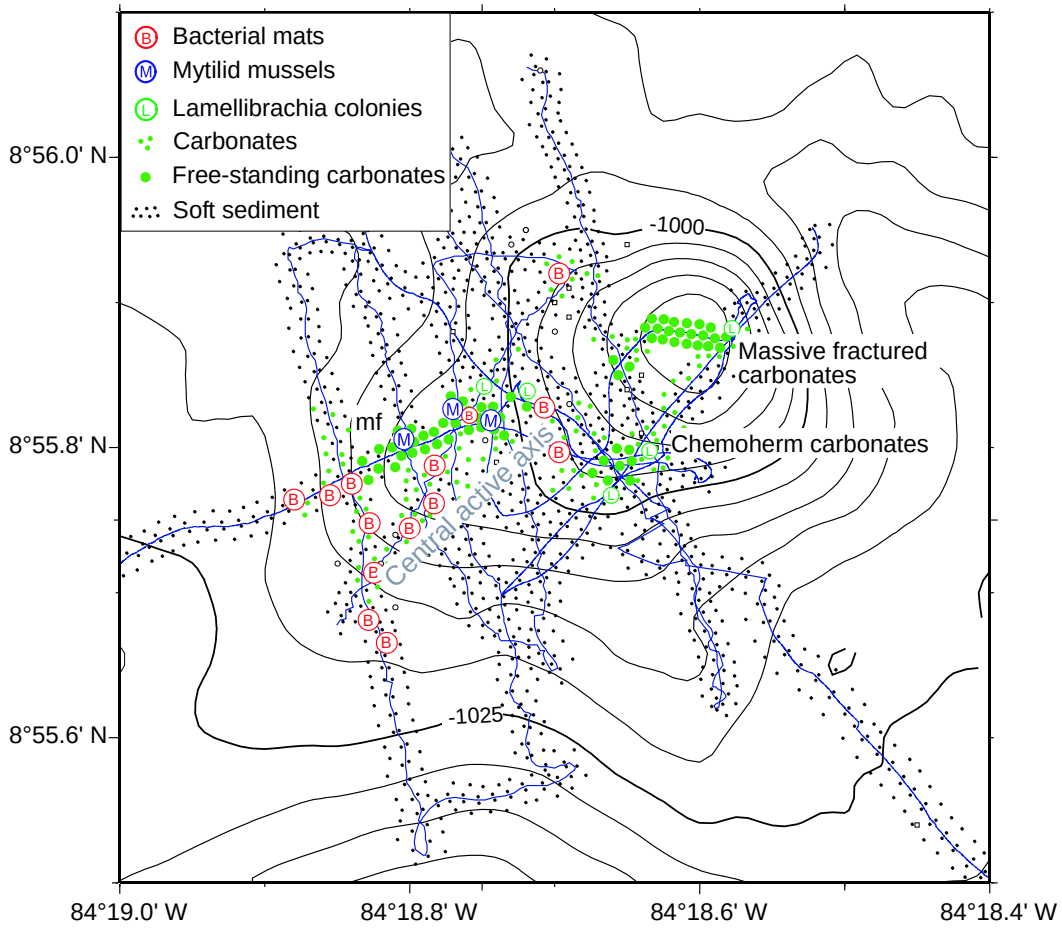

Fig. 9 Seafloor observations at Mound 12. OFOS-tracks are indicated by thin lines. The mound is elongated with a morphologically weakly developed northeast-southwest trending axis and an apparent zonal distribution of carbonates and chemosynthetic communities. Massive carbonates occur at the top area. A mélange of pebble-sized carbonates, shells and sediments is present along the axis. Bacterial mats are most abundant in the southwest. Mytilid mussels occur in fractures of massive carbonates. Chemosynthetic communities partly buried by sediments indicate recent mud flows (mf). Contour interval: 5 m.

The distribution in the water column above Mound 12 suggests that methane is mainly emitted from areas covered by bacterial mats. Increasing methane concentrations towards the seafloor were found in all CTD and BWS stations along the central axis southwest of the summit (Fig. 11). The shape of the profiles indicates only weak vertical transport of methane through the water column, e.g., at station M 54 BWS 168 the methane concentration decreases from 68.9 nmol L^{-1} 14 cm above seafloor to 17.4 nmol L^{-1} at 120 cm. This strong

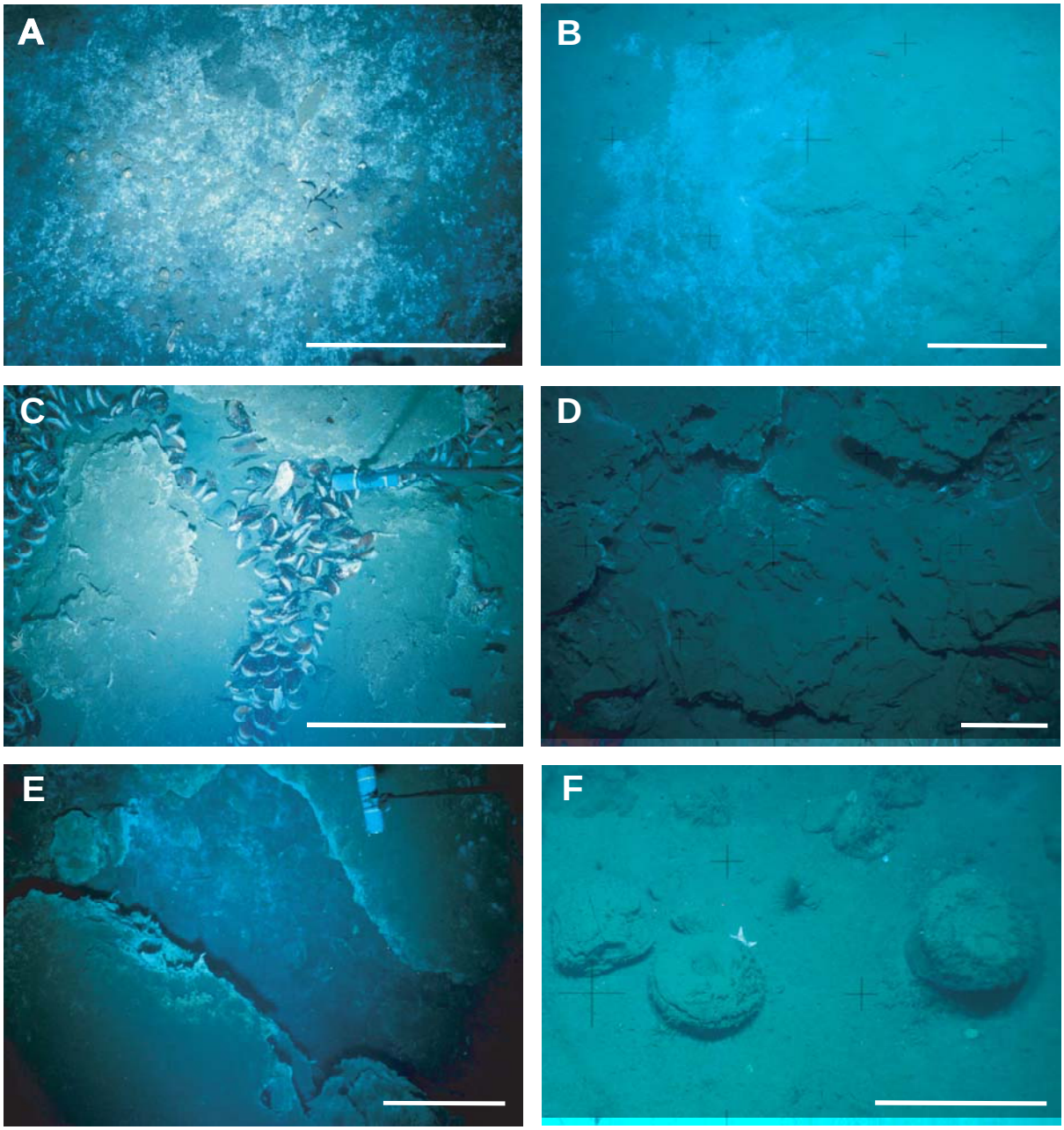

Fig. 10 Seafloor pictures taken by the video sled OFOS at Mound 12 (A, C, D, E) and Mound 11 (B, F). (A) Bacterial mats covering a melange of sediments, carbonates and shells. Note the sediment-covered decapod (M 54 OFOS 161, photo: 6_29). (B) Bacterial mats on soft sediments (SO 173 OFOS 107, photo: 07:02:37). (C) Mytilid bivalves in cracks between carbonates (M 54 OFOS 161, photo: 5_14). (D) Carbonates and mytilid bivalves buried below a thin cover of sediment. (SO 163 OFOS 21, photo: 18:23:55). (E) Fragmented massive carbonates at the summit of Mound 12 (M 54 OFOS 161, photo: 9_16). (F) Exposed doughnut-shaped carbonates at Mound 11 (SO 173 OFOS 107, photo: 04:39:23). Scale bar 50 cm.

decrease may be caused either by horizontal transport, effective oxidation in the bottom layer, or both.

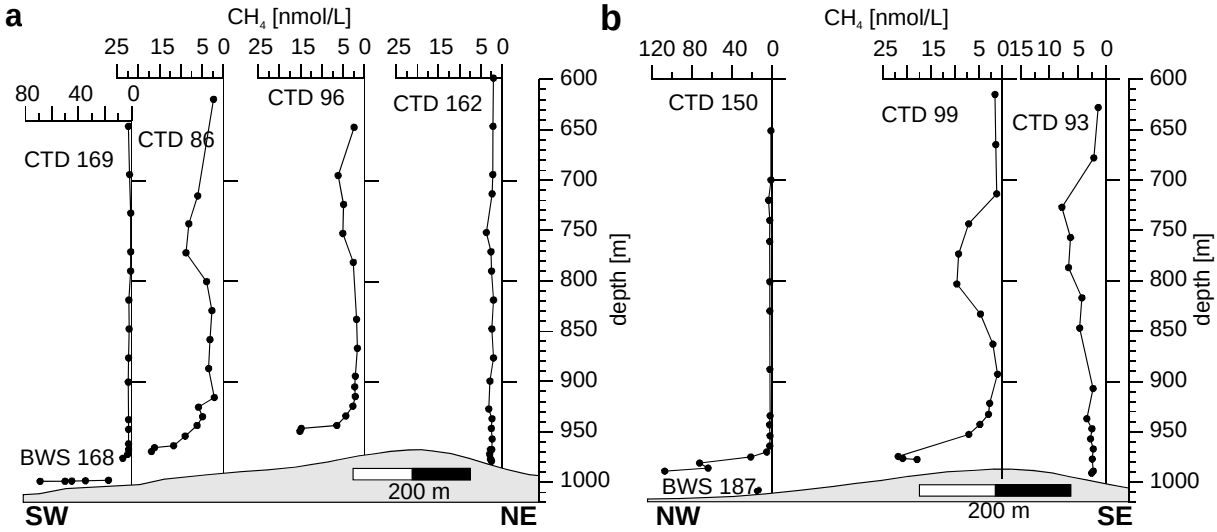

Fig. 11: CH_4 concentrations in the water column above Mound 12 (for location see Fig. 8). Note different scales of individual diagrams. (a) profile from southwest to northeast and (b) profile from northwest to southeast. Methane venting occurs in the region southwest to northwest of the mound corresponding to areas covered by bacterial mats (see Fig. 9). The highest value of 107 nmol L^{-1} was measured at station M 54 CTD 150, most likely originating from a vent site close-by. CH_4 is carried to the northwest with the bottom water current.

Ocean currents strongly affect the methane distribution. The highest methane concentration of all investigated mud extrusions, with a value of 107.3 nmol L^{-1}, was measured at 995 m depth at station M 54 CTD 150 northwest of the mound. It most likely originates from the small vent site nearby (see isolated bacterial mat, Fig. 9). The methane was carried to the northwest with the bottom water flowing with 3.2 ± 2 cm s^{-1} 1 – 10 m above seafloor, according to our ADCP data. This interpretation is supported by the low methane concentrations in the bottom water (M 54 BWS 187) sampled at this location. The injection of methane into the bottom water at the central axis of the mound with subsequent transport to the northwest is further verified by two hydrocasts in the northeast (M 54 CTD 162) and southeast (M 54 CTD 93) that did not show any elevated methane concentrations.

Mound 11

Mound 11 is located southeast of Mound 12 and also has a weak morphological expression. It is about 20 m high with complex small-scale seafloor structures. It consists of two separated elevations at which bacterial mats were found (Fig. 12). At present, only two small *Lamellibrachia* colonies and one cluster of vesicomyid clams were observed at the mound, however, the remains of a diverse chemosynthetic community were found in the sediments. Remarkably, the presence of all sizes of vesicomyid clams indicates that the entire community was killed during a single event. The distribution of carbonates is also chaotic. Mostly, carbonate talus of pebble to boulder-size were exposed at the summits or on the flanks. Hydrate-related as well as dolomitic carbonates were sampled and analyzed (Han et al., 2004). We observed evidence for mud flows in two areas (Fig. 12). Living vesicomyid clams and a *Lamellibrachia* colony were almost completely buried by a layer of very uniform sediments similar to the observation at Mound 12 (Fig. 10 D). Mud flows were also found in sediment cores at this mound (Moerz et al., in press). In order to estimate the active seepage

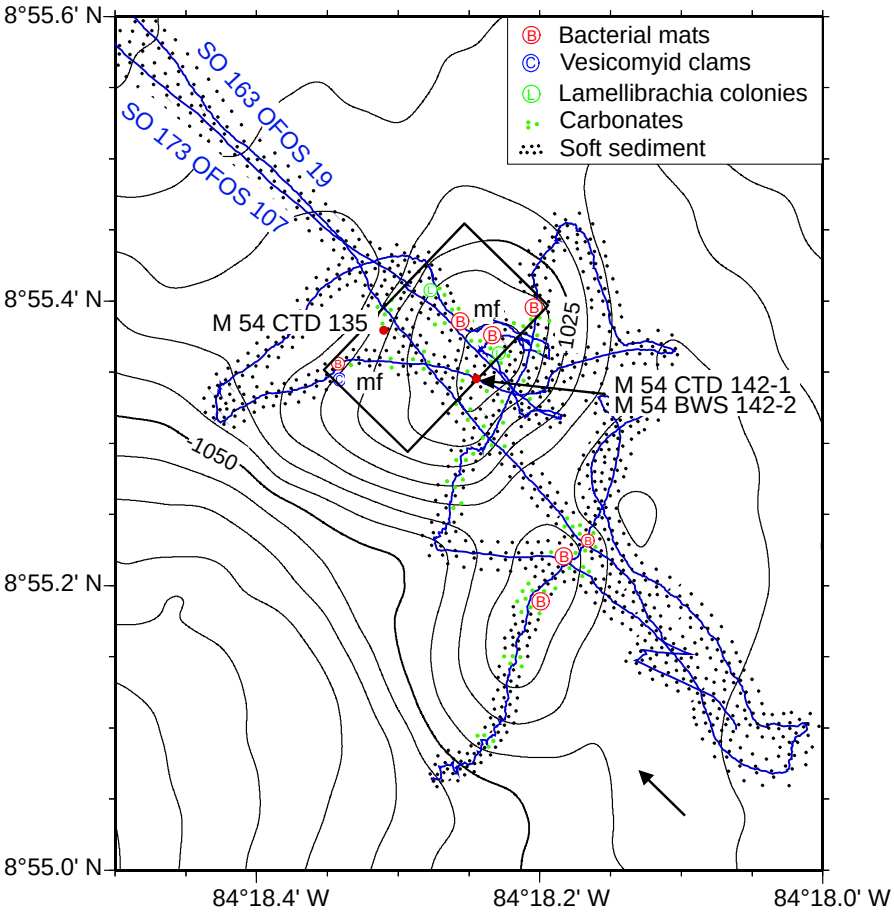

Fig. 12 Seafloor observations and stations at Mound 11. The mound has a complex surface morphology consisting of two elevations where bacterial mats occur. Buried chemosynthetic communities gave evidence of mud flows (mf). The rectangle indicates the area of main venting at the northern summit used for calculating the CH_4 output. The main current direction is indicated by the arrow in the right, lower corner (Contour interval: 5 m).

area we calculated the bacterial mat-covered area which is smaller than the area on Mound 12 (Tab. 1).

The methane concentration was measured above the northern elevation of Mound 11 (Fig. 13). Continuous increasing concentrations towards the seafloor indicate that methane is released in dissolved form like at the other mounds. However, the methane concentrations at Mound 11 are distinctly lower. Bottom waters at 14 cm above ground had values of 16.9 nmol L^{-1} (M 54 BWS 142-1) decreasing to 8.7 nmol L^{-1} at 120 cm and hydrocast profiles display even lower values of 4.2 nmol L^{-1} (M 54 CTD 135) and 5.3 nmol L^{-1} (M 54 CTD 142-2) at 16 m and 23 m above seafloor, respectively (Fig. 13).

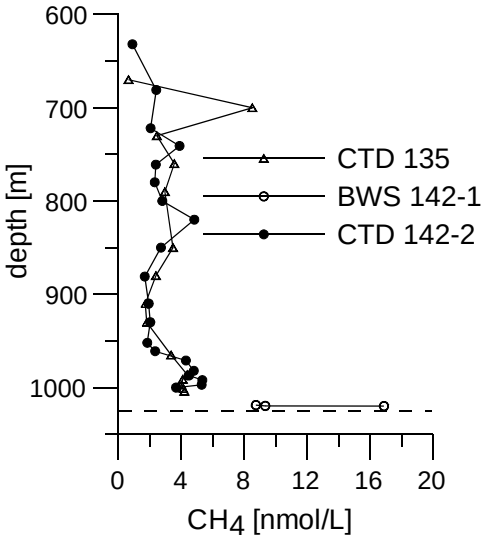

Fig. 13 CH_4 concentrations in the water column above Mound 11. The dashed line marks the depth at the top of the mud extrusion. Water samples contained less methane than samples of the other mounds.

Discussion

Evolution of the mounds

All four mud extrusions occur at mid slope depths on the continental margin. They are connected to deep-reaching fault systems (Moerz et al., in press). All mounds show evidence for venting of methane-rich fluids such as chemosynthetic communities, authigenic carbonates and methane anomalies in the water column.

The mud extrusions differ in their morphology. Mound Culebra and Mound 10 are cone shaped, about 100 m high and with steep flanks, while Mound 11 and 12 are flat with maximum elevations of 30 m and very gentle slopes. Moerz et al. (in press) proposed conceptual models of the formation of these mounds. The concepts assume that the major mound growth occurs during eruptive phases. Mound Culebra is suggested to originate from a diapiric rise of sediments leading to the occurrence of mud breccia and deformed clays in sediments at the surface. In a post eruptive stage, hydrofracturing by fluids and low viscous mud causes formation of conduits and subsequent growth of fauna and authigenic carbonates.

Mound 12 and Mound 11 are considered to be mud volcanoes. A flow sequence in a sediment core of Mound 12 is proposed as evidence for a violent, gas-driven destruction of the summit. During this phase, brecciation and chaotic relocation of shells and carbonate pieces occurred which were subsequently covered by mud flows. Even though Mound 11 and Mound 12 are in a rather quite phase at present, we found areas where mud covers chemosynthetic communities and carbonates (Fig. 10 D). This may indicate a rather recent outflow of low viscous mud or deposition of a suspension cloud generated during a mud flow (co-mud flow deposits).

Chemosynthetic communities

Differences in the geochemical environment at the mounds cause differences in the composition of the chemosynthetic communities as well as in the types of authigenic carbonates. High methane supply causes anaerobic oxidation of methane (AOM) close to the sediment-seawater interface. Low methane supply leads to AOM deeper in the sediments (Luff and Wallmann, 2003; Han et al., 2004). Thus, the methane supply mainly influences the depth of this zone. We did not find any evidence for the emission of methane as free gas and the methane distribution in the lower water column strongly suggests that methane is mainly transported dissolved in vent fluids. Methane supply is therefore directly coupled to fluid advection rates and methane concentration in the fluid.

The chemosynthesis-based species depend, in general, on hydrogen sulfide rather than methane (Fisher, 1990). Thus, the species indicate at what sediment depth hydrogen sulfide is produced in the course of AOM. Bacterial mats live at or close to the surface of soft sediments and mytilid bivalves were predominantly observed in fractures of carbonates. Both organisms indicate AOM close to the sediment-seawater interface and thus, indicate high fluid flow rates. In contrast, vesicomyid clams live in soft sediments and have access to sulfide that is produced deeper in the sediment at depths of several centimeter and decimeter, indicating lower flow rates. This simple concept of variation in flow rates causing vertical shifts in the zone of anaerobic methane oxidation is also supported by carbonate formation: high fluid flow rates pushes AOM out of the sediment into, e.g., fractures of previously existing carbonates that are subsequently lined by aragonitic cements (Han et al., 2004). Low fluid flow causes the precipitation of carbonates in the sediments. Based on this concept we infer that the fluid flow rate at Mound 12 is high, indicated by the prevalence of bacterial mats,

mytilid mussels and aragonite linings. Fluid flow rates at Mound 11 are also high, indicated by the occurrence of bacterial mats, and supported by reported fluid advection rates of 300 cm yr^{-1} derived from modeling of pore water data (Hensen et al., 2004). In contrast, the fluid flow at Mound Culebra and Mound 10 appears to be lower, as indicated by vesicomyid clams, a lack of bacterial mats and carbonates that formed by cementation of sediments (Han et al., 2004).

We briefly discuss the evidences for the concept proposed above that greatly depends on the fact that the observed fauna relies on hydrogen sulfide rather than on methane. The recovered bacterial filaments resembled morphologically *Beggiatoa*, a sulfur-oxidizing organism (Nelson and Jannasch, 1983). Mytilid bivalves have been described with both, thiotrophic as well as methanotrophic endosymbionts. The mytilids off Costa Rica probably belong to a new species, genetic studies on the host and endosymbionts are in process (S. Hourdez, pers. comm.). The $\delta^{13}C$ values obtained for two specimens recovered from Mound 12 fall in the range between -30 – -40 ‰ PDB (U. Struck, pers. comm.) which are typical for specimens that live in symbiosis with sulfur-oxidizing bacteria (Fisher, 1990). Furthermore, the $\delta^{13}C$ values of the seeping methane from that site are below -70 ‰ PDB (Rehder et al, in prep.). A significant contribution of this methane would result in more negative $\delta^{13}C$ values of the mytilid tissue than -30 – -40 ‰ PDB. Thus, we suppose that the mytilids live in symbiosis with thiotrophic endosymbionts. Various different species of vesicomyid clams were discovered off Costa Rica, some of which are new (E. Krylova, pers. comm.). The recovered tubeworms are genetically identical to *Lamellibrachia barhami* (McMullin et al., 2003). The endosymbionts of all vestimentiferan tubeworms and vesicomyid clams are described as thiotrophic (Fisher, 1990). Thus, evidences exist that all chemosynthesis-based specimens rely on hydrogen sulfide rather than on methane.

Methane seeps and methane anomalies in the water column

Methane is currently escaping through all four mounds, as clearly shown by elevated methane concentrations in the water column of up to two orders of magnitude above the regional background of 0.5 – 2 nmol L^{-1}. It is dissolved in the fluids, as evidenced by the continuous increase or decrease of CH_4 concentration with depth without any sudden peaks (Fig. 5, 7, 11, 13). Moreover, we did not observe any signs of bubbles using acoustic methods or video-guided instruments. Methane escapes from regions with chemosynthetic communities. This is

supported by the generally good agreement between the location and depth of the methane plumes and the occurrence of chemosynthetic communities at the mounds.

In general, methane concentrations at ~20 m above the seafloor are similar for all mounds except Mound 11. Here, the lower methane values can be explained by the fact that the CTD and BWS stations were not deployed exactly at the very small area of seepage. However, it can also be related to the relatively small area of venting compared to the other mounds, effective methane degradation and/or accumulation processes within the near-surface sediment. The latter assumption is based on findings of shallow gas hydrate deposits at Mound 11 described by Schmidt et al. (subm.).

When methane is emitted from the sediment into the ocean, it is subject to transport and dilution by ocean currents and aerobic oxidation. Near-bottom currents strongly influence the distribution of methane in the water column. The plumes mapped at Mound Culebra (Fig. 5) and Mound 12 (Fig. 11) indicate a northwestward flow. Highest methane concentrations were observed on the northwest-flanks of these mounds, pointing to an enrichment in the lee side of the mounds. Nevertheless, part of the enrichment probably originates from vent sites nearby. At Mound Culebra, vesicomyid clam fields were observed on the northwest-side of the mud diapir (Fig. 3) and at Mound 12 a small field covered by bacterial mats seems to contribute to the methane anomaly found slightly offset to the site (Fig. 9). The northwestward flow derived from the shape of the methane plume is in agreement with the major current direction directly measured above the mounds by ADCP. The velocities range from 2.4 ± 1.4 cm s^{-1} at Mound Culebra and from 3.2 ± 2 cm s^{-1} at Mound 11 and Mound 12. Therefore, vent methane will be carried over the mound area in direction of the current flow within hours to days.

The time frame of dilution by ocean currents is much shorter than that of methane oxidation. Valentine et al. (2001) studied methane oxidation rates and turnover times by incubation of tritium-labeled methane (^3H-CH_4) in water samples from an area of active seepage in the Eel River Basin, off the coast of northern California. Their results demonstrate that methane is oxidized more rapidly in areas of high methane concentration (20 – 300 nmol L^{-1}) than in waters of low methane concentration (3 – 10 nmol L^{-1}). Because of comparable CH_4 concentrations over the mounds we assume similar oxidation rates and turnover times. The data of Valentine et al. (2001), reported from a gas hydrate bearing, cold vent setting, suggest a turnover time of a few years for a concentration of ~20 nmol L^{-1}. In contrast, de Angelis et

al. (1993) reported turnover times in the range of weeks to one month for such concentrations in deep-sea hydrothermal plumes of the Juan de Fuca Ridge. They also measured oxidation rates by incubation, but used $^{14}CH_4$ instead of $^{3}H\text{-}CH_4$. However, fast mixing with background waters decreases CH_4 concentration and increases turnover time. This suggests that dilution rules over methane oxidation as shown by Damm and Budeus (2003), who examined carbon isotopic signatures in the plume water above the Håkon Mosby mud volcano (Norwegian Sea). They observed that the $\delta^{13}C$-depleted methane in the water column is consistent with mixing of ambient sea water and water containing vent methane.

Methane budgets

Calculation based on seafloor observation

The dominant chemosynthesis-based species are vesicomyid clams at Mound Culebra and Mound 10 and bacterial mats at Mound 11 and 12. The bacterial mat or clam-covered areas vary by one order of magnitude between Mound Culebra and Mound 10, and about a factor of two between Mound 12 and Mound 11 (Tab. 1). We carried out the following calculations based on the range of areas. The area estimates are conservative because we did not consider regions that were covered by *Lamellibrachia*-colonies or mytilid bivalves. Furthermore, we do not consider active seepage that is transient, too slow, or too fast to sustain chemosynthetic communities in this estimate.

The geochemical environment at bacterial-mat sites at Mound 12 was constrained by modeling in situ benthic chamber and porewater data (Linke et al., subm.). The methane flux is about 10.3 mol m^{-2} yr^{-1}, of which 5.9 mol m^{-2} yr^{-1} is oxidized in the sediments and 4.4 mol m^{-2} yr^{-1} are escaping into the overlaying bottom water. These values are at the lower end of a range of values reported from bacterial mats at various other sites. For example, the anaerobic oxidation of methane below bacterial mat sites at Hydrate Ridge was determined by radiotracer technique and porewater modeling to be between 1.8 and 51.1 mol m^{-2} yr^{-1} (Boetius et al., 2000; Knittel et al., 2003; Luff and Wallmann, 2003; Treude et al., 2003). Seepage of methane into the overlying bottom water was measured with a benthic barrel at Hydrate Ridge with values of 10.9 to 32.8 mol m^{-2} yr^{-1} (Torres et al., 2002). Thus, the values reported for Mound 12 used for our estimate lie at the lower end of the range of methane flux rates reported for areas covered by bacterial mats elsewhere.

The flux estimates for vesicomyid clams are less well defined; preliminary porewater data draw an inconclusive picture of methane oxidation rates in the vesicomyid habitat with values ranging from 0.05 to 3 mol m^{-2} yr^{-1} (Hensen, pers. comm.). Radiotracer techniques and porewater modeling yield methane oxidation rates (= sulfate reduction rates) in the range of 14.6 to 20.4 mol m^{-2} yr^{-1} at Hydrate Ridge (Knittel et al., 2003; Treude et al., 2003) and 19 mol m^{-2} yr^{-1} at the Aleutian trench (Wallmann et al., 1997). Almost all of the methane is oxidized in the sediments; only zero to < 0.2 mol m^{-2} yr^{-1} escaped into the bottom water, as determined by benthic barrel experiments at Hydrate Ridge (Torres et al., 2002). In general, less methane appears to be available at the vesicomyid clam habitat compared to bacterial mat sites. Therefore we assume, somewhat arbitrary, that only 20% of methane present at sites covered by bacterial-mats is available at vesicomyid clam sites. This amounts to 2 mol m^{-2} yr^{-1} largely as methane oxidized with an insignificant amount seeping into the bottom water. The derived methane output for the different mounds are summarized in Table 1.

Calculation based on methane measurements in the water column

In this approach, the methane output from the mud extrusions into the water column is assessed by dividing the inventory of excess methane above the mounds by the clearance time that defines the time needed to remove all excess CH_4 (Heeschen et al., subm.). Due to the sparseness of water column data and a complete lack of current measurements, we could not address Mound 10 by this method. For the other three mud extrusion sites, this approach results in output estimates in the order of 10^4 to 10^5 mol yr^{-1} for each mound (Tab. 2). 10 – 20% of the uncertainty results from variations of the local background methane concentration (from 0.5 to 2 nmol L^{-1}). More than 50% of the uncertainty is caused solely by the variation of current velocities. Unfortunately, the depth levels covered by the ADCP do not cover the full plume height, and we assumed that the velocities stay about the same above the recorded depths range. However, the average of the velocities and thus the average of the CH_4 discharge represent the most reasonable estimates. Long-term variations could not be assessed within this study, because the calculation is based on methane measurements collected over a month.

Similar methane discharge rates were calculated at Mound Culebra and Mound 12 whereas the output from Mound 11 is considerably lower. Measured current velocities at Mound 12 and Mound 11 are slightly higher than at Mound Culebra, but the range of velocities is greater

than the differences between the mounds. The results display the different spatial extent and activity of the three mounds. The area of Mound Culebra is almost twice as large as the one of Mound 12, but the CH_4-output is only one and a half times as large as the one of Mound 12 suggesting a lower venting activity over a larger area at Mound Culebra and more concentrated and enhanced outflow of methane at Mound 12. The low methane output of Mound 11 is due to an even smaller area in connection with low methane concentrations measured above this mound.

Tab. 2 Methane inventories, outputs, and flux rates (only methane seepage) derived from methane concentrations in the water column and current measurements.

Area	**Area** km^2	**Plume height** m	**Inventory** mol	**Current velocity** $cm\ s^{-1}$	**Clearance time** d	**CH_4-output** $10^3\ mol\ yr^{-1}$	**CH_4-flux rates** $mol\ m^{-2}\ yr^{-1}$
area covered by water column measurements							
Mound Culebra	0.22	260	410 – 486	2.4 ± 1.4	0.17 – 0.66	625 ± 398	1.0 – 4.7
Mound 12	0.12	80	102 – 117	3.2 ± 2.0	0.06 – 0.27	406 ± 270	1.1 – 5.6
area covered by vent indicative fauna							
Mound 11	0.04	80	6.9 – 11.3	3.2 ± 2.0	0.03 – 0.14	70 ± 53	0.4 – 3.1

Comparison of methane outputs

A minimum and maximum methane output is presented by the different methods of calculation. It is worthwhile to note that both approaches yield estimates of different quantities. The approach based on seafloor observation includes the area covered by the dominant chemosynthesis-based species (Tab. 1) whereas the approach based on measurements in the water column includes diffusive, focused as well as methane seepage too slow, too vigorous, or too transient for faunal growth to be established (Tab. 2). The role of the dominant vent fauna in methane seepage can be determined by comparing the flux rates listed in Table 1 and 2. However, the flow estimate based on water column sampling only considers the CH_4 output into the bottom water, neglecting the fraction consumed by AOM or by aerobic oxidation at the sediment-water interface. For a site covered with bacterial mats at Mound 12, the data by Linke et al. (subm.) suggest that roughly 60% of the methane is oxidized, while about 40% (4.4 mol $m^{-2}\ yr^{-1}$) reach the water column. As discussed earlier, at

clam sites only a minor fraction of methane is seeping into the water column. Nonetheless, the comparison of the distribution of chemosynthesis-based species and the methane plumes in the water column indicate that methane is generally seeping through these areas. This suggests, that the additional outflow, e.g. at areas covered by *Lamellibrachia*-colonies or diffuse seepage, is located in the near vicinity of the clam sites and/or that methane enters the water column through localized channels within or near to faunal covered areas. Such channels were found in sediments obtained by gravity corer (Moerz et al., in press). However, while the two approaches differ in quantity, both calculations show the same trend: a similar output at Mound Culebra and Mound 12 as the result of the difference in area (see discussion above) and a lower output at Mound 11 (Tab. 1 & 2).

Our estimates of methane outputs are lower than reported estimates from other mud extrusions (Tab. 3). Two examples from the Barbados accretionary wedge are described as diatremes by Henry et al. (1996). A higher CH_4 output from diatremes than from mud diapirs/volcanoes is very likely in view of a higher fluid content of the material of a diatreme in contrast to mud volcanoes or even mud diapirs (Brown, 1990; Kopf, 2002). Lance et al. (1998) demonstrated a higher fraction of fresh water from hydrate dissociation at these diatremes than at mud volcanoes. Methane seeps mainly through the central active area of a diatreme where warm mud is circulating and chemosynthesis-based species are absent (Henry et al., 1996). Håkon Mosby Mud Volcano off Norway is structured concentrally; a central zone, devoid of fauna and too warm for gas hydrate to form, is surrounded by gas hydrate rich mud covered by bacterial mats (Milkov et al. 2004). The structural and surficial differences of the flat structures with active central zones in contrast to the mound-shaped mud extrusions off Costa Rica could account for the differing CH_4-outputs.

The discrepancy between our estimates and the reported values might also be caused by the different approaches of calculating the annual release of methane. Henry et al. (1996) assumed that a certain part of the fluids escaping from the diatremes at the Barbados margin comes from hydrate destabilization and calculated the resulting methane output. Ginsburg et al. (1999) suggest that the methane concentration in the fluid emitted at the Håkon Mosby mud volcano is close to its solubility and computed the methane output from the total amount of discharged water. Furthermore, Kopf and Behrmann (2000) estimated the annual output of methane at Milano and Napoli mud volcanoes at the Mediterranean Ridge based on their geometry and published methane concentrations of other mounds. These authors calculated

the total CH_4 output including the methane which becomes anaerobically oxidized in the sediment and the part emitted into the ocean. Thus, the data are not directly comparable with our estimates derived from methane measurements, which show only the fraction of methane actually reaching the hydrosphere. Taking into account that about 60% (Linke et al., subm.) to 80% (Drews et al., subm.) of the CH_4 output becomes oxidized in the sediments the discrepancy between the reported annual releases and our estimates is still one to two orders of magnitude. Therefore, the mud extrusions off Costa Rica appear to be less productive in terms of methane emission than the mud volcanoes and diatremes at accretionary margins and at passive margins.

Tab. 3 Comparison of CH_4 output from mud extrusions (s.o. - output derived from seafloor observations, w.m. – output calculated using water column measurements).

Area	**CH_4-output** in mol yr^{-1}	**Reference**
Mound Culebra off Costa Rica	$3 \cdot 10^4$ s.o. – $6 \cdot 10^5$ w.m.	this study
Mound 10 off Costa Rica	$3 \cdot 10^3$ s.o.	this study
Mound 12 off Costa Rica	$3 \cdot 10^4$ s.o. – $4 \cdot 10^5$ w.m.	this study
Mound 11 off Costa Rica	$1 \cdot 10^4$ s.o. – $7 \cdot 10^4$ w.m.	this study
Atalante, Barbados	$2 \cdot 10^8$	Henry et al., 1996
Cyclops, Barbados	$1 \cdot 10^7$	Henry et al., 1996
Håkon Mosby, Norwegian Sea	$7 \cdot 10^6$	Ginsburg et al., 1999
Milano, Mediterranean Sea	$6 – 28 \cdot 10^6$	Kopf & Behrmann 2000
Napoli, Mediterranean Sea	$12 – 45 \cdot 10^6$	Kopf & Behrmann 2000

Conclusions

Four mud extrusions, which all show signs of active fluid seepage, were investigated offshore Costa Rica. Two of them are diapiric structures and the other two are classified as mud volcanoes. Methane emitted from the mud extrusions is rapidly diluted rather than aerobically oxidized. Estimates of the amount of CH_4 discharging per mud extrusion range from 10^3 to 10^4 mol yr^{-1} as estimated from areas covered by vent indicative fauna and from 10^4 to 10^5 mol yr^{-1} derived from methane measurements in the water column. Our estimates indicate a lower methane discharge in comparison to mud extrusions at accretionary and passive margins,

partly resulting from the effect of anaerobic oxidation of methane, but most likely resulting from structural differences. The erosional nature of the subduction zone which limits the accumulation of thick sedimentary sequences, usually the source of organic carbon for methane formation, could be the reason for the different style and activity of the mud extrusions.

The methane plumes are assumed to be locally bound to the extrusions; thus, the CH_4 emitted contributes to the carbon budget in the ocean rather than reaching the atmosphere. Similar results from cold vent sites were reported from the Aleutian subduction zone (Suess et al., 1998), the Hydrate Ridge on the Cascadia Margin (Suess et al., 1999) as well as from the Håkon Mosby Mud Volcano in the Norwegian Sea (Damm and Budeus, 2003). If all 48 mud extrusions observed along the Pacific coast of Costa Rica are as active as the four representative examples described here (taking $4 \cdot 10^5$ mol yr^{-1} as the average CH_4-output) and if they would emit methane continuously over time, then 19.2 Mmol yr^{-1} (307 Mg yr^{-1}) methane would enter the ocean along this part of the erosive subduction zone. This only accounts for the mud extrusions excluding emissions from scarps (Mau et al., in prep.), landslides and fault zones in the area, which also emit methane into the water column. The estimate reveals that methane output from these mud extrusions does not significantly contribute to the global methane discharge from the seafloor which was estimated to be in the order of 20 Tg yr^{-1} (Kvenvolden et al., 2001). Nevertheless, to improve the highly speculative global estimates currently in use, the contribution from erosive margins such as derived here, must be included.

Acknowledgements

Many thanks to the scientists, masters and crews aboard research vessels SONNE and METEOR during cruises SO 144, SO 163, M 54 and SO 173 for their support, information and discussion. We are grateful for the skilful laboratory assistance by Karen Stange and the many other helpful hands during sampling. Thanks also to Jens Greinert for help with the post-processing of current meter data. This publication is contribution no. 66 of the Sonderforschungsbereich 574 “Volatiles and Fluids in Subduction Zones” at the University of Kiel.

References

Bialas, J., Flüh, E. and Bohrmann, G., 1999. FS SONNE, cruise report SO 144/1&2 PAGANINI; San Diego - Caldera (September 7 - November 7, 1999). GEOMAR Report, 94, 437 pp.

Boetius, A., Ravenschlag, K., Schubert, C.J., Rickert, D., Widdel, F., Gieskes, A., Amann, R., Joergensen, B.B., Witte, U. and Pfannkuche, O., 2000. A marine microbial consortium apparently mediating anaerobic oxidation of methane. Nature, 407: 623-626.

Bohrmann, G., Jung, C., Heeschen, K., Weinrebe, W., Baranov, B., Cailleau, B., Heath, R., Hühnerbach, V., Hort, M., Masson, D. and Schaffer, I., 2002. Widespread fluid expulsion along the seafloor of Costa Rica convergent margin. Terra Nova, 14: 69-79.

Brown, K.M., 1990. The Nature and Hydrogeologic Significance of Mud Diapirs and Diatremes for Accretionary Systems. J. Geophys. Res., 95(B6): 8969-8982.

Damm, E. and Budeus, G., 2003. Fate of vent-derived methane in seawater above the Håkon Mosby mud volcano (Norwegian Sea). Marine Chemistry, 82: 1-11.

de Angelis, M.A., Lilley, M.D., Olson, E.J. and Baross, J.A., 1993. Methane oxidation in deep-sea hydrothermal plumes of the Endeavour Segment of the Juan de Fuca Ridge. Deep-Sea Research I, 40(6): 1169-1186.

Dimitrov, L.I., 2002. Mud volcanoes - the most important pathway for degassing deeply buried sediments. Earth-Science Reviews, 59: 49-76.

Drews, M., Wallmann, K., Aloisi, G. and Bohrmann, G., subm. Fluid expulsion from the Dvurechenskii mud volcano (Black Sea), Part II: Methane fluxes and their relevance to the Black Sea methane cycle. Earth and Planetary Science Letters.

Fisher, C.R., 1990. Chemoautotrophic and methanotrphic symbioses in marine invertebrates. Aquatic sciences, 2: 399-436.

Ginsburg, G.D., Milkov, A.V., Soloviev, V.A., Egorov, A.V., Cherkashev, G.A., Vogt, P.R., Crane, K., Lorenson, T.D. and Khutorskoy, M.D., 1999. Gas hydrate accumulation at the Håkon Mosby Mud Volcano. Geo-Marine Letters, 19: 57-67.

Grasshoff, K., Ehrhardt, M. and Kremling, K., 1997. Methods of seawater analysis. Verlag Chemie, Gulf Publishing, Houston, 757-773 pp.

Grevemeyer, I., Kopf, A., Fekete, N., Kaul, N., Villinger, H., Heesemann, M., Wallmann, K., Spieß, V., Gennerich, H.-H., Müller, M. and Weinrebe, W., 2004. Fluid flow through active mud dome Mound Culebra offshore Nicoya Peninsula, Costa Rica: evidence from heat flow surveying. Marine Geology, 207: 145-157.

Han, X., Suess, E., Sahling, H. and Wallmann, K., 2004. Fluid venting activity on the Costa Rica Margin: New results from authigenic carbonates. International Journal Earth Science (Geologische Rundschau), 93: 596-611.

Heeschen, K.U., Collier, R.W., de Angelis, M.A., Suess, E., Rehder, G., Linke, P. and Klinkhammer, G.P., subm. Methane sources, distributions, and fluxes from cold vent sites at Hydrate Ridge, Cascadia Margin. Global Biochemical Cycles.

Henry, P., Le Pichon, X., Lallement, S., Lance, S., Martin, J.B., Foucher, J.-P., Fiala-Medioni, A., Rostek, F., Guilhaumou, N., Pranal, V. and Castrec, M., 1996. Fluid flow in and around a mud volcano field seaward of the Barbados accretionary wedge: Results from Manon cruise. J. Geophys. Res., 101(B9): 20297-20323.

Hensen, C., Wallmann, K., Schmidt, M., Ranero, C. and Suess, E., 2004. Fluid expulsion related to mud volcanism at Costa Rica continental margin - a window to the subducting slab. Geology, 32: 201-204.

Inthorn, M., Kumbier, T. and Zabel, M., subm. BeaWieS - A new sampling and monitoring device for the benthic boundary layer. L&O:Methods.

Judd, A.G., Hovland, M., Dimitrov, L.I., Garcia Gil, S. and Jukes, V., 2002. The geological methane budget at continental margins and its influence on climate change. Geofluids, 2: 109-126.

Kimura, G., Silver, E., Blum, P. et al., 1997. Proceedings of the ocean drilling program, 170, 458 pp.

Knittel, K., Boetius, A., Lemke, A., Eilers, H., Lochte, K., Pfannkuche, O. and Linke, P., 2003. Activity, distribution, and diversity of sulfate reducers and other bacteria in sediments above gas hydrate (Cascadia Margin, OR). Geomicrobiology Journal, 20: 269-294.

Kopf, A. and Behrmann, J.H., 2000. Extrusion dynamics of mud volcanoes on the Mediterranean Ridge accretionary complex. In: B. Vendeville, Y. Mart and J.-L. Vigneresse (Editors), From the Artic to the Mediterranean: Salt, shale, and igneous diapirs in and around Europe. Journal of the Geological Society, Spec. Publ., London, pp. 169-204.

Kopf, A.J., 2002. Significance of mud volcanism. Reviews of Geophysics, 40: 1-52.

Kopf, A.J., 2003. Global methane emission through mud volcanoes and its past and present impact on the Earth's climate. International Journal Earth Science, 92: 806-816.

Kvenvolden, K.A., Lorenson, T.D. and Reeburgh, W.S., 2001. Attention turns to naturally occuring methane seepage. EOS, 82: 457.

Lammers, S. and Suess, E., 1994. An improved head-space analysis method for methane in seawater. Mar. Chem., 47: 115-125.

Lance, S., Henry, P., Le Pichon, X., Lallement, S., Chamley, H., Rostek, F., Faugeres, J.-C., Gonthier, E. and Olu, K., 1998. Submersible study of mud volcanoes seaward of the Barbados accretionary wedge: sedimentology, structure and rheology. Marine Geology, 145: 255-292.

Linke, P., Wallmann, K., Suess, E., Hensen, C. and Rehder, G., subm. In-situ benthic fluxes from an intermittently active mud volcano at the Costa Rica convergent margin. Earth and Planetary Science Letters.

Luff, R. and Wallmann, K., 2003. Fluid flow, methane fluxes, carbonate precipitation and biogeochemical turnover in gas hydrate-bearing sediments at Hydrate Ridge, Cascadia Margin: Numerical modeling and mass balances. Geochimica et Cosmochimica Acta, 67(18): 3403-3421.

McAdoo, B.G., Orange, D.L., Silver, E.A., McIntosh, K., Abbott, L., Galewsky, J., Kahn, L. and Protti, M., 1996. Seafloor structural observations, Costa Rica accretionary prism. Geophysical Research Letters, 23(8): 883-886.

McMullin, E., Hourdez, S., Schaeffer, S.W. and Fisher, C.R., 2003. Phylogeny and biogeography of deep sea vestimentiferan tubeworms and their bacteria symbionts. Symbiosis, 34: 1-41.

Milkov, A.V., Sassen, R., Apanasovich, T.V. and Dadashev, F.G., 2003. Global gas flux from mud volcanoes: A significant source of fossil methane in the atmoshere and the ocean. Geophysical Research Letters, 30(2): 9-1 - 9-4.

Moerz, T., Fekete, N., Kopf, A. et al., in press. Styles and productivity of mud diapirism along the Middle American Margin Part II: Mound culebra and Mound 11, and 12. NATO ASI Series.

Nelson, D.C. and Jannasch, H.W., 1983. Chemoautotrophic growth of marine *Beggiatoa* in sulfide-gradient cultures. Archives of Microbiology, 136: 262-269.

Ranero, C.R. and von Huene, R., 2000. Subduction erosion along the Middle America convergent margin. Nature, 404: 748-752.

Rehder, G., Keir, R.S., Suess, E. and Rhein, M., 1999. Methane in the Northern Atlantic controlled by microbial oxidation and atmospheric history. Geophysical Research Letters, 26(5): 587-590.

Sahling, H., Rickert, D., Lee, R.W., Linke, P. and Suess, E., accepted. Macrofaunal community structure and sulfide flux at gas hydrate deposits from the Cascadia convergent margin. Marine Ecology Progress Series.

Schmidt, M., Hensen, C., Moerz, T., Mueller, C., Grevemeyer, I., Wallmann, K., Sahling, H., Mau, S. and Brueckmann, W., subm. Shallow surface methane hydrate accumulation related to mud diapirism at "Mound 11" (Costa Rica forearc). Marine Geology.

Shipley, T.H., McIntosh, K.D., Silver, E.A. and Stoffa, P.L., 1992. Three-dimensional imaging of the Costa Rica accretionary prism: structural diversity in a small Volume of the lower slope. Journal of Geophysical Research, 97: 4439-4459.

Suess, E., Bohrmann, G., von Huene, R., Linke, P., Wallmann, K., Lammers, S., Sahling, H., Winckler, G., Lutz, R.A. and Orange, D., 1998. Fluid venting in the eastern Aleutian subduction zone. J. Geophys. Res., 103(B2): 2597-2614.

Suess, E., Torres, M.E., Bohrmann, G., Collier, R.W., Greinert, J., Linke, P., Rehder, G., Trehu, A., Wallmann, K., Winckler, G. and Zuleger, E., 1999. Gas hydrate destabilization: enhanced dewatering, benthic material turnover and large methane plumes at the Cascadia convergent margin. Earth Planet. Sc. Lett., 170: 1-15.

Torres, L.M., McManus, J., Hammond, D.E., de Angelis, M.A., Heeschen, K.U., Colbert, S.L., Tryon, M.D., Brown, K.M. and Suess, E., 2002. Fluid and chemical fluxes in and out of sediments hosting methane hydrate deposits on Hydrate Ridge, OR, I: Hydrological provinces. Earth Planet. Sc. Lett., 201: 525-540.

Treude, T., Boetius, A., Knittel, K., Wallmann, K. and Jorgensen, B.B., 2003. Anaerobic oxidation of methane above gas hydrates at Hydrate Ridge, NE Pacific Ocean. Marine Ecology Progress Series, 264: 1-14.

Valentine, D.L., Blanton, D.C., Reeburgh, W.S. and Kastner, M., 2001. Water column methane oxidation adjacent to an area of active hydrate dissociation, Eel River Basin. Geochimica et Cosmochimica Acta, 65(16): 2633-2640.

von Huene, R., Ranero, C.R. and Vannucchi, P., 2004. Generic model of subduction erosion. Geology, 32(10): 913-916.

Wallmann, K., Linke, P., Suess, E., Bohrmann, G., Sahling, H., Schlüter, M., Dählmann, A., Lammers, S., Greinert, J. and Mirbach, N.v., 1997. Quantifying fluid flow, solute mixing, and biogeochemical turnover at cold vents of the eastern Aleutian subduction zone. Geochimica et Cosmochimica Acta, Vol. 61(24): 5209 - 5219.

Wiedicke, M., Sahling, H., Delisle, G., Faber, E., Neben, S., Beiersdorf, H., Marchig, V., Weiss, W., von Mirbach, N. and Afiat, A., 2002. Characteristics of an active vent in the fore-arc basin of the Sunda Arc, Indonesia. Marine Geology, 184: 121-141.

Sources, fate and output of methane from cold seeps at Jaco Scarp, an embayment caused by seamount subduction offshore Costa Rica

S. Mau[1,*], G. Rehder[2,1], E. Soeding[1], H. Sahling[3,1], E. Suess[2,1], K. Stange

[1] Sonderforschungsbereich 574, Kiel University, Wischhofstr. 1-3, 24148 Kiel, Germany

[2] IFM-GEOMAR, Wischhofstr. 1-3, 24148 Kiel, Germany

[3] DFG Forschungszentrum Ozeanränder, Bremen University, Klagenfurter Str., 28359 Bremen, Germany

* corresponding author: S. Mau, smau@geomar.de, Fax: +49-431-600-2915

Abstract

Methane concentrations and their stable carbon isotopic composition ($\delta^{13}C_{CH4}$) were investigated in the water mass semi-enclosed by a scarp created by massive landslides caused by the subduction of a seamount offshore Costa Rica. Such a mass wasting process can open up deep sedimentary layers from which accumulated methane can escape. In Jaco Scarp we revealed numerous active vent sites. Large methane sources are located at the eastern rim of the scarp and at an outcropping sedimentary sequence in the northwest corner, where concentrations in the adjacent water column reached up to 1500 nmol L^{-1}. Repeated sampling of these sites indicates continuous venting over time, even though the internal structure of the methane plume changes. Several small methane-sources located on the talus, on the terrace and on the uplifted area of the scarp were identified by their light isotopic ratios. The $\delta^{13}C_{CH4}$ values of all sources range between -50 ‰ and -62 ‰ VPDB pointing to bacterial methane production. The vent-derived CH_4 is distributed and diluted in the water mass enclosed by the scarp by mixing with water containing background CH_4 concentrations. A measurable effect of CH_4 oxidation was revealed in the center of the main plume, where concentrations of methane are high, as well as along the walls of the scarp. Increased oxidation near the wall is probably due to diminished current flow and a different pathway of oxidation. At Jaco Scarp the water flow is directed mainly along the isobaths towards the northwest transporting CH_4 out of the scarp. The total CH_4 output was estimated to be 58 – 65 Mg yr^{-1} (1 Mg = 10^6 g) which is comparable to e.g. the hydrothermal vent site of Izena Cauldron in the Okinawa Trough or cold fluid venting from the northern or southern summit of Hydrate Ridge off

Oregon. This finding and the global abundance of scarps created by seamount subduction suggest a not yet considered contribution to natural methane sources on the seafloor.

Introduction

The determination of the extent of seep occurrences and the output of methane from various sources is one of the most significant hurdles to estimate the role of natural methane seepage in the global methane budget (Kvenvolden et al., 2001). One of the least known submarine source of methane is related to mass wasting along continental margins. Submarine landslides can be caused by earthquakes (e.g. von Huene et al., 2003), dissolution of gas hydrates (e.g. Katz et al., 1999), basal erosion of the continental plate (von Huene et al., 2004) and by seamount subduction. Tracks of subducting seamounts on continental margins were reported from the Aleutian subduction zone (Suess et al., 1998), the Japan Trench (Lallemand and Le Pichon, 1987), the New Hebrides subduction zone (Collot and Fisher, 1989), the Tonga Trench (Ballance et al., 1989). Even though mass wasting associated with seamount subduction was frequently reported, hardly anything is known about methane seepage related to these structures, least of all the amount of methane discharging and its role in the global methane cycle.

Seamount subduction has been inferred from high resolution bathymetry offshore Costa Rica (Ranero and von Huene, 2000; von Huene et al., 2000). The oceanic plate offshore Costa Rica is covered by ~40% seamounts, rising up to 1.5 to 2.5 km in height (von Huene et al., 2000, Fig. 1). They intercept and destroy the frontal prism while being carried down the subduction zone. The prism grows rapidly afterwards to its former extent, but tracks in the form of deeply cut grooves mark the further path of the seamount on the continental margin. Subducted seamounts are indicated by circular uplifts and steep scarps as a result of massive landslides (Fig. 1). These mass wasting processes affect only the upper part of the slope sediments, that are 1 – 2 km thick, lying atop of igneous rocks of which the continental margin off Costa Rica mainly consists (Ranero and von Huene, 2000). Pervasive fracturing was observed at the crest of the uplifts due to bending of overlaying strata above the seamount. Seawards, oversteepened sediments fail leading to the formation of scarps. Traces of more than one landslide can be found within scarps displayed by small embayments and the step like structure of the steep hanging walls (Fig. 1, Bohrmann et al., 2002).

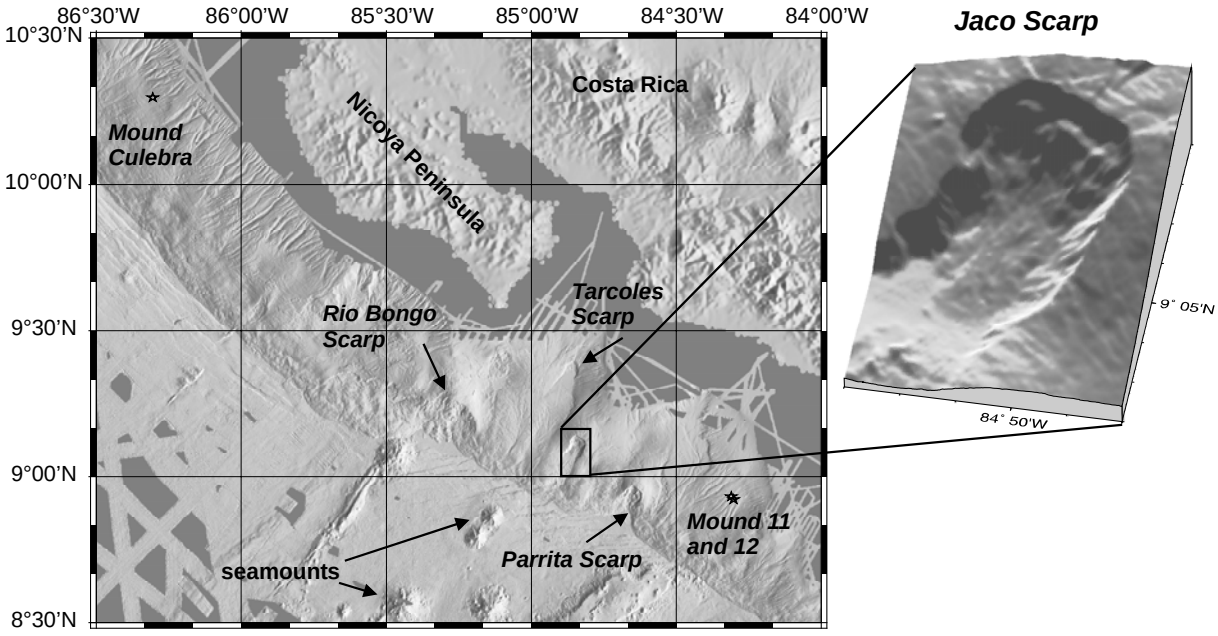

Fig. 1 Bathymetry of the continental margin off Costa Rica and the location as well as a close-up of Jaco Scarp. Other scarps (pointed out by arrows) and methane-emitting mud extrusions (mounds = stars) along this part of the continental margin referred to in the text are also indicated.

We investigated methane seepage from Jaco Scarp as one of the prominent slope failures observed offshore Costa Rica in detail (Fig. 1 & 2). Highest CH_4 concentrations of all water column stations investigated during PAGANINI expedition in 1999 (SO144, CTD02) (Bohrmann et al., 2002) were obtained inside this scarp. The observed plume originates at the foot of the hanging wall. In addition, we identified several other point sources of methane in the scarp and the fate of methane in the water column by high-resolution sampling and isotopic characterization of methane. Moreover, we estimated the inventory and output of excess methane for comparison with other natural sources of methane.

Methods

Methane concentration and isotopic ratios were measured in water samples at 16 stations within the water body enclosed by Jaco Scarp (Fig. 2). Sea water samples were collected during cruises of research project SFB 574 "Volatiles and Fluids in Subduction Zones" at the University of Kiel in April/May 2002 (SONNE 163-2), August/September 2002 (METEOR 54-2/3) and September 2003 (SONNE 173-3/4). In addition, current meters (Aanderaa RCM 8) were deployed during the last cruise.

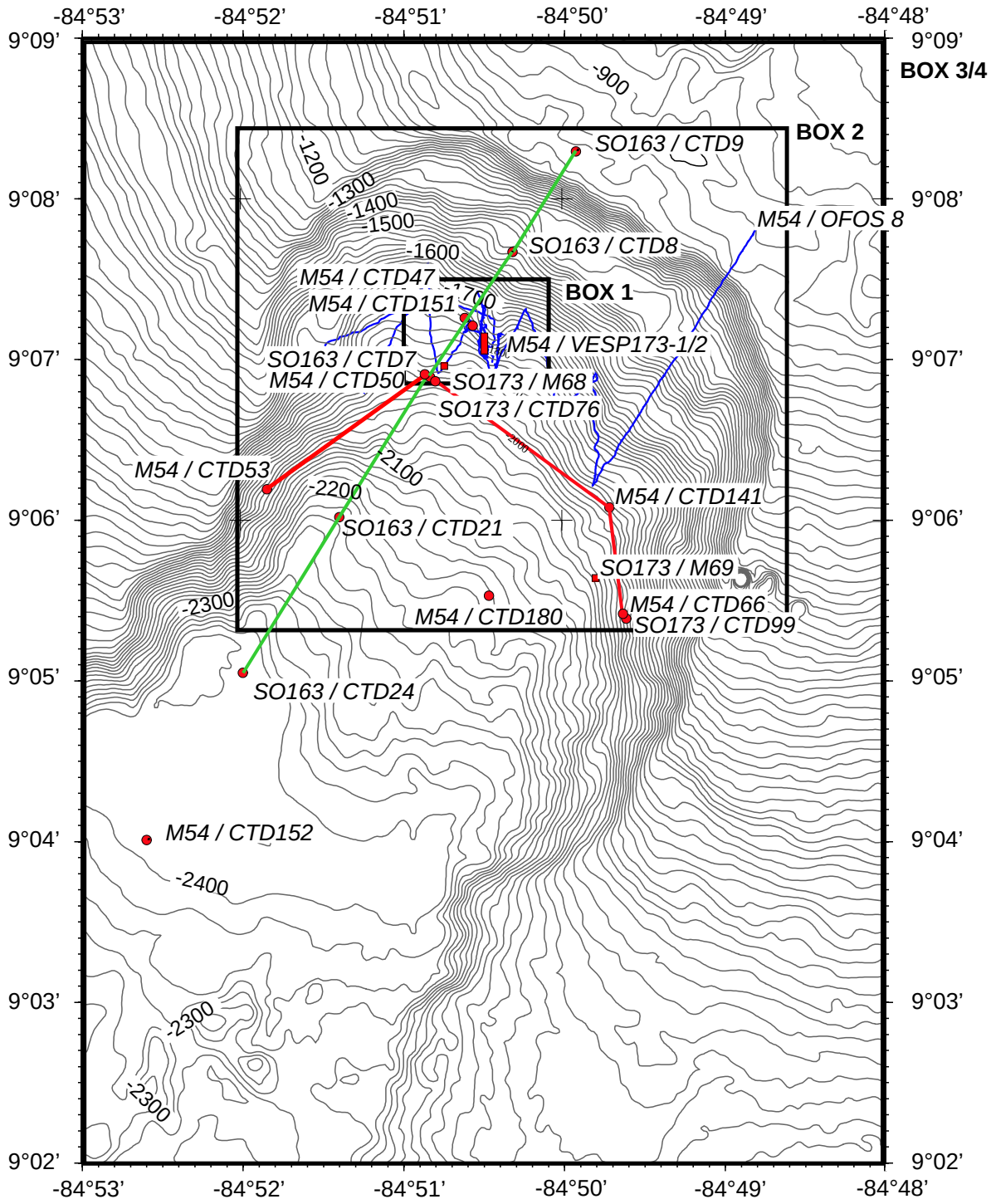

Fig. 2 Bathymetry of Jaco Scarp. Sampling stations are marked by filled circles. The labels of the stations include the sampling method: CTD – hydrocast sampling, VESP – video-guided sampling; M – moorings. The green line illustrates sampling along a transect through the scarp during SO163 and the red line sampling along the 1900 m isobath during M54. Highest CH_4 concentrations were found in the northwest corner of the scarp (e.g. SO163/CTD7) together with vent indicative fauna (M54/OFOS8 – blue line). Another main vent site is inferred from the data at station M54/CTD66. These two sites have been sampled repeatedly revealing continuous venting over time. The boxes were used for calculating the inventory of excess methane and the CH_4 output. Box 3 (depth range ground to 1500 m) and Box 4 (depth range 1500 to 1000 m) cover the whole area of the map.

Water samples for CH_4 analyses were collected by CTD/rosette and a video guided VESP-MUC. The VESP-MUC consists of five 5 L water bottles (HYDRO-BIOS) attached to the central piston of a modified multicorer frame (Linke et al., 1994). The ship's coaxial cable was used for bidirectional transmission of the video images, commands, data and power supply of the underwater units (ADITEC/SCHOLZ). The instrument is towed in view of the seafloor approximately 2 – 3 m above the sediment and is deployed if signs of seepage become visible e.g. clam colonies, bacterial mats, carbonate crusts. Water samples taken by CTD/rosette were collected with decreasing depth intervals towards the seafloor. For CH_4-analyses aboard a modification of the vacuum degassing method described by Lammers and Suess (1994) was used, modified by Rehder et al. (1999). The oxygen content was determined by Winckler titration (Grasshoff et al., 1997) in addition to the oxygen sensor of the CTD.

Only a subsample of the extracted gas from the vacuum degassing method is needed for the gas-chromatographic analyses of the CH_4 content aboard a ship, and the remainder was transferred to an evacuated 20 ml vial, preserved with 7 ml of 1:250 saturated $HgCl_2$:dest. H_2O (V/V) solution, and stored for shore-based analysis of stable isotopes. Gas samples were analyzed by an isotope-ratio-monitoring gas-chromatography/mass-spectrometry (irm-GC/MS). In preparation, aliquots of gas samples were purged using $Mg(ClO_4)_2$, NaOH, and HayeSep D in a ethanol bath at -110°C. The methane is separated by gas-chromatography and oxidized to CO_2 in a combustion reactor. The water generated by oxidation was removed by a naphion tubing and P_2O_5. The methane-derived CO_2 peak is cryofocussed again. Controlled warming of the trap injects the gas into a continuous flow of He entering the mass spectrometer. The volume of the injected samples was chosen based on the CH_4 concentration measured aboard to allow constant mass injections (e.g. less gas is injected of a sample of high CH_4 concentration), thus reproducibility of stable carbon isotope determination is 0.6 ‰ for all samples. All isotope ratios are given in δ-notation versus Vienna Pee Dee Belemnite (VPDB) standard.

Two moorings were deployed within Jaco Scarp to obtain ocean current data (Fig. 2). Each was equipped with an Aanderaa-current meter (RCM 8) at about 10 m above seafloor. The mooring placed close to the headwall of the scarp included an additional RCM8 approximately 120 m above ground. The second mooring was located at the southeastern rim. Both devices were deployed from September 16th to 23rd 2003.

Results and Discussion

CH_4 distribution and temporal variability

Enhanced CH_4 concentrations were found throughout the water mass enclosed by the scarp. The concentrations reach up to 360 nmol L^{-1} CH_4, that is two orders of magnitude above the regional background of 0.5 – 2 nmol L^{-1}. Highest values were observed at the northwestern corner of the slide mass, on the western slope of a small ridge (M54/47, SO163/07). Concentrations decrease along a transect that is slightly offset to the northwest of the axis of the scarp from the hanging wall towards the talus filled basin in the southeast (Fig. 3, green line in Fig. 2). The observed methane plume is situated at 1600 – 2000 m depth. The concentration in the basin shows a maximum value of 7.2 nmol L^{-1}. Thus, the CH_4 content decreased by two orders of magnitude along the transect. The plume was also observed in samples of four hydrocasts taken along the 1900 m isobath (Fig. 4a, red line in Fig. 2) and at station M54/180 centrally located above the talus (Fig. 4b). This indicates that the plume

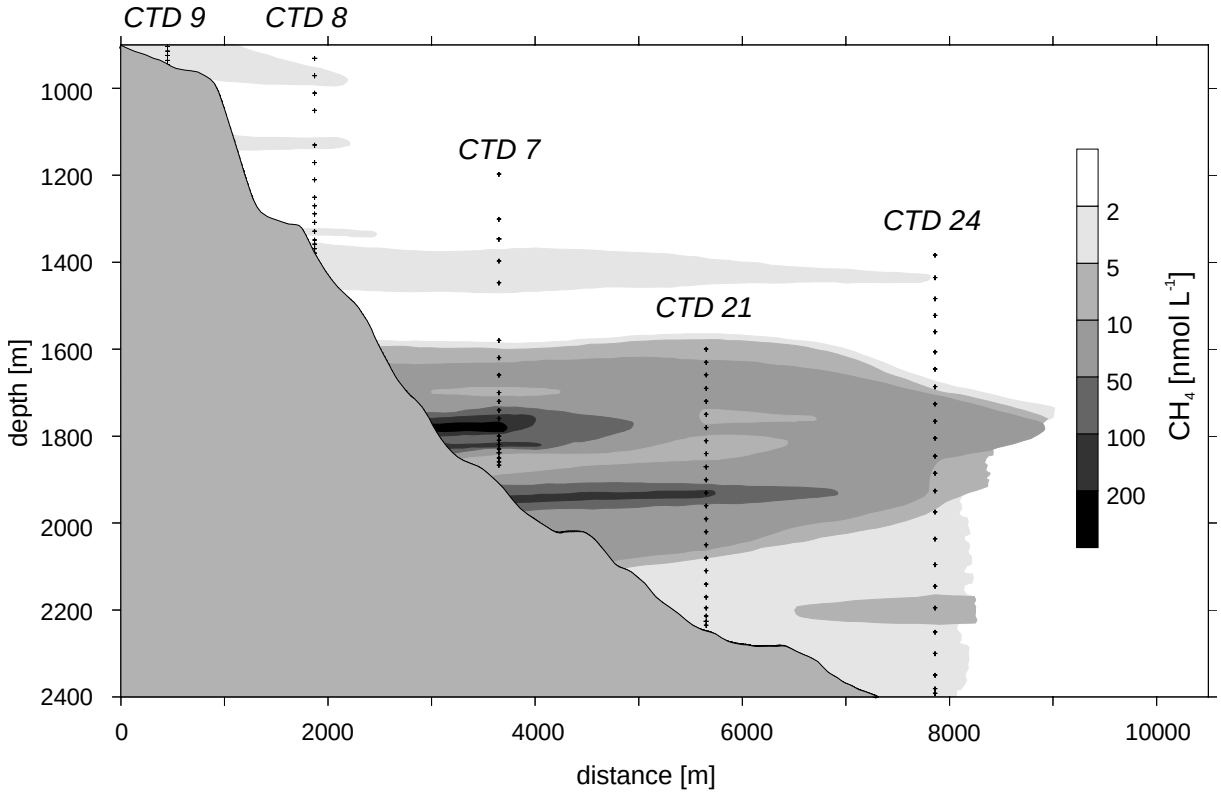

Fig. 3 Hand contoured section of CH_4 concentration based on data sampled during SO163 (Fig. 2). The crosses mark the sampling points. CH_4 concentrations of the regional background range between 0.5 – 2 nmol L^{-1} whereas CH_4 values reach up to 360 nmol L^{-1} in the water column above the main vent site in the northwest corner of the scarp; for locations of CTDs see Fig. 2. The plume generated at this site spreads along the transect from the hanging wall to the basin.

spreads horizontally from the small ridge in the northwestern corner over the entire water mass inside the scarp. However, elevated CH_4 concentrations (99 nmol L^{-1}) were found at the eastern rim of the scarp (M54/66; Fig. 4a) at a depth correlating with the center of the plume, but the stations in-between the rim and the small ridge show lower concentrations. Moreover, current meter measurements point to a predominantly counterclockwise flow along isobaths inside the scarp. If that flow is continuous, the methane enrichment can only be explained by another point source located on the southeastern rim (M54/66). Water is still enriched in methane below the plume pervading the scarp whereas mainly background concentrations have been observed above 1500 m.

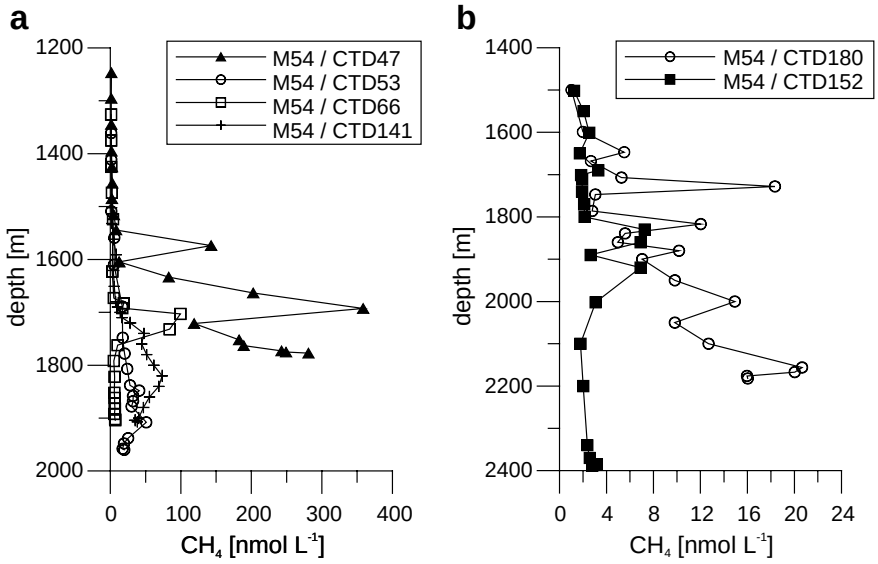

Fig. 4 CH_4 concentration versus depth a) along the 1900 m isobath including the stations of the main vent sites (M54/47 and M54/66) and b) above the talus (see Fig. 2 for locations of CTDs). Note different scales.

Seepage of methane rich fluids was found to vary with time and space. Water was sampled repeatedly at two locations in the scarp of which one is situated in the northwest corner and the other on the southeastern rim of the scarp (Fig. 2). The northwest corner was sampled in April (SO163) and August 2002 (M54) as well as in September 2003 (SO173) and the southeastern rim during cruises M54 and SO173. These repeated stations indicate continuous methane venting over two years, but also reveal changes of seepage activity.

Highest methane concentrations were observed repeatedly in the northwest corner. However, the internal structure of the plume (CH_4 concentration and depth of CH_4 maxima) fluctuates

considerably with time (Fig. 5a). The isotopic ratios of C-CH_4 of the concentration-maxima vary only slightly which may result from mixing with background methane having a value between –38 and –43 ‰ (unpublished data) or oxidation. Both processes lead to less negative $\delta^{13}C$ values. A detailed discussion of this issue is given in the following sections. In general, the similar isotopic signatures point to the same origin of the methane emitted, but fluids seem to discharge from more than one location over a certain depth range. Analogous results were obtained at the southeastern rim (Fig. 5b).

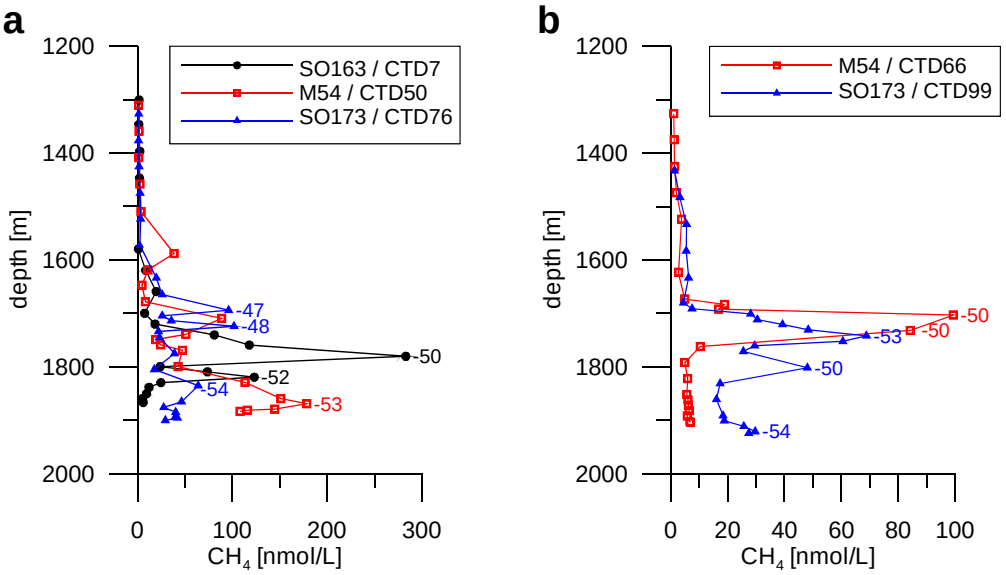

Fig. 5 Profiles of CH_4 concentration including $\delta^{13}C_{CH4}$ values of the CH_4-concentration-maxima from the repetitively sampled main vent sites (see Fig. 2 for location). a) stations in the northwest corner and b) at the eastern rim of the scarp. Samples were taken in April 2002 = SO163, August 2002 = M54 and in September 2003 = SO173.

Shifts of maximum methane concentrations with depth illustrate most likely long-term changes linked to variations of the fluid pathways. Short-term variations result mainly from changes of hydrostatic pressure associated with e.g. tides, ocean swells and storm surges (Boles et al., 2001). They influence the seepage rate (Linke et al., 1994; Boles et al., 2001; Torres et al., 2002) but an affect on the distribution of a methane plume has not been reported yet and is probably difficult to observe. The variations in methane profiles of the water column could also be due to gaseous venting which has a rapid impact on CH_4 concentrations in the water column as shown at Hydrate Ridge offshore Oregon (Heeschen et al., subm.). However, bubble streams have not been detected during any of the video guided operations in Jaco Scarp (Weinrebe and Flueh, 2002; Soeding et al., 2003). Sahling et al. (2003) describe the vent area in the northwest corner of Jaco Scarp as a sedimentary sequence exposed after a

slumping event. Thus, we suggest that the variability in space and time is due to tectonic events cutting of old fluid pathways and creating new ones and/or due to changes of the internal structure of the sedimentary sequence. Three earthquakes with magnitudes ranging between 2 – 3 occurred in the area of Jaco Scarp during half a year of seismic data recording (J. Gossler, pers. comm.). This indicates ongoing tectonic activity related to seamount subduction. The permeability of the sediments can be reduced because of carbonate precipitation as a product of anaerobe methane oxidation in sediments (Han et al., 2004) and formation of gas hydrates (Reed et al., 1990). These sealing effects could force fluids in the sedimentary sequence to find new passages. However, the origin of the fluid seems to be the same as proposed by the methane isotopic characteristics. Most of the strongly CH_4-enriched samples have $\delta^{13}C_{CH4}$ values of -50 to -55 ‰ (Fig.5).

Sources of methane

The major seepage area is situated in the northwest corner of the scarp where the highest CH_4 concentrations were measured (M54/47; Fig. 4). Biological evidence for seepage was found during OFOS M54/147 survey which revealed a small stretch of extremely high abundance of vent-associated biota (pogonophoran tubeworm of the genus *Lamellibrachia*; Fig. 6a) in 1750 –1850 m depth growing on steep sedimentary outcrops on the western flank of a small ridge. Vent indicative clams were also abundant, in particular on less steep locations and on the debris below the ridge. The investigation showed focused fluid seepage from the outcrops, but non from the slide debris. A video guided VESP-MUC was used for near-bottom sampling above the field of pogonophora. The CH_4 concentrations of these samples reached values of up to 1500 nmol L^{-1} (Fig. 6b) – the highest values observed along the entire Costa Rican subduction zone, which are comparable with hydrothermal vent sites (de Angelis et al., 1993; Watanabe et al., 1995; Tsunogai et al., 2000). Other evidence from OFOS surveys for additional vent sites have been scarce. It appears that this one site generates most of the widespread methane anomaly within Jaco Scarp.

Samples of methane collected in the water right above the major vent site show $\delta^{13}C$-values of -55 ‰ pointing to microbial methane production rather than to a thermogenic source. Whiticar (1996) reported C isotope ratios of bacterial methane varying in $\delta^{13}C_{CH4}$ between -110 ‰ to -50 ‰ whereas thermogenic CH_4 is enriched in ^{13}C. Such $\delta^{13}C_{CH4}$ values range

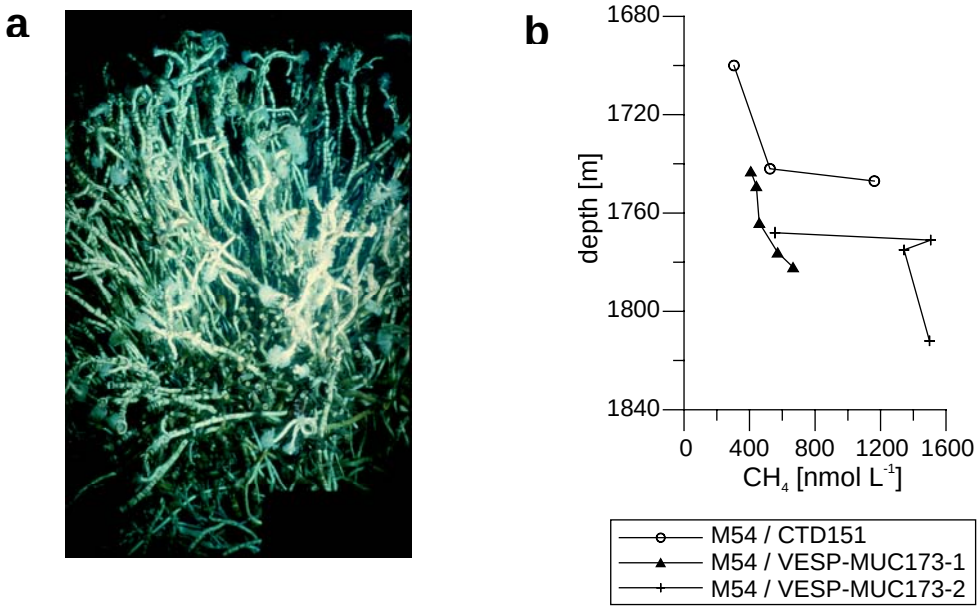

Fig. 6 The main seep site in the northwest corner of Jaco Scarp a) assemblage of pogonophora b) CH_4 concentrations measured in the near vicinity of the vent site (M54/CTD151), above the field of pogonophora (M54/VESP-MUC173-1) and within the field (M54/VESP-MUC173-2). These are the highest values observed offshore Costa Rica.

from -50 ‰ to -20 ‰. The methane/ethane ratio is commonly used to clarify the origin. A ratio of > 1000 is typically for bacterial CH_4 whereas a methane/ethane ratio of less than 100 is characteristic for thermogenic CH_4 (Bernard et al., 1978). Our results are illustrated in Figure 7 and show that a bacterial production of the methane is more likely. Moreover, thermogenic methane is produced at temperatures over ~120 °C which requires burial depths greater than ~ 1 km (Tissot and Welte, 1984), in contrast, bacterial methane is produced under anoxic conditions at low temperatures in burial depths of a few meters only (Whiticar, 1999), i.e. below the zone where sulfate levels have been depleted by sulfate-reducing bacteria (Judd et al., 2002). Using the regional geothermal gradient of 28 °C km^{-1}, the temperature in the sedimentary layer (700 – 800 mbsf), that was identified as the pathway of the fluids, is about 20 °C. Hence, assuming this layer to be the source of the methane strongly suggests a bacterial origin of the CH_4. CO_2 reduction is the preferred methanogenic pathway in marine sediments. It is indicated by a depletion in ^{13}C and results in $\delta^{13}C$-values below -60 ‰ (Whiticar, 1999). However, our results show heavier isotopic ratios, also in comparison with other vent sites where methane is bacterially produced, e.g. CH_4 from Hydrate Ridge has a stable carbon isotope values of -65.4 to -69 ‰ (Grant and Whiticar, 2002) and CH_4 escaping from the Håkon Mosby Mud Volcano has an average $\delta^{13}C_{CH4}$ value of -61.6 ‰ (Damm and

Budeus, 2003). Paull (2000) and Whiticar (1999) observed a trend to heavier $\delta^{13}C_{CH4}$ values with increasing sediment depth that could explain our results; as the methane in the northwest corner of Jaco Scarp originates probably from a deep sedimentary layer. Also, the isotopic characteristics of the CH_4 in the water column can be already enriched in ^{13}C due to oxidation which would suggest a lighter isotopic signature of the CH_4-source than directly inferred from the measurements. This would also explain the trend in C_1/C_n ratios towards lower values, because methane is preferably oxidized. A physical mixing of bacterial and thermogenic methane in response to vertical and lateral migration cannot be ruled out completely. Still, at least the dominant fraction seems to originate from microbial methane production.

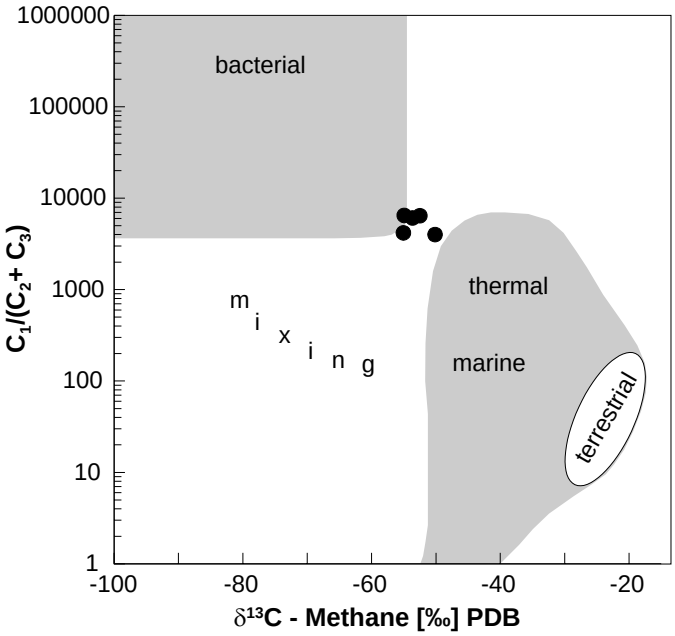

Fig. 7 Modified "Bernard" diagram (after Bernard et al., 1978) combining the molecular and the isotope compositional information. The samples shown in the diagram were taken at the major cold seep site in the northwest corner of the scarp within a field of pogonophoran tubeworm and above. The high C_1/C_n ratio indicates a rather bacterial origin of the CH_4.

Another main vent site is proposed to occur at the eastern slope of Jaco Scarp. A maximum CH_4 concentration of 99 nmol L^{-1} was observed here at 1700 m water depth with a $\delta^{13}C$-value of -50 ‰ (Fig. 5; CTD 66). We assume a similar source and mechanism to explain the isotopic ratio as described for the major vent site above. That is, the $\delta^{13}C$-values most likely result from oxidation of light CH_4 within the sediments and water column or are produced by mixing of different methane pools. Apart from the similar isotopic ratios, the methane-plume is located in the same depth range as the one in the northwest corner. To date, we cannot infer if both seepage sites have a common source i.e. the same sedimentary sequence outcropping at these two places. Ranero (2002) described a terrace downslope of the scarps edge displaying a block that slipped a few hundred meters downwards (Fig. 1). This mass wasting process was observed along the headwall probably not affecting the western and eastern

slopes of the scarp. This argues against a common source-layer; only a closer investigation of this second proposed vent site by video-guided instruments can answer that question.

Apart from these main vent sites, more sources were identified based on the isotopic signature of CH_4 samples. Data of the transect through the scarp (SO163) is presented in Figure 8a showing three additional sources. These sources with methane concentrations of 2.7, 2.9 and

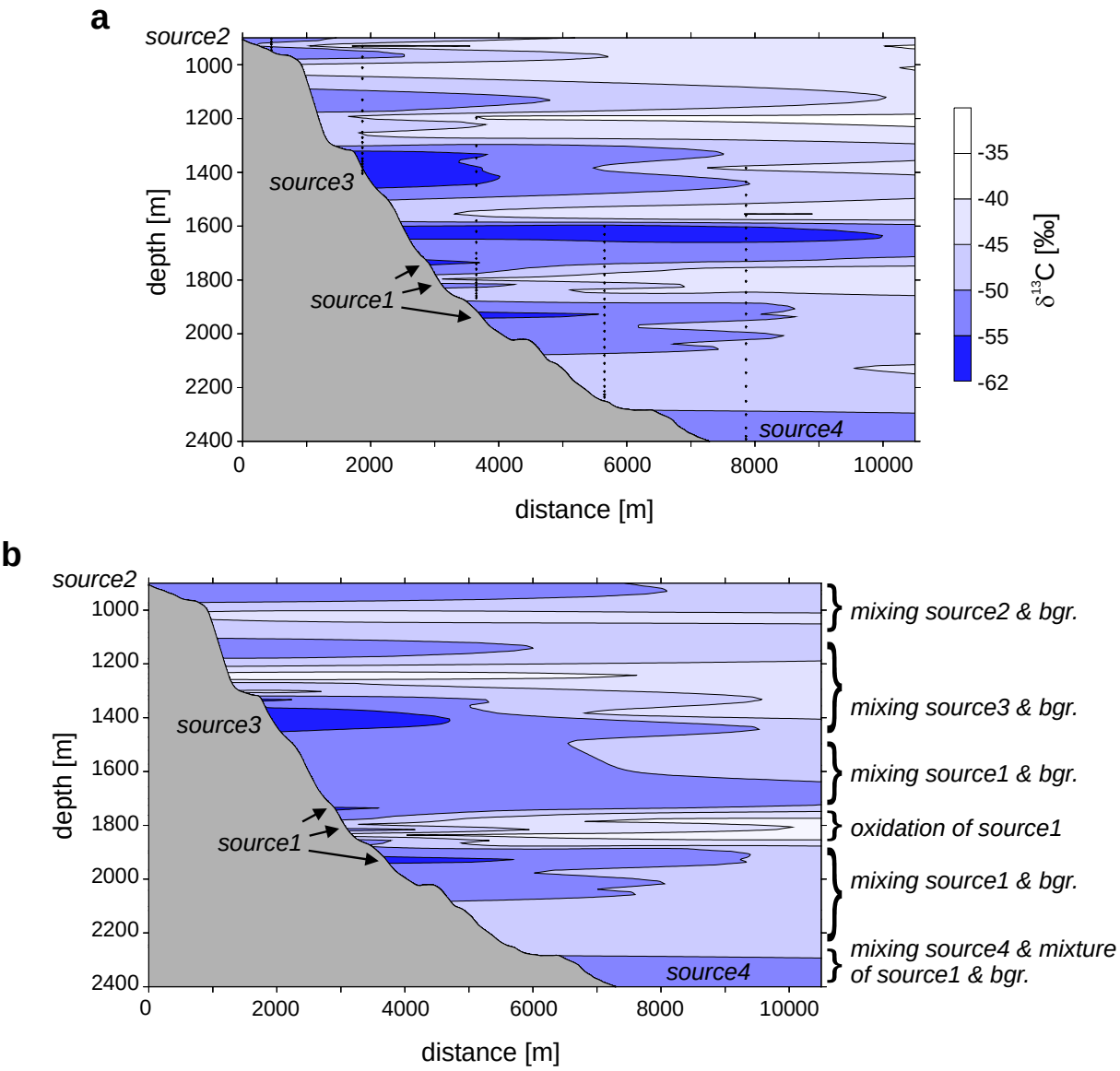

Fig. 8 Contoured section of $\delta^{13}C_{CH4}$ values of samples collected along the transect during SO163 (Fig. 2). The crosses mark the sampling points. Source 1 illustrates the main vent site in the northwest corner of the scarp and sources 2 to 4 represent minor seepage sites with CH_4 concentrations below 3 nmol L^{-1} (Fig. 3). a) measured data, b) calculated $\delta^{13}C_{CH4}$ values from CH_4 concentrations using the equations derived from Fig. 9. The identification of the different mixing processes and oxidation point out the layered structure in the scarp due to the dominant horizontal transport.

2.7 nmol L^{-1}, marked as source 2, source 3 and source 4 in Figure 8, have $\delta^{13}C_{CH4}$ values of -55, -62, and -54 ‰, respectively. We also discovered sources at sites M54/CTD 180 and M54/CTD 152 with low concentrations and $\delta^{13}C$-values of -57 and -56 ‰ closest to the seafloor. The isotope characteristics of these small sources point to a bacterial origin. Similar to our findings at the major vent sites, the $\delta^{13}C$-values are heavier than -60 ‰, but to light for a thermogenic source, which is probably due to ongoing oxidation of CH_4 (see discussion above).

The small sources are probably located at sites of enhanced fluid flow. Once CH_4 is generated, is starts migrating towards the surface, but most of it is rapidly oxidized by microbial consortia using pore water sulfate as oxidizing agent (Boetius et al., 2000). Only in certain areas where methane is transported with ascending fluids with flow rates exceeding ~ 80 cm yr^{-1}, dissolved CH_4 can escape into the bottom water (Luff and Wallmann, 2003). Fluid flow is increased along fractures and in porous and highly permeable sediments. Thus, we suggest that the small sources occur at sites where such sediment layers outcrop, which could be near the terrace, or where fractures exist, presumable on the uplifted area of the scarp and on the talus. CH_4 venting on the latter could also be due to breaking of blocks of rocks and, hence, opening up pathways for methane-rich fluids.

Fate of methane derived from isotopic characterization

To obtain information on the fate of methane, we interpreted the samples separately for each cruise to cancel out temporal variability. First we examined the results of the cruise SO163 located along the transect and then the ones of the cruise M54 located along the hanging wall.

The decline of the methane content along the transect results from mixing and oxidation of vent-derived CH_4. Methane is emitted into the water column at the major vent site, a point source, in the northwest corner and at three minor seepage sites (sources indicated in Fig. 8). Mixing of these sources and background CH_4 was identified using a $1/CH_4$ vs. $\delta^{13}C$ plot (Fig. 9) in which mixing of two end members should result in a straight line. The value defining the background in Figure 9 was confirmed by samples collected offshore Costa Rica in similar depth intervals where the scarp is situated (unpublished data). Their $\delta^{13}C$-values range from -38 to -43 ‰ with concentrations from 0.4 to 2.4 nmol L^{-1}. Figure 9 illustrates that most of the data fall onto mixing lines between sources 1, 2, 3 and background water. Methane of source

4 which escapes at the bottom layer of the scarp, mixes with the overlaying water which in turn is displayed as a mixture of source 1 and background concentrations. However, some values cannot be explained solely by mixing (crosses in Fig. 9). Instead we favor an oxidation trend based on the averaged data of source 1 (140 nmol L^{-1} and -53 ‰) using Rayleigh fractionation after e.g. Coleman (1981) together with a fractionation factor of 1.005, representing the lower end of published values (Barker and Fritz, 1981; Whiticar and Faber, 1986). This value was chosen, because small fractionation factors were reported from other low temperature environments (~4 °C) like in the methane plumes above Hydrate Ridge (Grant and Whiticar, 2002) and in the methane-rich hydrothermal plume in the Myojin Knoll Caldera (Tsunogai et al., 2000). Figure 9 shows that only a few samples fall right on the oxidation trend. The data located between the oxidation line and the Source 1 - background mixing line are most likely controlled by the combined effects of mixing and oxidation. For simplicity, further calculations were conducted by assigning the samples marked as crosses on Figure 9 to oxidative modification of the source-methane rather than to mixing.

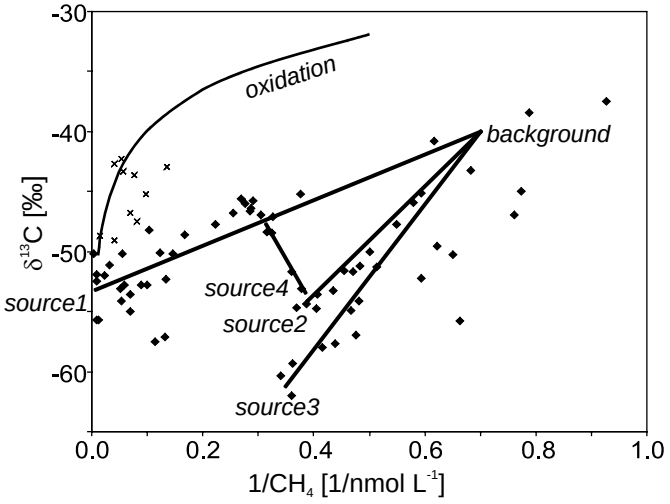

Fig. 9 $1/CH_4$ vs. $\delta^{13}C_{CH4}$ of samples of the transect - SO163 (Fig. 2 & 3). Sources 1 to 4 of Figure 8 are included and represent the end members of the mixing lines (straight lines). The background value is verified by measurements at background stations offshore Costa Rica (unpublished data, not shown). An oxidation trend using a fractionation factor of 1.005 was calculated for source 1. Samples between the oxidation line and the mixing line of source 1 and the background are likely to be controlled by ongoing mixing and oxidation. Nevertheless, data indicated as crosses are assigned to oxidation rather than to mixing.

Most samples can be ascribed to one of the mixing processes or to oxidation. After identifying the processes, the samples were divided according to their anticipated fate, i.e. to one of the five equations derived from Figure 9. Isotopic ratios shown in Figure 8b were calculated using these equations and the measured CH_4 concentrations. This figure illustrates the predicted horizontally layered structure of the methane distribution and its stable carbon isotopes in the scarp. Methane of source 4 mixes with already mixed source 1-water in the

bottom layer. Above, the plume of mixed methane of source 1 and the background is centered by oxidized methane of source 1. Farther up in the water column, CH_4 of source 3 is mixed with background water and the uppermost water of the scarp indicates mixing of source 2 and background methane. Nevertheless, the one layer of ^{12}C enriched methane of low concentrations (Fig. 8a) as well as few other data cannot be explained by these processes. They hint to further mechanisms. However, most of measured data are well represented indicating that the most important processes are identified and considered.

In general, mixing is the dominating process in the scarp, and the effect of oxidation ins the water column can only be revealed in some cases. Oxidation is recognized in the center of the main plume. De Angelis et al. (1993) who measured oxidation rates in the deep-sea hydrothermal plume of the Juan de Fuca Ridge showed enhanced oxidation at highest CH_4 concentrations. Valentine et al. (2001) obtained similar results in the water column of Eel River Basin (offshore northern California). This agrees well with our results. The isotopic ratios of CH_4-enriched samples indicate oxidation, even though in combination with ongoing mixing, whereas samples with low CH_4 concentration were dominated by mixing (Fig. 9).

Water samples taken during cruise M54 indicate that methane becomes also oxidized in the vicinity of the scarp walls. Samples of CTD 53, CTD 66 and CTD 141 show a strong enrichment in ^{13}C (Fig. 10). A stronger fractionation during oxidation of methane is also inferred from water samples taken right above the field of pogonophora (VESP-MUC 173-2) and in the immediate environment of the seepage site (CTD 151) in the northwest corner, i.e. near the slope (Fig. 10b). The $\delta^{13}C$-values of all of these samples lie above the calculated oxidation trend used for the interpretation of the transect data (i.e. $\alpha = 1.005$) representing the oxidation in the main plume (Fig. 9). Therefore, the methane is more depleted in ^{12}C than the oxidized methane in the main plume. It appears that stronger fractionation characterizes the oxidation near the major vent site where high methane concentrations are prevailing. The measured concentrations reach up to 1500 nmol L^{-1} at this site which is at least one order of magnitude higher than the concentration of any other sample gathered inside the scarp by CTD/rosette casts. However, concentrations are lower at the other sites (CTD 53, 66, 141). The higher fractionation factors at those locations can result from a different pathway of methane oxidation near the walls in contrast to the one in the center of the scarp. A change of the pathway of the reaction was observed by Coleman (1981) during the course of a laboratory culture study who suggest accumulation or depletion of some component as

possible cause. Evidence for that process could be that the most depleted values were only measured in the vicinity of slope sediments (lowermost samples of CTD 53, 66). Hence, other components could be available near the slope than in the water column farther off the slopes. Oxidation over a longer time period could also explain these values as shown by Barker and Fritz (1981) who recorded increasing $\delta^{13}C$-values due to aerobic CH_4 oxidation over 20 days in laboratory. Current velocity is lower near the ground (wall) increasing the residence time for oxidation, thus, oxidation could here be more complete than in the main methane plume.

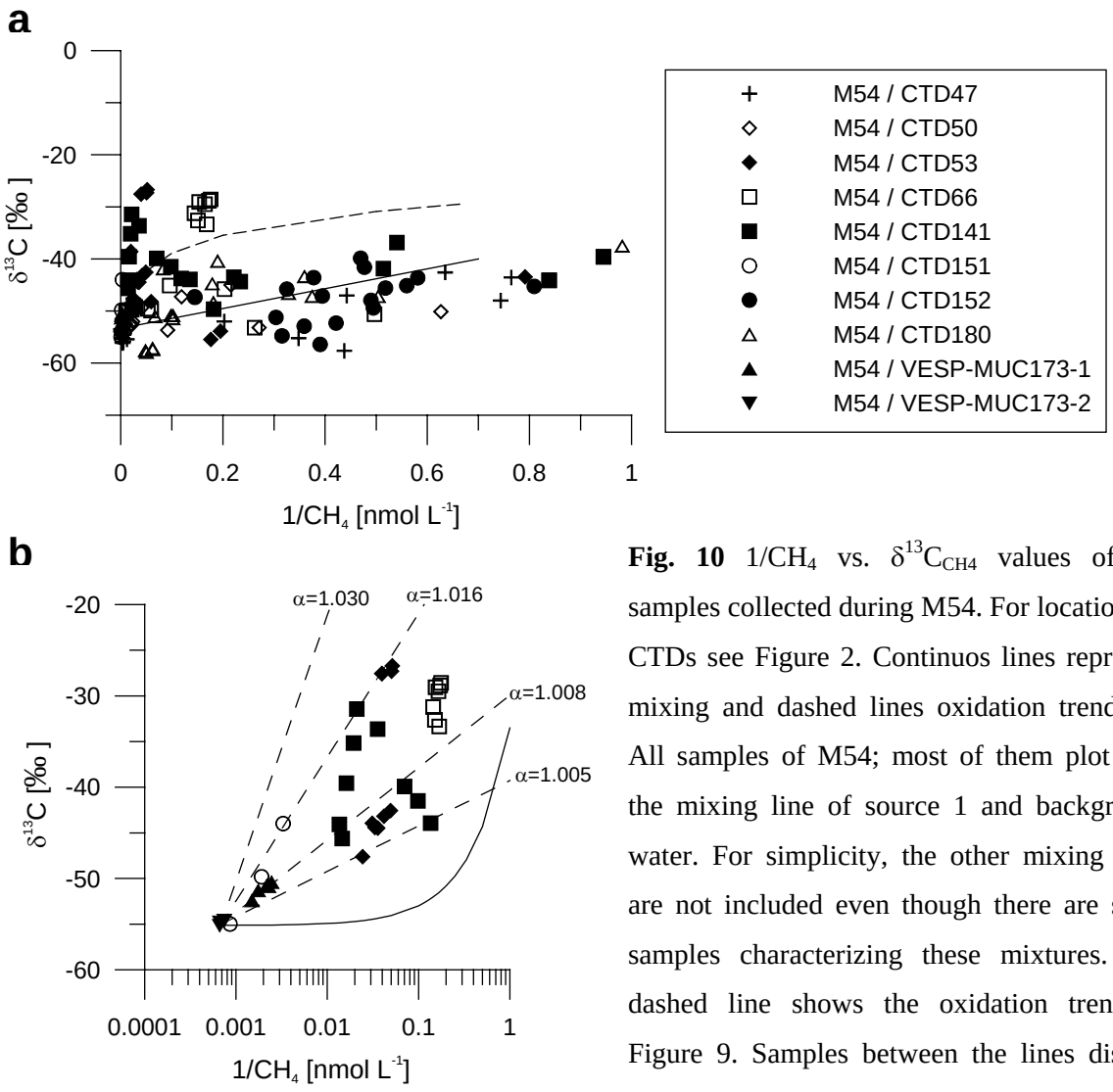

Fig. 10 $1/CH_4$ vs. $\delta^{13}C_{CH4}$ values of the samples collected during M54. For locations of CTDs see Figure 2. Continuos lines represent mixing and dashed lines oxidation trends. a) All samples of M54; most of them plot near the mixing line of source 1 and background water. For simplicity, the other mixing lines are not included even though there are some samples characterizing these mixtures. The dashed line shows the oxidation trend of Figure 9. Samples between the lines display ongoing oxidation and mixing whereas samples above the oxidation trend point to oxidation with a higher fractionation factor. These samples were collected in the vicinity of the walls of the scarp and are presented in b). Note the logarithmic scale of the x-axis. The dashed lines indicate various oxidation trends using different fractionation factors (α) but always source 1 as endmember. Shown are samples of CTD53 from 1960 – 1778 m water depth, samples of CTD66 from 1904 – 1792 m (in both cases the lowermost samples) and samples of CTD141 from 1840 – 1680 m (~100 m above seafloor).

In summary, both processes appear to lead to accelerated oxidation in combination with larger fractionation factors in the vicinity of the walls and to reduced oxidation farther away from the slope.

Current measurements

Current meter measurements indicate a counterclockwise flow along isobaths inside the Jaco Scarp; three current meters were placed here. Two of them in the northwest corner at 10 and 120 m above ground and one at 10 m above seafloor at the southeastern rim. The recorded data indicates that the water flows predominantly towards the northwest at the station on the southeastern side along the slope of the scarp turning southwest 10 m above ground in the northwest corner whereas the northwest flow continues 120 m above seafloor (Tab. 1). Current measurements at the station in the northwest corner also show flow which is occasionally directed to the east. Besides, the small coverage by current measurements does not confirm nor exclude eddy formation. Various sized eddies could form inside the scarp. For example eddies could develop in the northwest corner leading to a water mass strongly enriched in CH_4 as was discovered, but circulation could also form a closed-loop covering the entire area of the scarp. Only an expanded coverage of current measurements can clarify the current pattern in the scarp.

In spite of that, the assumed current flow along bathymetric lines in northwesterly direction corresponds reasonably well to the distribution of methane. The transect data indicates methane being transported from the northwest corner towards the southwest, i.e. along the wall in direction of the anticipated flow. Enhanced methane concentrations were observed below the rim of the western wall of the scarp but not above (M54/CTD53) emphasizing that methane-enriched water is already carried out of the scarp, thus, supporting the transport along isobaths. This transport pattern explains also the low CH_4 concentrations found at M54/180 near the center of the scarp. Moreover, a counterclockwise circulation would confirm the input of methane from the other seepage site at the eastern rim (M54/CTD66). However, at certain times the flow is reversed as current measurements at the northwest corner indicate (Tab. 1). Hence, methane from the major source is carried occasionally to the east. This would explain the elevated methane concentrations of station 141 positioned in the same depth range as the main plume (1600 – 2000 m). Based on this relatively good

correspondence between assumed current flow and CH_4-distribution, we used this flow pattern to calculate the methane output (see below).

Tab. 1 Current velocities and directions near to the two main vent sites located in the northwest corner and at the eastern rim of the scarp (Fig. 2). The velocities are given in cm s^{-1} and refer to the averaged velocity per day.

location	north-west-corner		north-west-corner		eastern rim	
longitude	84°50.74		84°50.74		84°49.80	
latitude	9°06.96		9°06.96		9°05.64	
depth	1870m		1760m		2030m	
	velocity	**direction**	**velocity**	**direction**	**velocity**	**direction**
17.-18.09.03	0.57	NW	0.54	SE	1.59	SW
18.-19.09.03	1.06	SW	1.49	NW	1.75	NW
19.-20.09.03	1.04	SW	0.84	NE	2.2	NW
20.-21.09.03	3.81	SW	1.39	NW	0.40	NW
21.-22.09.03	1.23	NE	1.17	NW	0.87	NW
22.-23.09.03	2.45	SE	0.49	NE	1.65	NW

Methane inventory and output

The inventory of excess methane (i.e. methane above background levels derived from seepage) in Jaco Scarp was calculated using boxes of different sizes (Fig. 2) instead of layers as in the approaches of Tsunogai and Watanabe. The Myojin Knoll Caldera (Tsunogai) and the Izena Cauldron (Watanabe) are closed structures with a basin floor surrounded by steep walls. CH_4 concentrations are similar within layers of same depth or salinity, thus, Tsunogai and Watanabe calculated the methane inventory using layers. In the half open structure of Jaco Scarp the CH_4 concentrations vary in a layer of equal depth, therefore, we had to find another approach. Instead of layers we used boxes. Box 1 covers the northwest corner including the source where highest CH_4 concentrations were measured. Box 2 contains most of the sampled CTD-hydrocasts inside the northern part of the scarp, which is surrounded by steep walls. Box 3 contains measurements farthest from the main source, above the small basin located at the southwestern end. Box 1, 2 and 3 extend from the ground to 1500 m whereas box 4 covers the water depths from 1500 to 1000 m. The boxes exclude one another, that is, box 2 does not include box 1 etc.. We only calculated the methane inventory within the scarp's volume. Thus, box 4 contains only the volume of water above 1500 m, but below the rim of the scarp's walls.

The volumes of the boxes were determined using the bathymetric map of the area and the software Generic Mapping Tools (GMT 3.4, Wessel and Smith, 1998). Initially, a bathymetric map was created as it would look like without the scarp. Hence, we cut all data from the bathymetric grid within the scarp and calculated a virtual surface (using the ”surface” tool) spanning between the rims of Jaco Scarp. A tension factor of 1 was used, to achieve the most ”tightened” surface possible leading to the best volume estimation. Then, the volume of a box was calculated using the GMT tool ”grdvolume”. This function calculates the volume from a defined bottom-layer (e.g. 2400 m water depth) to the surface of the bathymetric grid. Hence, the difference of the volumes calculated from the bathymetric grid with the scarp and the bathymetric grid without the scarp or a defined surface-layer (e.g. 1500 m water depth) yields the volume of the box.

The inventory is then calculated as the product of the volume and the averaged CH_4 concentration for each box (Tab. 2). Methane concentrations of each depth-profile were first of all averaged over layers of 10 m in height. If no data of a 10 m – layer was available, we extrapolated from the CH_4 concentrations above and below. Then, the data of the hydrocasts situated in a box consisting of the 10 m – averages were averaged within the individual layers. Thus, within the boxes, the horizontal distribution of a layer is assumed to be uniform. Finally, we averaged the CH_4 concentrations of the layers of the box. Due to the temporal variability, we calculated the inventory separately based on SO163 data and M54 data, but also based on the entire data set (data of SO163, M54 and SO173). For the latter, the CH_4 concentrations of the hydrocasts of the different cruises collected at one site were averaged over 10 m layers, before averaging over the individual layers of a box. A background value of 1.5 nmol L^{-1} was subtracted from the averaged values of a box representing the average of all methane concentrations below 2 nmol L^{-1} inside the scarp. Background concentrations between 0.5 and 2 nmol L^{-1} were measured outside of the scarp, defining the criteria for background values inside the scarp. The results of these calculations are shown in Table 2.

The output of methane was calculated by dividing the inventory by the clearance time (Tab. 3). The time needed to transport the CH_4 enriched water out of the scarp is defined by the ratio of the distance through the scarp and the net current velocity (Heeschen, 2002). According to the results of current meter deployments (Tab. 1), which indicate a flow along isobaths, we calculated the length as the averaged lengths of the isobaths with a contour

distance of 100 m. We estimated the output of methane by taking that length, the average of the velocities representing the flow along the walls (Tab. 1) and the inventory.

Tab. 2 Inventories of excess methane of the different sized boxes and the total inventories of the scarp based on different data sets. 'all' – includes data of SO163, M54 and SO173. The base of the boxes are shown in Figure 2.

box no.	depth range m	volume km^3	ave. exc. CH4 nmol L^{-1}			inventory mol		
			SO163	**M54**	**all**	**SO163**	**M54**	**all**
1	ground - 1500	0.5	36.9	89.3	60.1	19071	46187	31070
2	ground - 1500	6.6	16.7	18.6	18.8	110044	122671	123839
3	ground - 1500	6.1	2.3	0.9	1.9	14217	5541	11851
4	1500 - 1000	2.5	0.5	0.4	0.4	1233	1025	1075
					total	144565	175425	167835

Tab. 3 Total inventories of excess CH_4 (i.e. sum of all boxes, see Tab. 2) and CH_4-outputs based on the average clearance time (15 days) and the maximum clearance time in the depth range of the main methane plume (17 days).

	inventory mol	**clearing time** d	**CH_4-output** Mg yr^{-1}
SO163	144565	15.0	56.3
M54	175425	15.0	68.3
all	167835	15.0	65.3
SO163	144565	17.2	49.2
M54	175425	17.2	59.7
all	167835	17.2	57.1

The total inventory of excess methane in the water mass enclosed by Jaco Scarp ranges from 145 to 175 kmol (Tab. 2). CH_4 concentrations are always highest in box 1 covering the area of the major source in the northwest corner. However, the inventory of that box is lower than the ones from box 2 and 3, because of the smaller volume of box 1. The inventories decrease from box 2 to box 4 due to the decreasing concentrations farther away from the source; though their volume increases. The variation of the inventories calculated from the different data sets (Tab. 2) result from sampling water at other locations during SO163 than during M54. The high inventory of box 1 based on M54 data results from higher CH_4 concentrations in the water sampled closer to the source. In box 3, the averaged concentration of methane of SO163-data is greater than the one from M54 data, because the latter samples were taken

much farther away from the two main sources. Despite of these variations due to sampling locations, the inventories of the boxes and the total inventories based on the different averages deviate within one order of magnitude at the most.

Assuming, that the current carries the excess methane out of the scarp along isobaths. The average residence time or clearing time for the whole inventory of the scarp is calculated to be about 15 days (Tab. 3). The time increases towards greater water depth, because water has to travel increasing distances (Fig. 2, lengths of isobaths increases). For example, it ranges between 15 and 17 days at 1600 – 2000 m depth where the main plume is located. Thus, the CH_4 output of the Jaco Scarp embayment ranges between 58 and 65 Mg yr^{-1} (3.6 – 4.1 Mmol yr^{-1}) based on the flushing times of 15 and 17 days, respectively.

Comparison with other seepage sites

Maximum CH_4 concentrations and the total CH_4 inventory of Jaco Scarp are similar in magnitude to published data from hydrothermal vent sites (Tab. 4). Even though the concentrations of methane in the Izena Cauldron at the east side of the mid-Okinawa Through reach values of up to 700 nmol L^{-1} (Watanabe et al., 1995), other hydrothermal sites show similar or even lower values as those at Jaco Scarp. For example, a maximum of 11 nmol L^{-1} was measured in the Myojin Knoll Caldera at the Izu-Bonin arc in the western North Pacific (Tsunogai et al., 2000). In the hydrothermal plume of the Endeavour Segment of the Juan de Fuca Ridge CH_4 concentrations did not exceed 390 nmol L^{-1} (de Angelis et al., 1993). The highest value observed in a hydrocast-sample inside Jaco Scarp was 358 nmol L^{-1}. Inventories have been derived for the cauldron-like structures. Due to the different volumes of the structures and to make comparison easier, we normalized the methane inventory to unit volume of km^3 (Tab. 4). The results indicate that the mass of excess methane inside Jaco Scarp is higher than in the Myojin Knoll Caldera and lower than in the Izena Cauldron. Tsunogai (2000) and Watanabe (1995) also calculated the output of methane from these structures, assuming vertical eddy diffusion as major transport mechanisms, because of the closed structure of the cauldron/caldera. According to these authors most of the methane is consumed by oxidation and only a minor portion escapes into the open ocean. In contrast, we suggest advective transport in the half-open structure of Jaco Scarp, which of course facilitates flushing greatly compared to the cauldron-structures. Thus, more methane is emitted into the open ocean from scarps than from cauldron like structures (Tab. 4). This

emphasizes that cold vent sites such as at Jaco Scarp are of equal importance to the methane carbon budget of the ocean as small defined hydrothermal vent sites similar to the ones mentioned herein.

Furthermore, Jaco Scarp contributes a similar amount of methane to the ocean as mud extrusions and other cold vent sites. Our estimate of the annual CH_4 release is in the same order of magnitude as the outputs reported from the Håkon Mosby mud volcano (Ginsburg et al., 1999; Lein et al., 1999) and the Dvurechenskii mud volcano (Drews et al., subm.). The amount of methane emitted from the individual mud extrusions located offshore Costa Rica (Fig. 1) is less than from Jaco Scarp (Tab. 4). This illustrates that scarps generated by

Tab. 4 Inventories of excess CH_4 and CH_4 output of individual vent sites. The inventories are just given for similar structures. * CH_4 output calculated by Drews et al. (subm.) based on data of references.

area	vent type	inventory kmol	inventory kmol km^{-3}	output Mg yr^{-1}	reference
Jaco Scarp off Costa Rica	cold fluid venting	168	10.7	58 – 65	this study
Izena Cauldron, Okinawa Trough	hydrothermal	591	61.6	18	Watanabe et al., 1995
Myojin Knoll Caldera, Izu-Bonin arc	hydrothermal	21	3.2	0.5 – 2	Tsunogai et al., 2000
Mound Culebra off Costa Rica	cold fluid venting			9.6	Mau et al., subm.
Mound 12 off Costa Rica	cold fluid venting			6.4	Mau et al., subm.
Mound 11 off Costa Rica	cold fluid venting			1.1	Mau et al., subm.
Håkon Mosby Mud Volcano, Norwegian Sea	cold fluid venting			69*	Ginsburg et al., 1999 Lein et al., 1999
Dvurechenskii mud volcano, Black Sea	cold fluid venting			32	Drews et al., subm.
northern summit, Hydrate Ridge off Orgeon	cold fluid venting			75	Heeschen et al., subm.
southern summit, Hydrate Ridge off Orgeon	cold fluid venting			56	Heeschen et al., subm.

subducted seamounts may be as important as marine mud extrusions and should not be neglected in calculations addressing the amount of natural methane seepage from the seafloor.

Venting activity has also been observed at other scarps offshore Costa Rica and along the Aleuten subduction zone. However, analyses indicate lower methane concentrations at these sites than at Jaco Scarp. This could result from decreased fluid flow due to increasing water depth, from lower availability of methane and fluid pathways, or being an artefact of low-resolution sampling. Suess et al. (1998) detected a CH_4 content of 7 nmol L^{-1} in a scarp along the Aleutian subduction zone which is situated in 5000 m water depth. In contrast, Jaco Scarp is located in 2000 m depth. The higher hydrostatic pressure could cause less methane to be emitted. Even small pressure changes caused by the tidal cycle can have a considerable effect on methane seepage as reported by Boles et al. (2001) and Tryon et al. (1999). They demonstrated higher outflow rates at low tide and lower rates at high tide. Hence, the flow of methane rich fluids in the water could be decreased due to higher pressure. Moreover, high-resolution sampling in the scarp off the Aleutian chain was not conducted (Suess et al., 1998). Parrita Scarp, another scarp situated at the Costa Rican margin, has so far not been investigated in detail, but its maximum value did not exceed 20 nmol L^{-1}. This could be the result of sampling farther away from a source or in the opposite direction of the current. In contrast to Parrita Scarp, Jaco Scarp is located farther landward of the trench and the foot of the headwall is located at ~1900 m water depth whereas in Parrita Scarp the lower edge of the headwall is at 1620 m. Therefore, it is most likely that other sedimentary layers are outcropping at Jaco Scarp presumably tapping a larger CH_4-reservoir. One of these layers or the boundaries between certain layers seem to be an effective pathway of fluids. Hence, venting activity in scarps depends strongly on the outcropping rocks and their porosity, permeability as well as on the existence of a source of methane.

Conclusions

Jaco Scarp is one of the scarps along the Pacific coast offshore Costa Rica that formed by seamount subduction. Detailed investigations of the methane content inside that structure revealed two main vent sites and several small vent sites. The CH_4 originates most likely from bacterial breakdown of organic matter. It is distributed and mixed in the water mass occupying the scarps interior and partly oxidized in the center of the main plume and close to the walls of the scarp. Ocean currents flowing mainly counterclockwise along the isobaths of

the scarp towards the northwest, carry the CH_4 out of the scarp. Therefore, the CH_4 released from vent sites in the scarp contributes to the methane carbon budget of the ocean.

Scarps are common features along subduction zones, but little is known about their role in the methane cycle. The example of Jaco Scarp illustrates that if deeper sedimentary layers are tapped and accumulated methane can discharge, a remarkably high amount of methane is transferred into the ocean. Moreover, the continuous venting over time and the similarity to hydrothermal and other cold vent sites emphasize their importance. Remarkably, the role of these structures is completely lacking in calculations of the methane budget of the ocean.

Acknowledgements

Many thanks to the scientists, masters and crews aboard research vessels SONNE and METEOR during cruises SO 144, SO 163, M 54 and SO 173 for their support, information and discussion. We are grateful for the many helpful hands during sampling, most of all Bert Mantzke. Thanks also to our new colleges at the IFM Gerd Niehus and Antonius Kipping for providing technical support on RCM8 and Thomas Müller and Rolf Käse for helping interpreting the current meter data. For comments and discussion we like to thank Robin Keir, Jürgen Gossler, Christian Hensen, Warner Brückmann, Steffen Kutterrolf, Roger Luff, Oliver Bartdorff and Heidi Wehrmann. This publication is contribution no. xxx of the Sonderforschungsbereich 574 “Volatiles and Fluids in Subduction Zones” at the University of Kiel.

References

Ballance, P.F., Scholl, D.W., Vallier, T.L. and Herzer, R.H., 1989. Subduction of a late cretaceous seamount of the Loisville Ridge at the Tonga Trench: A model of normal and accelerated tectonic erosion. Tectonics, 8(5): 953-962.

Barker, J.F. and Fritz, P., 1981. Carbon isotope fractionation during microbial methane oxidation. Nature, 293: 289-291.

Bernard, B.B., Brooks, J.M. and Sackett, W.M., 1978. Light hydrocarbons in recent Texas continental shelf and slope sediments. Journal of Geophysical Research, 83: 4053-4061.

Boetius, A., Ravenschlag, K., Schubert, C.J., Rickert, D., Widdel, F., Gieskes, A., Amann, R., Joergensen, B.B., Witte, U. and Pfannkuche, O., 2000. A marine microbial consortium apparently mediating anaerobic oxidation of methane. Nature, 407: 623-626.

Bohrmann, G., Jung, C., Heeschen, K., Weinrebe, W., Baranov, B., Cailleau, B., Heath, R., Hühnerbach, V., Hort, M., Masson, D. and Schaffer, I., 2002. Widespread fluid expulsion along the seafloor of Costa Rica convergent margin. Terra Nova, 14: 69-79.

Boles, J.R., Clark, J.F., Leifer, I. and Washburn, L., 2001. Temporal variation in natural methane seep rate due to tides, Coal Oil Point area, California. J. Geophys. Res., 106(C11): 27077-27086.

Coleman, D.D., Risatti, J.B. and Schoell, M., 1981. Fractionation of carbon and hydrogen isotopes by methane-oxidizing bacteria. Geochimica et Cosmochimica Acta, 45: 1033-1037.

Collot, J.-Y. and Fisher, M.A., 1989. Formation of forearc basins by collision between seamounts and accretionary wedges: An example from the New Hebrides subduction zone. Geology, 17: 930-933.

Damm, E. and Budeus, G., 2003. Fate of vent-derived methane in seawater above the Håkon Mosby mud volcano (Norwegian Sea). Marine Chemistry, 82: 1-11.

de Angelis, M.A., Lilley, M.D., Olson, E.J. and Baross, J.A., 1993. Methane oxidation in deep-sea hydrothermal plumes of the Endeavour Segment of the Juan de Fuca Ridge. Deep-Sea Research I, 40(6): 1169-1186.

Drews, M., Wallmann, K., Aloisi, G. and Bohrmann, G., subm. Fluid expulsion from the Dvurechenskii mud volcano (Black Sea), Part II: Methane fluxes and their relevance to the Black Sea methane cycle. Earth and Planetary Science Letters.

Ginsburg, G.D., Milkov, A.V., Soloviev, V.A., Egorov, A.V., Cherkashev, G.A., Vogt, P.R., Crane, K., Lorenson, T.D. and Khutorskoy, M.D., 1999. Gas hydrate accumulation at the Håkon Mosby Mud Volcano. Geo-Marine Letters, 19: 57-67.

Grant, N.J. and Whiticar, M.J., 2002. Stable carbon isotopic evidence for methane oxidation in plumes above Hydrate Ridge, Cascadia Oregon Margin. Global Biochemical Cycles, 16(4): 71-1 - 71-13.

Grasshoff, K., Ehrhardt, M. and Kremling, K., 1997. Methods of seawater analysis. Verlag Chemie, Gulf Publishing, Houston, 757-773 pp.

Han, X., Suess, E., Sahling, H. and Wallmann, K., 2004. Fluid venting activity on the Costa Rica Margin: New results from authigenic carbonates. International Journal Earth Science (Geologische Rundschau), 93: 596-611.

Heeschen, K., 2002. Processes and fluxes controlling methane in different marine settings: Continental margins of Cascadia and Costa Rica and the Weddell Basin, Christian-Albrechts-Universität, Kiel, 128 pp.

Heeschen, K.U., Collier, R.W., de Angelis, M.A., Suess, E., Rehder, G., Linke, P. and Klinkhammer, G.P., subm. Methane sources, distributions, and fluxes from cold vent sites at Hydrate Ridge, Cascadia Margin. Global Biochemical Cycles.

Judd, A.G., Hovland, M., Dimitrov, L.I., Garcia Gil, S. and Jukes, V., 2002. The geological methane budget at continental margins and its influence on climate change. Geofluids, 2: 109-126.

Katz, M.E., Pak, D.K., Dickens, G.R. and Miller, K.G., 1999. The source and fate of massive carbon input during the Latest Paleocene Thermal Maximum. Science, 286(19): 1531-1533.

Kvenvolden, K.A., Lorenson, T.D. and Reeburgh, W.S., 2001. Attention turns to naturally occuring methane seepage. EOS, 82: 457.

Lallemand, S. and Le Pichon, X., 1987. Coulomb wedge model applied to the subduction of seamounts in the Japan Trench. Geology, 15: 1065-1069.

Lammers, S. and Suess, E., 1994. An improved head-space analysis method for methane in seawater. Mar. Chem., 47: 115-125.

Lein, A., Vogt, P., Crane, K., Egorov, A. and Ivanov, M., 1999. Chemical and isotopic evidence for the nature of the fluid in CH_4-containing sediments of the Håkon Mosby Mud Volcano. Geo-Marine Letters, 19: 76-83.

Linke, P., Suess, E., Torres, M., Martens, V., Rugh, W.D., Ziebis, W. and Kulm, L.D., 1994. In situ measurement of fluid flow from cold seeps at active continental margins. Deep-Sea Res. Pt.I, 41(4): 721-739.

Luff, R. and Wallmann, K., 2003. Fluid flow, methane fluxes, carbonate precipitation and biogeochemical turnover in gas hydrate-bearing sediments at Hydrate Ridge, Cascadia Margin: Numerical modeling and mass balances. Geochimica et Cosmochimica Acta, 67(18): 3403-3421.

Paull, C.K., Lorenson, T.D., Borowski, W.S., Ussler III, W., Olsen, K. and Rodriguez, N.M., 2000. 7. Isotopic composition of CH_4, CO_2 species, and sedimentary organic matter within samples from the Blake Ridge: Gas source implications. In: C.K. Paull, R. Matsumoto, P.J. Wallace and W.P. Dillon (Editors), Proceedings of the Ocean Drilling Program, Scientific Results. Ocean Drilling Program, College Station, TX, pp. 67-78.

Ranero, C.R. and Thierer, P.O., 2002. Multibeam bathymetry. In: W. Weinrebe and E. Flueh (Editors), RV Sonne, Cruise Report SO 163, Subduction I, Balboa-Caldera-Balboa (March 13 - May 21, 2002). GEOMAR, Kiel, pp. 55-68.

Ranero, C.R. and von Huene, R., 2000. Subduction erosion along the Middle America convergent margin. Nature, 404: 748-752.

Reed, D.L., Silver, E.A., Tagudin, J.E., Shipley, T.H. and Vrolijk, P., 1990. Relations between mud volcanoes, thrust deformation, slope sedimentation, and gas hydrate, offshore north Panama. Marine and Petroleum Geology, 7: 44-54.

Rehder, G., 1999. Quellen und Senken marinen Methans zwischen Schelf und offenem Ozean, GEOMAR, Kiel.

Sahling, H., Brückmann, W., Scholten, J., Soeding, E. and Suess, E., 2003. Seafloor observations. In: E. Söding, K. Wallmann, E. Suess and E. Flueh (Editors), RV METEOR, Cruise Report M54/2+3, Fluids and subduction Costa Rica 2002. GEOMAR, Kiel.

Soeding, E., Wallmann, K., Suess, E. and Flueh, E., 2003. RV METEOR Cruise Report M54/2+3 Fluids and Subduction Costa Rica 2002. GEOMAR Report, 111, Kiel, 366 pp.

Suess, E., Bohrmann, G., von Huene, R., Linke, P., Wallmann, K., Lammers, S., Sahling, H., Winckler, G., Lutz, R.A. and Orange, D., 1998. Fluid venting in the eastern Aleutian subduction zone. J. Geophys. Res., 103(B2): 2597-2614.

Tissot, B.P. and Welte, D.H., 1984. Petroleum Formation and Occurrence. Springer Verlag, Heidelberg.

Torres, L.M., McManus, J., Hammond, D.E., de Angelis, M.A., Heeschen, K.U., Colbert, S.L., Tryon, M.D., Brown, K.M. and Suess, E., 2002. Fluid and chemical fluxes in and out of sediments hosting methane hydrate deposits on Hydrate Ridge, OR, I: Hydrological provinces. Earth Planet. Sc. Lett., 201: 525-540.

Tryon, M.D., Brown, K.M., Torres, M.E., Trehu, A.M., McManus, J. and Collier, R.W., 1999. Measurements of transience and downward fluid flow near episodic methane gas vents, Hydrate Ridge, Cascadia. Geology, 27(12): 1075-1078.

Tsunogai, U., Yoshida, N., Ishibashi, J. and Gamo, T., 2000. Carbon isotopic distribution of methane in deep-sea hydrothermal plume, Myojin Knoll Caldera, Izu-Bonin arc: Implications for microbial methane oxidation in the oceans and applications to heat flux estimation. Geochimica et Cosmochimica Acta, 64(14): 2439-2452.

Valentine, D.L., Blanton, D.C., Reeburgh, W.S. and Kastner, M., 2001. Water column methane oxidation adjacent to an area of active hydrate dissociation, Eel River Basin. Geochimica et Cosmochimica Acta, 65(16): 2633-2640.

von Huene, R., Ranero, C.R. and Vannucchi, P., 2004. Generic model of subduction erosion. Geology, 32(10): 913-916.

von Huene, R., Ranero, C.R. and Watts, P., 2003. Tsunamigenic slope failure along the Middle America Trench in tw tectonic settings. Marine Geology, 3415: 1-15.

von Huene, R., Ranero, C.R. and Weinrebe, W., 2000. Quaternary convergent margin tectonics of Costa Rica, segmentation of the Cocos Plate, and Central American volcanism. Tectonics, 19(2): 314-334.

Watanabe, S., Tsurushima, N., Kusakabe, M. and Tsunogai, S., 1995. Methane in Izena Cauldron, Okinawa Trough. Journal of Oceanography, 51: 239-255.

Weinrebe, W. and Flueh, E., 2002. RV Sonne, Cruise Report SO 163, Subduction I, Balboa-Caldera-Balboa (March 13 - May 21, 2002). GEOMAR Report, 106: 534.

Wessel, P. and Smith, W.H.F., 1998. New, Improved Version of Generic Mapping Tools Released,. EOS Trans., AGU, 79(47): 579.

Whiticar, M.J., 1996. Isotope tracking of microbial methane formation and oxidation. Mitt. Internat. Verein. Limnol., 25: 39-54.

Whiticar, M.J., 1999. Carbon and hydrogen isotope systematics of bacterial formation and oxidation of methane. Chemical Geology, 161: 291-314.

Whiticar, M.J. and Faber, E., 1986. Methane oxidation in sediment and water column environments - Isotope evidence. Organic Geochemistry, Vol. 10: 759-768.

Variations in CH_4 seepage from mud extrusions and landslides offshore Costa Rica affected by seismo-tectonics

Susan Mau[a,*], Gregor Rehder[b,a], Ivonne G. Arroyo[a], Jürgen Gossler[a], and Erwin Suess[b,a]

[a] Sonderforschungsbereich 574, Kiel University, Wischhofstr. 1-3, 24148 Kiel, Germany

[b] IFM-GEOMAR Leibniz-Institut für Meereswissenschaften an der Universität Kiel, Wischhofstr. 1-3, 24148 Kiel, Germany

* corresponding author: Susan Mau, smau@ifm-geomar.de, Fax: +49-431-600-2916

Abstract

Repeated measurements of CH_4 concentrations in the bottom-near water column above different cold vent sites at the Pacific margin off Costa Rica indicate long-term variations of methane release. Methane is emitted from mud extrusions and landslides in 1000 – 2300 m water depth. CH_4 concentrations were measured in spring and autumn 2002, autumn 2003, and are compared with data from 1999. The results show higher CH_4 concentrations above all observed vent sites in 1999 and 2002 correlating with major earthquakes that occurred in these years, whereas the CH_4 content was diminished in 2003 – a year of significantly lower seismic activity. Some other potential causes for our observations, like seasonality or changes in bottom current velocity, are ruled out. The largest variations of the methane plume were observed above mud extrusions, which are located above faults and, thus, more strongly affected by tectonic movements. This supports the contention that earthquake activity has an impact on methane seepage.

Introduction

Natural methane seeps of varying intensity are found along most convergent continental margins. Several of these sites have been investigated e.g. at the Cascadian Margin (Suess et al., 1999), offshore Peru (Dia et al., 1993), and at the Barbados prism (Henry et al., 1996). Convergent margins are crucial regions in terms of element recycling (Moore and Vrolijk, 1992); fluids and volatiles are mobilized due to the compaction of sediments that accrete in or subduct beneath margin wedges. CH_4 is one of the compounds migrating from various sediment depths towards the sediment-water-interface. Most of it becomes oxidized

anaerobically in the near-seafloor sediments leading to the precipitation of authigenic carbonates (Kulm et al., 1986) providing energy for vent-specific biota (Sibuet and Olu, 1998). Only a fraction of CH_4 is injected into the water column, its extent depending on the fluid pathway, the efficiency of oxidation processes and the rate of upward flow.

Numerous cold seeps were examined in detail along the Costa Rican subduction zone over the past years. The vent sites are associated with mud extrusions and scarps (Fig. 1). Mud extrusions are driven by buoyancy forces that arise from bulk density differences between undercompacted fluid-rich clayey sediments and denser overlying sediments (Brown, 1990). All mud extrusions reported in this paper are located at the mid-slope of the margin wedge, 25 – 40 km landward from the Middle American Trench, in water depths ranging from 2300 – 1000 m. Off Middle America, submarine landslides are often triggered by seamount subduction, which leads to an temporary uplift of the continental wedge during passage of the mount and causes landslides on the seaward side of the uplift. Several circular uplifts associated with steep scarps have been identified along the continental margin of Costa Rica (von Huene et al., 2000), and are here referred to as scarps. All of these different structures show the typical signs of active methane seepage.

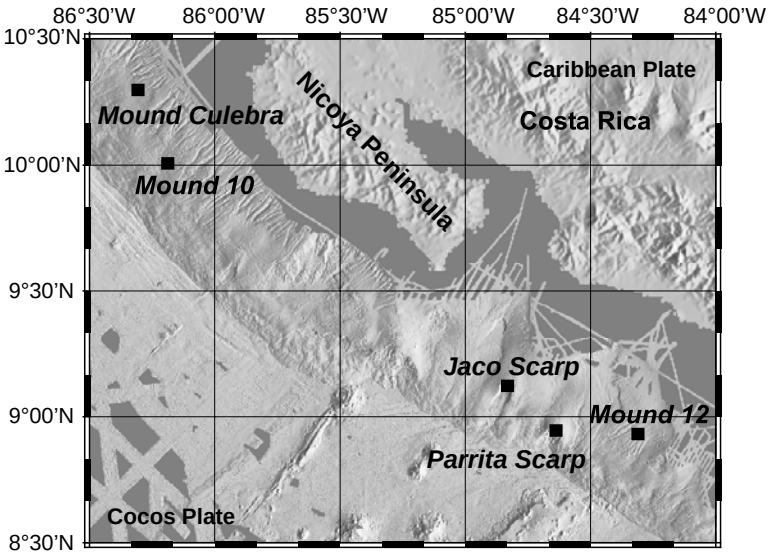

Fig. 1 Bathymetry of a segment of the Costa Rica margin showing the repeatedly sampled cold seep sites.

The amount of CH_4 discharging from cold seeps is difficult to estimate because of the high variability in space and time (Linke et al., 1994; Tryon et al., 1999) in particular on longer time scales. Using data of a survey in 1999 (Bohrmann et al., 2002) followed by intensive investigations of cold seeps offshore Costa Rica in 2002 and 2003, we had the opportunity to repeatedly measure CH_4 concentrations at several vent sites offshore Costa Rica (Fig. 1). These data combined with oceanographic and seismic data are used to identify possible reasons for the temporal variability observed.

Methods

CH_4 concentrations were measured in water samples collected with standard CTD/rosette equipment at 5 different cold seep sites offshore Costa Rica (Fig. 1). Sampling took place in May/April 2002 and September 2003 aboard RV SONNE (SO163-2 & SO173-3/4) and in August/September 2002 using RV METEOR (M54-2/3). For CH_4-analyses aboard a modification of the vacuum degassing method described by Lammers and Suess (1994) was used (Rehder, 1999). Replicate analysis of samples of a single hydrocast yield a precision of ± 10% for samples with CH_4 concentration < 2 nmol/L and ± 5% for CH_4 concentration > 2 nmol/L.

Current measurements were obtained by upward looking ADCPs (Acoustic Doppler Current Profiler; RD Instruments) attached to different lander devices and short moorings (~140 m) equipped with two Aanderaa current meters (RCM 8). The velocities given in Table 1 represent the average velocities for 1 day.

Earthquakes located in the area of Figure 1 were selected from the data set provided by the Red Sismológica Nacional (RSN: ICE-UCR). Earthquakes located by less than 5 stations and with a travel time error of > 0.6 s (rms) were excluded. The energy released by earthquakes was calculated using the Gutenberg-Richter formula (Gutenberg and Richter, 1954): $\log E = 11.8 + 1.5\ M_L$, where E is energy in TJ (Terra Joule) and M_L is local magnitude. Only earthquakes with a $M_L > 3$ were included in the calculation, because the seismological network was not capable to detect lower magnitude earthquakes completely.

Results

Long-term variations of methane venting were observed at all cold seep sites investigated along the continental slope of Costa Rica, regardless of their geological setting. The most dramatic changes occurred between August/September 2002 and September 2003. Figure 2 illustrates the decline of CH_4 concentration over this time at five seep sites. The CH_4 concentrations found in autumn 2003 are up to 94% lower than the concentrations recorded in 2002. The values above the NW-flank of Mound Culebra, which had increased from 15.9 nmol/L to 42.3 nmol/L between May 2002 and August 2002, dropped to 2.4 nmol/L in September 2003 (Fig. 2A). At the summit of Mound Culebra the CH_4 concentration decreased

from 21.4 nmol/L to 4.04 nmol/L between the investigations in 2002 and 2003 (Fig. 2B). The values above Mound 10 and Mound 12 indicate the same trend (Fig. 2C/D/E). CH_4 concentrations at the upper edge of the talus apron at Jaco Scarp seem to be highly variable with time. However, from August 2002 to September 2003, the maximum value decreased from 178.5 nmol/L to 101.8 nmol/L (Fig. 2F). Measurements at the SE-rim of Jaco Scarp indicate a drop by 30% (Fig. 2G). A decline of CH_4 concentrations was also determined at Parrita Scarp from 33.9 nmol/L to 19.7 nmol/L (Fig. 2H).

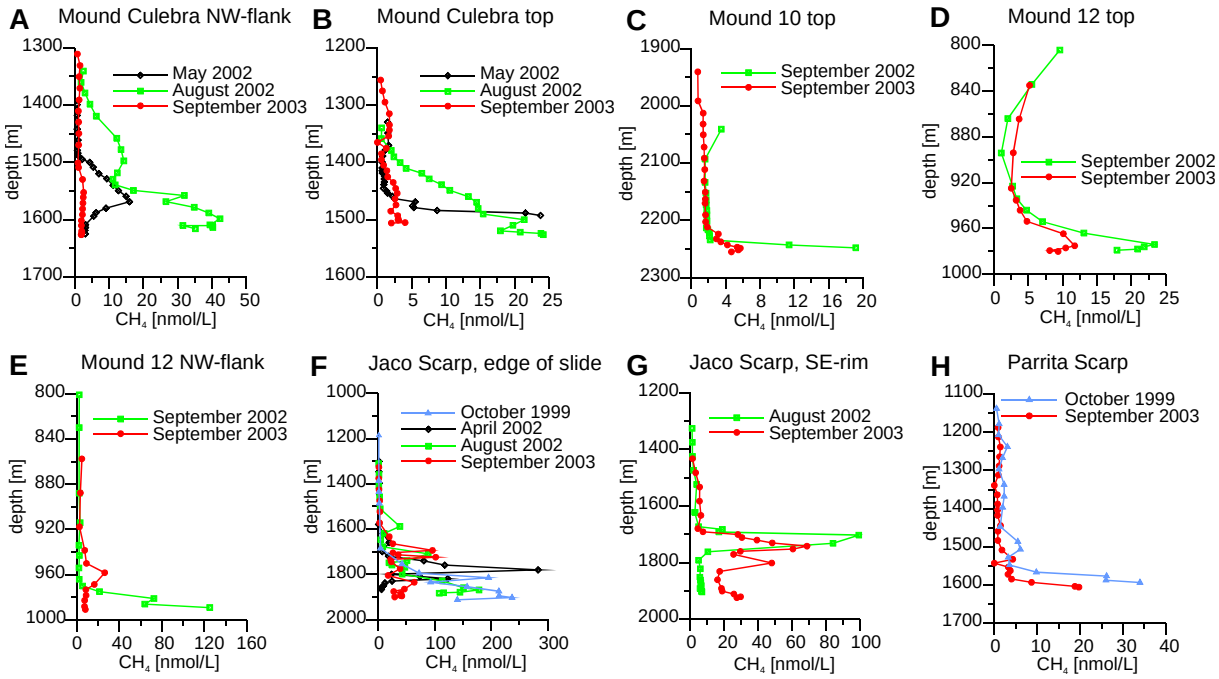

Fig. 2 CH_4 concentration versus depth at the several seep sites. Note different scales.

Discussion

Unlikely causes of the temporal changes observed

The compelling evidence of variations in methane emissions recorded interannually is seen in the large magnitude of change and the large areal extent. The variations cannot be caused by seasonal productivity changes, because we determined the CH_4 concentration during the same season in each year, in particularly in August/September 2002 and September 2003, when the most dramatic changes in CH_4 concentrations were observed.

Tidal control on fluid venting as a result of changing hydrostatic pressure has been shown for different fluid seep sites (Boles et al., 2001; Torres et al., 2002). However, the general

decrease in the inventory above repeatedly sampled locations disproves this mechanism as a reason for our observation. Sampling has been performed during all phases of the tidal cycles during all sampling campaigns.

Another potential mechanism which would produce lower concentrations even on constantly emitting locations is a change in the advective transport from the sources, i.e. changes in the oceanographic current regime. If seepage of methane-rich fluids was constant over time, a higher current velocity would cause faster dilution of CH_4, which in turn would decrease the CH_4 concentration in the water column. Current velocities were measured at Mound Culebra and at Mound 12 in 2002 as well as in 2003 (Tab. 1). Both data sets indicate similar flow velocities during these times. At Mound Culebra the velocities vary within two orders of magnitude in a time frame of 11 days in 2002. The data obtained in 2003 fall into the same range. The differences in current velocity at Mound 12 are less than those observed at Mound Culebra. The measurements of both years at Mound 12 vary within one order of magnitude and cover mainly the same range of current velocities (Tab. 1). Hence, the observed drop in CH_4 concentration is very unlikely related to changes in current flow.

Tab. 1 Averaged current velocities per day at the mud extrusions Mound Culebra and Mound 12. Minimum and maximum velocities are given when data over a certain depth range was recorded.

area/ water depth [m]	date	v_{min} [m/s]	v_{max} [m/s]	instrument
Mound Culebra				
1533-1513	16.-17.09.02	0.0104	0.0282	ADCP
	17.-18.09.02	0.0123	0.0234	ADCP
	18.-19.09.02	0.0002	0.0206	ADCP
	19.-20.09.02	0.0105	0.0147	ADCP
	20.-21.09.02	0.0031	0.0071	ADCP
	21.-22.09.02	0.0088	0.0232	ADCP
	22.-23.09.02	0.0171	0.0234	ADCP
	23.-24.09.02	0.0277	0.0388	ADCP
	24.-25.09.02	0.0330	0.0470	ADCP
	25.-26.09.02	0.0420	0.0536	ADCP
	26.-27.09.02	0.0376	0.0420	ADCP
1512	12.-13.09.03	0.0169		RCM 8
1510	20.-21.09.03	0.0338		ADCP
Mound 12				
1018-1014	19.-20.09.02	0.0106	0.0142	ADCP
1015-1010	23.-24.09.02	0.0420	0.0601	ADCP
1011	24.-25.09.03	0.0393		RCM 8
1003	24.-25.09.03	0.0117		ADCP
1011	25.-26.09.03	0.0161		RCM 8
1003	25.-26.09.03	0.0054		ADCP
1011	26.-27.09.03	0.0297		RCM 8
1003	26.-27.09.03	0.0275		ADCP

Correlation to earthquake activity

The decline in CH_4 concentration could be connected to changes in seismic activity, i.e. earthquakes. The seepage sites are situated above a convergent plate boundary, an area of pronounced and continuous seismic activity. The relationship between methane venting, geological structures, and seismic activity in the marine realm was recently hypothesized by Obzhirov et al. (2004) and Shakirov et al. (2004) based on methane data and earthquake events in the Sea of Okhotsk. The vent sites in the Okhotsk Sea occur at a strike slip plate boundary. Obzhirov et al. (2004) observed new gas flares along the North-East Sakhalin Shear Zone during periods of enhanced seismic activity between 1998 and 2002. Moreover, background CH_4 concentrations increased in the Okhotsk Sea after the 1988 Neftegorsk earthquake. Preceding an earthquake, Shakirov et al. (2004) recorded a gradual increase of gas emission and temperature over a mud volcano located at the Central Sakhalin Shear Zone. These examples illustrate the potential connection between plate tectonics, seismic activity, and methane seepage in the marine environment, although the data sets are less rigorous and were not systematically taken.

To identify a possible relationship of CH_4 seepage and seismic activity off Costa Rica, we compared preliminary earthquake data of 1999, 2002, and 2003 provided by the RSN. Overall seismic activity was diminished in 2003 compared to 1999 and 2002. However, if only the sampling periods are considered, similar ranges were obtained in view of the number of earthquakes and the amount of energy released (Fig. 3). In contrast, the total number of earthquakes recorded per year was less in 2003 than in 1999 and 2002 along this part of subduction zone (Fig. 3). The number of earthquakes with magnitudes ≥ 4 was also less. The high number of earthquakes in 1999 and 2002 is mainly the consequence of the two major events which occurred in these years. The large earthquake in 1999 as well as the one in 2002 have been located north-west of Osa Peninsula. 300 aftershocks have been reported following the M_W 6.9 earthquake on 20th of August 1999 (DeShon et al., 2003). The hypocenter was located in 21 km depth, near the plate interface, reflecting the interactions of the plates along the Central American subduction zone. On the 16th of June 2002, a large M_W 6.4 earthquake occurred again near the plate interface (DeShon et al., 2003). We suggest that the changes in CH_4 concentration are mainly related to the large events associated with major shifts along the subduction zone.

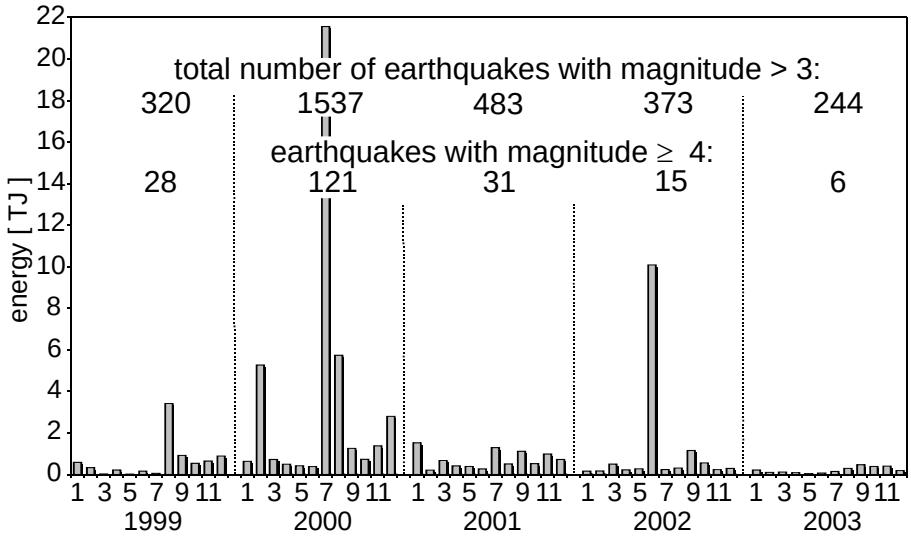

Fig. 3 Energy released per month by earthquakes of magnitude > 3 in the area of Fig. 1 from 1999 to 2003; energy was calculated from the local magnitude using the Gutenberg-Richter magnitude-energy relation.

The measured CH_4 anomalies along the margin of Middle America do not correspond one-to-one to the earthquake data. This was also noted by other investigations relating geochemical anomalies and seismicity (King, 1986). For example, the time scales of the occurrence of geochemical anomalies induced by seismic energy reported in literature vary widely. Obzhirov (2004) observed increasing CH_4 concentration in the water column several years prior and subsequent to 1995 – a year in which a number of earthquakes occurred. King (1986) showed in an overview on gas geochemistry applied to earthquake prediction on land, that gas concentrations change few hours to many months before large earthquakes occurred. In our case, higher CH_4 concentrations were measured two months after the main energy release in 1999, two months preceding and two months following the earthquake in 2002 corresponding to the time scales reported. Favara et al. (2001) and Italiano (2001) measured variations in fluid and gas venting in the Umbria region (Italy) during the 1997 – 1998 seismic swarm. However, they could not relate the anomalies to a single event. This suggests that geochemical anomalies are not connected solely to the time of an earthquake. Instead the anomalies are assumed to be linked to the entire seismogenic process including the slow deformation process and the sharp release of elastic energy (Favara et al., 2001; Italiano et al., 2001).

The decline in CH_4 concentration is more pronounced at the mud extrusions than at the scarps. The maximum concentrations observed above the mud extrusions in September 2003 do not even reach 50% of the maxima in the years before, whereas the maxima at the scarps

reach at least 55% of the values of the previous year (Fig. 2). In contrast to the scarps, mud extrusions are situated above deep-seated faults. Hensen et al. (2004) showed that one endmember of the fluids expelled from mud extrusions originate from 10 – 15 km depth, i.e. from the subducting sediments, migrating most likely upwards along the faults. Ascending fluids push the zone of anaerobic oxidation of methane into shallow sediment depth or even through the sediment-water interface. Thus, higher fluid discharge results in enhanced CH_4 seepage. Active faults are weak parts of the crust and thus, it is not surprising that gases and fluids escape along this zones of least resistance (King, 1986; Favara et al., 2001). Tectonic strain may be greatly amplified (King, 1986) at active faults, and so the influence of seismic activity on fluid pathways connected to these geological structures is expected to be high, in accordance to the observations at mud extrusions related to active faults. In contrast, the influence of tectonic activity is less pronounced at scarps, where gas and fluid escape is mainly a result of the exposure of deeper sedimentary layers, hosting reduced geochemical compounds at elevated pore pressures. Thus, CH_4 concentration vary less at vent sites related to scarps.

Summary

CH_4 concentration decreased drastically from autumn 2002 to autumn 2003 in the water column above mud extrusions and in the area of scarps offshore Costa Rica. The decline could not be related to seasonal, tidal, and oceanographic variations. Instead, we identified enhanced methane seepage in years in which great earthquakes occurred along the seismogenic zone of Central America. Methane seepage from mud extrusions were considerably more affected than seeps at scarps because mud extrusions are located above deep-seated faults where tectonic stresses and strains are amplified. At least some temporal variations of methane venting in the ocean appear to be caused by changes in seismic activity.

Acknowledgements

Many thanks to scientists, masters, and crews of research cruises SO 163, M 54, and SO 173 for their support, information, and discussion. Thanks also to the Red Sismológica Nacional (ICE-UCR) for providing the earthquake data. This publication is contribution no. 64 of the SFB 574 “Volatiles and Fluids in Subduction Zones” at the University of Kiel.

References

Bohrmann, G., Jung, C., Heeschen, K., Weinrebe, W., Baranov, B., Cailleau, B., Heath, R., Hühnerbach, V., Hort, M., Masson, D. and Schaffer, I., 2002. Widespread fluid expulsion along the seafloor of Costa Rica convergent margin. Terra Nova, 14: 69-79.

Boles, J.R., Clark, J.F., Leifer, I. and Washburn, L., 2001. Temporal variation in natural methane seep rate due to tides, Coal Oil Point area, California. J. Geophys. Res., 106(C11): 27077-27086.

Brown, K.M., 1990. The Nature and Hydrogeologic Significance of Mud Diapirs and Diatremes for Accretionary Systems. J. Geophys. Res., 95(B6): 8969-8982.

DeShon, H.R., Schwartz, S.Y., Bilek, S.L., Dorman, L.M., Gonzalez, V., Protti, J.M., Flueh, E.R. and Dixon, T.H., 2003. Seismogenic zone structure of the southern Middle America Trench, Costa Rica. J. Geophys. Res., 108(B10): 2491-2505.

Dia, A.N., Aquilina, L., Boulègue, J., Bourgois, J., Suess, E. and Torres, M., 1993. Origin of fluids and related barite deposits at the vent sites along the Peru convergent margin. Geology, 21: 1099-1102.

Favara, R., Italiano, F. and Martinelli, G., 2001. Earthquake-induced chemical changes in the thermal waters of the Umberia region during the 1997-1998 seismic swarm. Terra Nova, 13: 227-233.

Gutenberg, B. and Richter, C.F., 1954. Seismicity of the earth and associated phenomena, 310. Princeton University Press.

Henry, P., Le Pichon, X., Lallement, S., Lance, S., Martin, J.B., Foucher, J.-P., Fiala-Medioni, A., Rostek, F., Guilhaumou, N., Pranal, V. and Castrec, M., 1996. Fluid flow in and around a mud volcano field seaward of the Barbados accretionary wedge: Results from Manon cruise. J. Geophys. Res., 101(B9): 20297-20323.

Hensen, C., Wallmann, K., Schmidt, M., Ranero, C. and Suess, E., 2004. Fluid expulsion related to mud volcanism at Costa Rica continental margin - a window to the subducting slab. Geology, 32: 201-204.

Italiano, F., Martinelli, G. and Nuccio, P.M., 2001. Anomalies of mantle-derived helium during the 1997-1998 seismic swarm of Umbria-Marche, Italy. Geophys. Res. Lett., 28(5): 839-842.

King, C.-Y., 1986. Gas geochemistry applied to earthquake prediction: An overview. J. Geophys. Res., 91(B12): 12269-12281.

Kulm, L.D., Suess, E., Moore, J.C., Carson, B., Lewis, B.T., Ritger, S.D., Kadko, D.C., Thornburg, T.M., Embley, R.W., Rugh, W.D., Massoth, G.J., Langseth, M.G., Cochrane, G.R. and Scamman, R.L., 1986. Oregon Subduction Zone: Venting, Fauna, and Carbonates. Science, 231: 561-566.

Lammers, S. and Suess, E., 1994. An improved head-space analysis method for methane in seawater. Mar. Chem., 47: 115-125.

Linke, P., Suess, E., Torres, M., Martens, V., Rugh, W.D., Ziebis, W. and Kulm, L.D., 1994. In situ measurement of fluid flow from cold seeps at active continental margins. Deep-Sea Res. Pt.I, 41(4): 721-739.

Moore, J.C. and Vrolijk, P., 1992. Fluids in accretionary prisms. Rev. Geophys., 30(2): 113-135.

Obzhirov, A., Shakirov, R., Salyuk, A., Suess, E., Biebow, N. and Salomatin, A., 2004. Relation between methane venting, geological structure and seismo-tectonics in the Okhotsk Sea. Geo-Mar. Lett., 24: 135-139.

Rehder, G., 1999. Quellen und Senken marinen Methans zwischen Schelf und offenem Ozean, GEOMAR, Kiel.

Shakirov, R., Obzhirov, A., Suess, E., Salyuk, A. and Biebow, N., 2004. Mud volcanoes and gas vents in the Okhotsk Sea area. Geo-Mar. Lett., 24(3): 140-149.

Sibuet, M. and Olu, K., 1998. Biogeography, biodiversity and fluid dependence of deep-sea cold-seep communities at active and passive margins. Deep-Sea Res. Pt.II, 45: 517-567.

Suess, E., Torres, M.E., Bohrmann, G., Collier, R.W., Greinert, J., Linke, P., Rehder, G., Trehu, A., Wallmann, K., Winckler, G. and Zuleger, E., 1999. Gas hydrate destabilization: enhanced dewatering, benthic material turnover and large methane plumes at the Cascadia convergent margin. Earth Planet. Sc. Lett., 170: 1-15.

Torres, L.M., McManus, J., Hammond, D.E., de Angelis, M.A., Heeschen, K.U., Colbert, S.L., Tryon, M.D., Brown, K.M. and Suess, E., 2002. Fluid and chemical fluxes in and out of sediments hosting methane hydrate deposits on Hydrate Ridge, OR, I: Hydrological provinces. Earth Planet. Sc. Lett., 201: 525-540.

Tryon, M.D., Brown, K.M., Torres, M.E., Trehu, A.M., McManus, J. and Collier, R.W., 1999. Measurements of transience and downward fluid flow near episodic methane gas vents, Hydrate Ridge, Cascadia. Geology, 27(12): 1075-1078.

von Huene, R., Ranero, C.R. and Weinrebe, W., 2000. Quaternary convergent margin tectonics of Costa Rica, segmentation of the Cocos Plate, and Central American volcanism. Tectonics, 19(2): 314-334.

Summary and Conclusions

Methane concentrations in the near-bottom water were measured in the vicinity of 15 vent sites in the research area of the "Sonderforschungsbereich 574" offshore Costa Rica and Nicaragua. Increased CH_4 concentrations were found at 14 sites, indicating active CH_4 emission. The CH_4 concentration profiles together with a short description of the vent sites and first interpretations can be found in the GEOMAR Reports 106, 111, and 115 (Flueh et al., 2004; Soeding et al., 2003; Weinrebe and Flueh, 2002). Emission of methane was discovered at mud extrusions and landslides. Several large-scale landslides, also called scarps, are created by seamount subduction. Four mud extrusions and one scarp were investigated in detail to explore the fate of CH_4 in the water column and to estimate the CH_4 output at these sites. Mud extrusions are abundant along continental slopes around the world. 81 mud extrusions have been found offshore Costa Rica and Nicaragua (Sahling et al., in prep.). Nevertheless, estimations of the total CH_4 input from submarine mud extrusions to the carbon budget of the ocean and atmosphere vary widely from 181 to 12891 Gg yr^{-1} in recent literature (Dimitrov, 2002; Kopf, 2003; Milkov et al., 2003). The present study contributes to the small data set currently existing on CH_4 outputs from mud extrusions and also provides the first estimate from such extrusions occurring along an erosive subduction zone. Hardly any CH_4 concentrations and no methane outputs have been reported up to date from submarine scarps. Hence, the detailed investigation of Jaco Scarp presents the first work on that subject. In addition, collection of data over several years in the research area made it possible to investigate long-term variations of methane seepage and their potential reasons.

Methane is released from these vent sites into deep, intermediate and subsurface waters. In general, the CH_4 plumes are confined to the vent sites because the rather low CH_4 output is quickly diluted. No indications of vent derived CH_4 reaching the atmosphere were found although the upwelling region of the Costa Rica Dome (CRD) is situated in the research area. However, the upwelling from the CRD does not extend deeper than ~500 m and the mean position of the dome is at 9°N and 90°W, i.e. 300 – 400 km away from the shallowest vent sites (Fiedler, 2002), suggesting no interference of venting and upwelling.

Two mechanisms control the extent of a CH_4 plume in the water column: mixing by ocean currents and aerobic oxidation. Methane from the mud extrusions becomes rapidly diluted by ocean currents, because the velocity of the ocean currents inducing mixing is faster than the

turnover by oxidation. The general CH_4 concentration above the mud extrusions is rather low, ~20 nmol L^{-1}. Valentine et al. (2001) reported a turnover time of a few years for a CH_4 concentration of ~20 nmol L^{-1} and de Angelis et al. (1993) a turnover time of weeks to months. In contrast, the efficiency of bottom currents is much higher; the currents transport and dilute the CH_4 within hours to days over the area of the mud extrusion. The fate of CH_4 at Jaco Scarp was deduced from the carbon isotopic signature of CH_4. The results show again that mixing dominates over oxidation. Still, oxidation can be observed along the walls of the scarp and in the center of the plume. Oxidation of CH_4 along the walls of the scarp is enhanced most likely due to the diminished current velocity and/or the availability of different components affecting oxidation whereas oxidation within the plume is enhanced as the result of higher CH_4 concentrations. However, our investigations indicate that mixing dominates generally at open structures like mud extrusions and scarps where ocean currents rapidly dilute vent-derived methane and at vent sites with rather low CH_4 emission where the oxidation rate is low. In contrast, oxidation has a stronger impact in closed structures like calderas (Tsunogai et al., 2000) where current flow is less and at vent sites of high CH_4 emission where oxidation rates are high (de Angelis et al., 1993; Valentine et al., 2001).

The main focus of this work is: how much methane is emitted into the ocean from mud extrusions and scarps located at an erosive subduction zone and how significant is their contribution to the global ocean carbon budget of 20 Tg yr^{-1} (Kvenvolden et al., 2001). Many cold seeps have been described in the literature, but only for a few of them the CH_4 output was estimated (Tab 1). Most of these published CH_4 outputs include the amount of CH_4 anaerobically oxidized in the sediments which amounts to 60 – 80%. Only the remaining methane breaches the sediment-water-interface and escapes into the ocean. Recent examples on that issue are presented by Linke et al. (subm.) who showed that 4.4 mol $m^{-2}yr^{-1}$ CH_4 escapes into the ocean whereas 5.9 mol $m^{-2}yr^{-1}$ is anaerobically oxidized at a site covered by bacterial mats at Mound 12 (Chapter II). Similarly, Drews et al. (subm.) point out that 80% of CH_4 is oxidized before reaching the sediment-water-interface at the Dvurechneskii mud extrusion located in the Black Sea. Hence, less methane than the published values suggest is emitted into the water.

We used two approaches to estimate the CH_4-output from mud extrusions. The first is based on seafloor observations and fauna-specific CH_4 emission rates and the second is based on an inventory derived from measurements of CH_4 concentrations in the water column and current

Tab. 1 Comparison of cold vent sites

location	geological setting	seafloor manifestations	depth of site [m]	mode of CH_4-venting	max. CH_4 conc. [nmol L^{-1}]	CH_4-output [mol yr^{-1}]	references
northern Peru convergent margin, subduction erosion	scarps, canyon	barite deposits, clams, tube worms, bacterial mats	2500 - 5400				Dia et al., 1993
fore-arc basin of Sunda Arc, Indonesia, - accretionary prism	intersection fault and anticline	clams, tube worms, bacterial mats, authigenic carbonates	2910 - 2920	gaseous, dissolved	~220		Wiedicke et al., 2002
Makran accretionary wedge off Pakistan	fault related canyon	clams, tube worms	2300 - 2580	dissolved	~45 in water		von Rad et al., 2000
	oriented along fault	bacterial mats, carbonates	350 - 800	gaseous, dissolved	~1600 in sediments		
eastern Nankai accretionary wedge off central Japan	intersection fault and ridge	clams, tube worms, carbonates	2000				Lallemand et al., 1992
Mediterranean ridge, accretionary prism	mud extrusion (Napoli)	clams, tube worms	> 1900	gaseous, dissolved			Cita et al., 1995
Mediterranean Ridge accretionary complex	mud extrusions (Milano and Napoli)		~1900			17 x 10^6 (Milano), 28 x 10^6 (Napoli) with AOM	Kopf and Behrmann, 2000
Mediterranean Ridge accretionary complex	fault controlled mud extrusion (Kazan)	tube worms, clams, bacterial mats, carbonates	2000		844	5 x 10^6 with AOM	Haese et al., 2003, Zitter et al., 2002
seaward of the Barbados accretionary wedge	mud diatremes (Atlanta and Cyclops)	clams, sponges (only Atlanta) outside of eye, carbonates (only Atlanta)	~4925 (Atlanta) ~4960 (Cyclops)			185 x 10^6 (Atlanta), 14 x 10^6 (Cyclops) with AOM	Henry et al., 1996
eastern Aleuten subduction zone	scarp, faults, ridges, canyon	bacterial mats, tube worms, clams, carbonate, barite	~4000 - 5500	dissolved	~7		Suess et al., 1998

Tab 1 continued

location	geological setting	seafloor manifestations	depth of site [m]	mode of CH_4-venting	max. CH_4 conc. [nmol L^{-1}]	CH_4-output [mol yr^{-1}]	references
Northern and Southern Hydrate Ridge (NHR and SHR), Cascadia accretionary wedge	intersection fault and ridge	carbonates, bacterial mats, clams, tube worms	590 (NHR), 790 (SHR)	gaseous, dissolved	4400 (NHR), 1400 (SHR)	33 x 10^6 (NHR), 23 x 10^6 (SHR)	Suess et al., 1999, Heeschen et al., subm.
Håkon Mosby mud volcano, Norwegian Sea, passive continental margin	mud extrusion	bacterial mats, carbonates	~1200	dissolved	340	6 x 10^6 with AOM	Damm et al., 2003, Ginsburg et al., 1999
Black Sea	fault controlled mud extrusion (Dvurechneskii)		2080	gaseous, dissolved		2 x 10^6	Drews et al., subm.
erosive convergent margin of Costa Rica	fault controlled mud extrusions (ME), scarps (SC)	carbonates, bacterial mats, clams, tube worms	1000 - 2400 (ME), 900 - 2400 (SC)	dissolved	107 (ME), 1500 (SC)	9 x 10^4 - 7 x 10^5 (ME), 3.9 x 10^6 (SC)	this study

velocities. The first approach yields $10^3 – 10^4$ mol yr^{-1} which is only a minor part of the CH_4 actually emitted at mud extrusions. This approach excludes all methane seepage that is too transient, too fast and too slow for faunal growths. In contrast, the estimates based on CH_4 concentration include all kinds of seepage and, thus, yield the total amount of CH_4 escaping into the water column. The estimates derived by this approach range between $10^4 – 10^5$ mol yr^{-1}. The estimated amounts of CH_4 emitted from mud extrusions offshore Costa Rica are lower compared to estimates published elsewhere (Tab. 1), even when the amount of anaerobically oxidized CH_4 is subtracted. This discrepancy could result from differences in the structural and tectonic setting. The mud extrusions offshore Costa Rica have been described as morphological mounds whereas the mud diatremes observed at the Barbados margin and the Håkon Mosby mud volcano off Norway were described as flat structures with an active central zone. Mound-like structures indicate the rise of mud with a rather low fluid and CH_4 content compared to flat structures like mud volcanoes and mud diatremes where less cohesive mud with a high portion of fluids and methane extrudes (Kopf, 2002). The reason for the different style and activity of the mud extrusions could be the erosional nature of the subduction zone which limits the accumulation of thick sedimentary sequences, usually the source of organic carbon for CH_4 formation.

Apparently, less methane is emitted at erosional margins considering solely mud extrusions, even though data of CH_4 outputs in the literature are too sparse (Tab. 1) to really substantiate this hypothesis. In addition, other vent sites have to be taken into account along erosional margins which are uncommon at accretionary subduction zones, for example scarps. The CH_4 output estimated from Jaco Scarp is the first one reported and higher than the CH_4 outputs per mud extrusion. Jaco Scarp emits ~10 times as much as a mud extrusion (taking the average CH_4 output from the four investigated mud extrusions); the CH_4 output is even higher than outputs from some hydrothermal sites (Tsunogai et al., 2000; Watanabe et al., 1995). Yet, other scarps offshore Costa Rica seem to be not as active. 307 Mg yr^{-1} (1 Mg = 10^6 g) are emitted from the 48 mud extrusions discovered in the area between 8°30’N to 10°30’N and 84°00’W to 86°30’W assuming constant CH_4 seepage and a similar amount of CH_4 discharged as from the investigated mud extrusions. A similar approach can be undertaken for the four scarps shown in Figure 1 of Chapter III (Hühnerbach et al., subm.). CH_4 analysis revealed much higher CH_4 concentrations in Jaco Scarp (360 nmol L^{-1}) than in Parrita Scarp (18 nmol L^{-1}). Thus, venting activity of 5% at Parrita Scarp compared to Jaco Scarp is assumed. Seafloor surveys at the other two scarps indicate also CH_4 venting, but

unfortunately, no CH_4 analysis have been carried out so far at these scarps. For estimating the total CH_4 output from all scarps, somewhat arbitrary, a similar venting activity as at Parrita Scarp may be assumed. Accordingly, 70 Mg yr^{-1} would be emitted from all four scarps. However, one has to keep in mind that venting at scarps appears to be strongly dependent on the exposed layers and the amount of reduced chemical species. Based on this order-of-magnitude estimate of CH_4 output from the scarps, a total of 377 Mg yr^{-1} is added to the carbon budget of the ocean from this 350 km wide part of an erosional subduction margin. The estimate amounts to ~0.2 ‰ of the global CH_4 output from the seafloor, which lies in the order of 20 Tg yr^{-1}(Kvenvolden et al., 2001). This rather minor contribution does not include small landslides offshore Costa Rica, which also showed venting activity, and possible higher CH_4 outputs from geological structures, which have not been investigated in detail. More investigations like the ones presented in Chapter II and III at other structures are needed to clarify the significance of natural CH_4 seepage from continental slopes.

Methane seepage is highly variable in space and time. Spatial variations have been reported by Tryon et al. (1999) and Torres et al. (2002). Short-term variations can be explained by changes in seafloor pressure associated with tides, ocean swell, storm surges, bottom current velocities, and near surface sediment hydrology (Boles et al., 2001). Long-term variations, in contrast, are one of the least documented changes. The measured long-term variations offshore Costa Rica could not be related to seasonality or oceanographic changes. Instead, a correlation with earthquake data was identified. Similar results were recently reported by Obzhirov (2004) and Shakirov (2004) who hypothesized a relationship between seismic activity and CH_4 seepage in marine settings. The CH_4 emission offshore Costa Rica was increased in years of occurrence of large earthquakes and diminished in 2003 – a year without a major earthquake along the subduction zone. The drop in CH_4 concentration was enhanced at mud extrusions situated above deep-seated faults compared to scarps where CH_4 escapes from stratigraphic layers. Faults are weak zones in the crust and more strongly affected by tectonic movements compared to stratigraphic layers. Thus, the larger drop at the mud extrusions support the relationship between methane seepage and seismic activity. These temporal changes of CH_4 emission should be kept in mind regarding our estimates of CH_4 outputs as well as reported ones which have only a limited validity.

The investigation of four mud extrusions and one scarp along the convergent margin off Costa Rica and the estimates of their CH_4 output is the first comprehensive study of CH_4 seepage at

an erosive continental margin. As almost 50% of the worlds subduction zones are erosive in nature (von Huene and Scholl, 1991) these results and their temporal variations are of great importance for estimations of the global methane output in general and of specific geological structures (e.g. mud extrusions) in particular.

References

Boles, J.R., Clark, J.F., Leifer, I. and Washburn, L., 2001. Temporal variation in natural methane seep rate due to tides, Coal Oil Point area, California. J. Geophys. Res., 106(C11): 27077-27086.

Cita, M.B., Woodside, J.M., Ivanov, M.K., Kidd, R.B., Limonov, A.F. and 2, S.S.o.C.T.-L., 1995. Fluid venting from a mud volcano in the Mediterranean Ridge diapiric belt. Terra Nova, 7: 453-458.

Damm, E. and Budeus, G., 2003. Fate of vent-derived methane in seawater above the Håkon Mosby mud volcano (Norwegian Sea). Marine Chemistry, 82: 1-11.

de Angelis, M.A., Lilley, M.D., Olson, E.J. and Baross, J.A., 1993. Methane oxidation in deep-sea hydrothermal plumes of the Endeavour Segment of the Juan de Fuca Ridge. Deep-Sea Research I, 40(6): 1169-1186.

Dia, A.N., Aquilina, L., Boulègue, J., Bourgois, J., Suess, E. and Torres, M., 1993. Origin of fluids and related barite deposits at the vent sites along the Peru convergent margin. Geology, 21: 1099-1102.

Dimitrov, L.I., 2002. Mud volcanoes - the most important pathway for degassing deeply buried sediments. Earth-Science Reviews, 59: 49-76.

Drews, M., Wallmann, K., Aloisi, G. and Bohrmann, G., subm. Fluid expulsion from the Dvurechenskii mud volcano (Black Sea), Part II: Methane fluxes and their relevance to the Black Sea methane cycle. Earth and Planetary Science Letters.

Fiedler, P.C., 2002. The annual cycle and biological effects of the Costa Rica Dome. Deep-Sea Research I, 49: 321-338.

Flueh, E., Soeding, E. and Suess, E., 2004. RV SONNE Cruise Report SO173/1, 3 & 4 Subduction II: The Central American Continental Margin. GEOMAR Report, 115, Kiel, 491 pp.

Ginsburg, G.D., Milkov, A.V., Soloviev, V.A., Egorov, A.V., Cherkashev, G.A., Vogt, P.R., Crane, K., Lorenson, T.D. and Khutorskoy, M.D., 1999. Gas hydrate accumulation at the Håkon Mosby Mud Volcano. Geo-Marine Letters, 19: 57-67.

Haese, R.R., Meile, C., van Cappellen, P. and de Lange, G.J., 2003. Carbon geochemistry of cold seeps: Methane fluxes and transformation in sediments from Kazan mud volcano, eastern Mediterranean Sea. Earth and Planetary Science Letters, 212: 361-375.

Heeschen, K.U., Collier, R.W., de Angelis, M.A., Suess, E., Rehder, G., Linke, P. and Klinkhammer, G.P., subm. Methane sources, distributions, and fluxes from cold vent sites at Hydrate Ridge, Cascadia Margin. Global Biochemical Cycles.

Henry, P., Le Pichon, X., Lallement, S., Lance, S., Martin, J.B., Foucher, J.-P., Fiala-Medioni, A., Rostek, F., Guilhaumou, N., Pranal, V. and Castrec, M., 1996. Fluid flow in and around a mud volcano field seaward of the Barbados accretionary wedge: Results from Manon cruise. J. Geophys. Res., 101(B9): 20297-20323.

Hühnerbach, V., Masson, D.G., Bohrmann, G., Bull, J.M. and Weinrebe, W., subm. Deformation and submarine landsliding caused by seamount subduction beneath the Costa Rican continental margin new insights from high-resolution sidescan sonar data. Geological Society.

Kopf, A. and Behrmann, J.H., 2000. Extrusion dynamics of mud volcanoes on the Mediterranean Ridge accretionary complex. In: B. Vendeville, Y. Mart and J.-L. Vigneresse (Editors), From the Artic to the Mediterranean: Salt, shale, and igneous diapirs in and around Europe. Journal of the Geological Society, Spec. Publ., London, pp. 169-204.

Kopf, A.J., 2002. Significance of mud volcanism. Reviews of Geophysics, 40: 1-52.

Kopf, A.J., 2003. Global methane emission through mud volcanoes and its past and present impact on the Earth's climate. International Journal Earth Science, 92: 806-816.

Kvenvolden, K.A., Lorenson, T.D. and Reeburgh, W.S., 2001. Attention turns to naturally occuring methane seepage. EOS, 82: 457.

Lallemand, S. and Le Pichon, X., 1987. Coulomb wedge model applied to the subduction of seamounts in the Japan Trench. Geology, 15: 1065-1069.

Linke, P., Wallmann, K., Suess, E., Hensen, C. and Rehder, G., subm. In-situ benthic fluxes from an intermittently active mud volcano at the Costa Rica convergent margin. Earth and Planetary Science Letters.

Milkov, A.V., Sassen, R., Apanasovich, T.V. and Dadashev, F.G., 2003. Global gas flux from mud volcanoes: A significant source of fossil methane in the atmoshere and the ocean. Geophysical Research Letters, 30(2): 9-1 - 9-4.

Obzhirov, A., Shakirov, R., Salyuk, A., Suess, E., Biebow, N. and Salomatin, A., 2004. Relation between methane venting, geological structure and seismo-tectonics in the Okhotsk Sea. Geo-Mar. Lett., 24: 135-139.

Shakirov, R., Obzhirov, A., Suess, E., Salyuk, A. and Biebow, N., 2004. Mud volcanoes and gas vents in the Okhotsk Sea area. Geo-Mar. Lett., 24(3): 140-149.

Soeding, E., Wallmann, K., Suess, E. and Flueh, E., 2003. RV METEOR Cruise Report M54/2+3 Fluids and Subduction Costa Rica 2002. GEOMAR Report, 111, Kiel, 366 pp.

Suess, E., Bohrmann, G., von Huene, R., Linke, P., Wallmann, K., Lammers, S., Sahling, H., Winckler, G., Lutz, R.A. and Orange, D., 1998. Fluid venting in the eastern Aleutian subduction zone. J. Geophys. Res., 103(B2): 2597-2614.

Suess, E., Torres, M.E., Bohrmann, G., Collier, R.W., Greinert, J., Linke, P., Rehder, G., Trehu, A., Wallmann, K., Winckler, G. and Zuleger, E., 1999. Gas hydrate destabilization: enhanced dewatering, benthic material turnover and large methane plumes at the Cascadia convergent margin. Earth Planet. Sc. Lett., 170: 1-15.

Torres, L.M., McManus, J., Hammond, D.E., de Angelis, M.A., Heeschen, K.U., Colbert, S.L., Tryon, M.D., Brown, K.M. and Suess, E., 2002. Fluid and chemical fluxes in and out of sediments hosting methane hydrate deposits on Hydrate Ridge, OR, I: Hydrological provinces. Earth Planet. Sc. Lett., 201: 525-540.

Tryon, M.D., Brown, K.M., Torres, M.E., Trehu, A.M., McManus, J. and Collier, R.W., 1999. Measurements of transience and downward fluid flow near episodic methane gas vents, Hydrate Ridge, Cascadia. Geology, 27(12): 1075-1078.

Tsunogai, U., Yoshida, N., Ishibashi, J. and Gamo, T., 2000. Carbon isotopic distribution of methane in deep-sea hydrothermal plume, Myojin Knoll Caldera, Izu-Bonin arc: Implications for microbial methane oxidation in the oceans and applications to heat flux estimation. Geochimica et Cosmochimica Acta, 64(14): 2439-2452.

Valentine, D.L., Blanton, D.C., Reeburgh, W.S. and Kastner, M., 2001. Water column methane oxidation adjacent to an area of active hydrate dissociation, Eel River Basin. Geochimica et Cosmochimica Acta, 65(16): 2633-2640.

von Huene, R. and Scholl, D.W., 1991. Observations at convergent margins concerning
sediment subduction, subduction erosion and the growth of continental crust. Reviews of Geophysics, 29: 279-316.

von Rad, U., Berner, U., Delisle, G., Doose-Rolinski, H., Fecher, N., Linke, P., Lückge, A., Roeser, H.A., Schmaljohann, R., Wiedicke, M. and Party, S.s., 2000. Gas and fluid venting at the Makran accretionary wedge off Pakistan. Geo-Marine Letters, 20: 10-19.

Watanabe, S., Tsurushima, N., Kusakabe, M. and Tsunogai, S., 1995. Methane in Izena Cauldron, Okinawa Trough. Journal of Oceanography, 51: 239-255.

Weinrebe, W. and Flueh, E., 2002. RV Sonne, Cruise Report SO 163, Subduction I, Balboa-Caldera-Balboa (March 13 - May 21, 2002). GEOMAR Report, 106: 534.

Wiedicke, M., Sahling, H., Delisle, G., Faber, E., Neben, S., Beiersdorf, H., Marchig, V., Weiss, W., von Mirbach, N. and Afiat, A., 2002. Characteristics of an active vent in the fore-arc basin of the Sunda Arc, Indonesia. Marine Geology, 184: 121-141.

Zitter, T.A.C., Woodside, J.M., Huguen, C. and party, M.M.s., 18-19 April 2002. Fluid venting activity in the eastern Mediterranean Sea: observations from sidescan sonar and submersible surveys, NAC VI, Veldhoven, The Netherlands.

Acknowledgements

First of all I would like to thank Prof. Erwin Suess and most of all Gregor Rehder for enabling this work as well as for their advises and discussions which greatly improved this thesis. They taught me all I know about methane in sediments and the water column. Special thanks also to the other co-authors of the submitted and prepared papers for their constant help, information and discussion.

I am very thankful to all the members of the SFB 574 especially those working in building 8A, second floor. They all contributed at least a slight part to this thesis, e.g. Heidi Wehrmann (also called Thesaurus) always helped with her knowledge of English, Steffen Kutterolf and Oliver Bartdorff helped with nerving computer problems and with geological discussions, Christian Hensen for reading part of this work and for engaging me as office-plant-sitter during his absence, Jürgen Gossler and Michael Schnabel who explained me various aspects of earthquake data, and all the others for discussing scientific as well as other problems of life.

My thanks also to Roger Luff for computer support especially concerning Matlab. Also thanks to Emanuel Söding and Jens Greinert for their help with GMT.

I am very grateful to Peter Linke, all the technicians from building 15, Thomas Müller, Gerd Niehus, Antonius Kipping and Rolf Käse helping and teaching me to carry out water-current measurements. For the great help at sea I would like to thank most of all Karen Stange and Bert Mantzke, but also the many others helping or visiting the “methane lab”. Karen Stange also analyzed a great number of samples at the irm-GC/MS in Kiel extending greatly the isotopic-data set used in this study. I am very grateful to Bettina Domeyer and Anke Bleyer for their help preparing everything for the laboratory work on board and to the masters and crews of research cruises SO 163, M 54 and SO 173.

Special thanks to my friend Mark Elbing and my family who always supported and encouraged me.

These investigations were financially supported by the Deutsche Forschungsgemeinschaft in the framework of the Sonderforschungsbereich 574 “Volatiles and Fluids in Subduction Zones” at the University of Kiel.

list of stations – Subduction I – SONNE 163/2

Station No. SO163/2	Instrument	Date 2002	Latitude [N°]	Longitude [W°]	Depth [m]	Area
1	CTD	24-Apr	10°05.40	85°59.28	740	Northern Transect
2	CTD	24-Apr	10°00.84	86°03.83	1340	Northern Transect
3	CTD	24-Apr	09°00.02	87°05.15	3215	Northern Transect
4	CTD	25-Apr	09°30.00	86°35.29	2085	Northern Transect
5	CTD	28-Apr	09°48.90	86°16.23	4230	Northern Transect
6	CTD	28-Apr	09°56.13	86°09.24	2395	Northern Transect
7	CTD	29-Apr	09°06.90	84°50.85	1877	Jaco Scarp
8	CTD	1-May	09°07.67	84°50.32	1413	Jaco Scarp
9	CTD	1-May	09°08.30	84°49.93	955	Jaco Scarp
10	CTD	2-May	09°01.95	84°37.25	1395	Quepos Mound
11	CTD	3-May	09°01.87	84°37.32	1415 drift	Quepos Mound
			09°02.02	84°37.32		
12	CTD	3-May	09°01.87	84°37.17	1435 drift	Quepos Mound
			09°02.02	84°37.17		
13	CTD	5-May	09°01.87	84°37.25	1419 drift	Quepos Mound
			09°02.02	84°37.25		
14	CTD	5-6-May	09°01.95	84°37.22	1400	Quepos Mound
15	CTD	7-May	08°47.23	84°11.60	420	Southern Transect
16	CTD	8-May	08°42.22	84°16.70	1454	Southern Transect
17	CTD	9-May	08°35.00	84°24.20	2815	Southern Transect
18	CTD	9-May	08°24.20	84°36.00	2498	Southern Transect
19	CTD	10-May	08°07.99	84°53.24	2575	Southern Transect
20	CTD	10-May	07°48.00	85°14.00	2480	Southern Transect
21	CTD	12-May	09°06.02	84°51.40	2255	Jaco Scarp
22	CTD	14-May	10°17.99	86°18.30	1515	Mound Culebra
23	CTD	15-May	10°18.14	86°18.53	1624	Mound Culebra
24	CTD	18-May	09°05.05	84° 52.00	2416	Jaco Scarp

list of stations – Fluids and Subduction Costa Rica 2002 – METEOR 54/2+3a

Station No. M54	Instrument	Date 2002	Latitude [N°]	Longitude [W°]	Depth [m]	Area
/2-19 (CTD 05)	CTD	19-Aug	10°18.17	87°18.38	1640	Mound Culebra
/2-25 (CTD 06)	CTD	20-Aug	10°18.00	86°18.31	1539	Mound Culebra
/2-28 (CTD 07)	CTD	21-Aug	10°17.91	86°18.18	1530	Mound Culebra
/2-47 (CTD 08)	CTD	25-Aug	09°07.24	84°50.65	1803	Jaco Scarp
/2-50 (CTD 09)	CTD	26-Aug	09°06.90	84°50.86	1922	Jaco Scarp
/2-53 (CTD 10)	CTD	26-Aug	09°06.22	84°51.84	2025	Jaco Scarp
/2-58/1 (CTD 11)	CTD	27-Aug	09°10.43	84°48.25	760	Jaco Scarp
/2-62/1 (CTD 12)	CTD	28-Aug	09°09.04	84°49.18	837	Jaco Scarp
/2-66 (CTD 13)	CTD	28-Aug	09°05.41	84°49.64	1960	Jaco Scarp
/2-69/2 (CTD 14)	CTD	29-Aug	09°01.98	84°37.28	1427	Quepos Mound
/2-73/1 (CTD 15)	CTD	30-Aug	09°02.01	84°37.24	1446	Quepos Mound
/2-79 (CTD 16)	CTD	31-Aug	09°01.95	84°37.25	1426	Quepos Mound
/2-86 (CTD 17)	CTD	1-Sep	08°55.79	84°18.71	1003	Mound 12
/2-93 (CTD 18)	CTD	2-Sep	08°55.84	84°18.51	1014	Mound 12
/2-96 (CTD 19)	CTD	3-Sep	08°55.84	84°18.64	986	Mound 12
/2-99 (CTD 20)	CTD	3-Sep	08°55.82	84°18.64	991	Mound 12
/2-104 (CTD 21)	CTD	4-Sep	08°51.00	84°12.97	408	Quepos Slide
/2-108 (CTD 22)	CTD	5-Sep	08°51.40	84°12.70	225	Quepos Slide
/2-110 (CTD 23)	CTD	5-Sep	08°49.84	84°13.78	600	Quepos Slide
/3a-114 (CTD 01)	CTD	11-Sep	10°17.89	86°18.37	1499	Mound Culebra
/3a-118 (CTD 02)	CTD	12-Sep	10°17.57	86°18.56	1670	Mound Culebra
/3a-125 (CTD 03)	CTD	15-Sep	10°00.47	86°11.45	2260	Mound 10
/3a-127 (CTD 04)	CTD	15-Sep	10°00.71	86°11.63	2385	Mound 10
/3a-128	BWS	16-Sep	10°18.00	86°18.31	1538	Mound Culebra
/3a-130	ADCP	16-Sep	10°18.00	86°18.32	1543	Mound Culebra
/3a-131	VESP-MUC	16-Sep	10°17.99	86°18.29	1535	Mound Culebra
/3a-135 (CTD 05)	CTD	17-Sep	08°55.37	84°18.28	1020	Mound 11
/3a-141 (CTD 06)	CTD	18-Sep	09°06.08	84°49.71	1927	Jaco Scarp
/3a-142/1	BWS	18-Sep	08°55.35	84°18.24	1020	Mound 11
/3a-142/2 (CTD 07)	CTD	18-Sep	08°55.35	84°18.24	1020	Mound 11
/3a-146	ADCP	19-Sep	08°55.39	84°18.22	1023	Mound 11
/3a-150 (CTD 08)	CTD	19-Sep	08°55.94	84°18.72	1000	Mound 12
/3a-151 (CTD 09)	CTD	20-Sep	09°07.24	84°50.56	1760	Jaco Scarp
/3a-152 (CTD 10)	CTD	20-Sep	09°04.10	84°52.60	2395	Jaco Scarp
/3a-162 (CTD 12)	CTD	22-Sep	08°55.95	84°18.57	1018	Mound 12
/3a-165	ADCP	22-Sep	08°55.87	84°18.85	1020	Mound 12
/3a-167 (CTD 13)	CTD	23-Sep	08°52.00	84°23.00	1600	Mound 12
/3a-168	BWS	23-Sep	08°55.72	84°18.82	1018	Mound 12
/3a-169 (CTD 14)	CTD	23-Sep	08°55.72	84°18.82	1018	Mound 12
/3a-173/1	VESP-MUC	23-Sep	09°07.19	84°50.05	1867 drift	Jaco Scarp
			09°07.00	84°50.50		
/3a-173/2	VESP-MUC	23-Sep	09°07.21	84°50.49	1845 drift	Jaco Scarp
			09°07.00	84°50.50		
/3a-176/1	VESP-MUC	24-Sep	08°55.88	84°18.71	1007 drift	Mound 12
			08°55.81	84°18.58		
/3a-176/2	VESP-MUC	24-Sep	08°55.87	84°18.72	1022 drift	Mound 12
			08°55.69	84°18.81		
/3a-180 (CTD 15)	CTD	25-Sep	09°05.53	84°50.48	2220	Jaco Scarp
/3a-183 (CTD 16)	CTD	26-Sep	09°11.61	84°39.73	615	BGR-Slide
/3a-186	VESP-MUC	26-Sep	08°55.62	84°18.83	1008 drift	Mound 12
			08°55.82	84°18.76		
/3a-187	BWS	27-Sep	08°55.94	84°18.73	1009	Mound 12
/3a-188	VESP-MUC	27-Sep	08°55.83	84°18.69	1009	Mound 12

list of stations – Subduction II – SONNE 173/3+4

Station No. SO173	Instrument	Date 2003	Latitude [N°]	Longitude [W°]	Depth [m]	Area
/3-7 (CTD 01)	CTD	6-Sep	11°12.25	87°10.99	1358	Mound Quetzal
/3-10 (CTD 02)	CTD	7-Sep	12°00.00	88°09.00	1622	Redox Transect
/3-12 (CTD 03)	CTD	7-Sep	11°28.00	88°27.00	4102	Redox Transect
/3-14 (CTD 04)	CTD	8-Sep	10°04.00	89°18.00	3450	Redox Transect
/3-16 (CTD 05)	CTD	8-Sep	10°45.00	88°53.00	3200	Redox Transect
/3-22 (CTD 06)	CTD	10-Sep	11°12.20	87°09.30	1230	Mound Iguana
/3-23 (CTD 07)	CTD	10-Sep	11°07.70	87°11.51	2270	Landslide
/3-31 (CTD 08)	CTD	11-Sep	11°16.43	87°15.24	1428	Mound Cajablanca
/3-32	BWS	11-Sep	11°16.43	87°15.24	1430	Mound Cajablanca
/3-41	Mooring	11-Sep	10°17.16	86°17.87	1604	Mound Culebra
/3-42	Mooring	11-Sep	10°18.86	86°18.82	1632	Mound Culebra
/3-43 (CTD 09)	CTD	12-Sep	10°17.61	86°17.83	1590	Mound Culebra
/3-44 (CTD 10)	CTD	12-Sep	10°18.31	86°16.50	1644	Mound Culebra
/3-47 (CTD 11)	CTD	13-Sep	10°17.35	86°18.55	1660	Mound Culebra
/3-48 (CTD 12)	CTD	13-Sep	10°18.45	86°18.10	1602	Mound Culebra
/3-53 (CTD 13)	CTD	14-Sep	10°17.51	86°18.14	1616	Mound Culebra
/3-54 (CTD 14)	CTD	14-Sep	10°18.20	86°18.84	1682	Mound Culebra
/3-58 (CTD 15)	CTD	15-Sep	09°11.65	84°40.00	632	BGR Slide
/3-60 (CTD 16)	CTD	15-Sep	09°11.70	84°37.26	660	GEOMAR slide
/3-65	BWS	16-Sep	08°51.10	84°13.04	413	Quepos Slide
/3-67	BWS	16-Sep	08°48.20	84°13.75	770	Quepos Slide
/4-72 (CTD 17)	CTD	18-Sep	08°51.19	84°13.17	397	Quepos Slide
/4-75	BWS	18-Sep	08°51.17	84°13.19	398	Quepos Slide
/4-76 (CTD 18)	CTD	19-Sep	09°06.88	84°50.85	1930	Jaco Scarp
/4-82	ADCP	19-Sep	10°17.17	86°17.89	1610	Mound Culebra
/4-83 (CTD 19)	CTD	20-Sep	10°18.04	86°17.79	1550	Mound Culebra
/4-84 (CTD 20)	CTD	20-Sep	10°17.90	86°18.30	1514	Mound Culebra
/4-86 (CTD 21)	CTD	21-Sep	10°17.99	86°18.30	1512	Mound Culebra
/4-91	BWS	21-Sep	10°00.50	86°11.41	2267	Mound 10
/4-92 (CTD 22)	CTD	22-Sep	10°00.47	86°11.44	2260	Mound 10
/4-93 (CTD 23)	CTD	22-Sep	10°18.17	86°18.38	1632	Mound Culebra
/4-99 (CTD 24)	CTD	23-Sep	09°05.41	84°49.64	1930	Jaco Scarp
/4-100	Mooring	22-Sep	09°06.69	84°50.74	1880	Jaco Scarp
/4-101	Mooring	22-Sep	09°05.64	84°49.80	2040	Jaco Scarp
/4-103	BWS	23-Sep	08°51.16	84°13.04	401	Quepos Slide
/4-104	Mooring	23-Sep	08°56.07	84°18.95	1021	Mound 12
/4-105	ADCP	23-Sep	08°55.62	84°18.41	1023	Mound 12
74-106 (CTD 25)	CTD	24-Sep	08°55.82	84°18.64	990 drift	Mound 12
			08°55.90	84°18.70		
/4-111 (CTD 26)	CTD	25-Sep	08°56.03	84°18.83	1003 drift	Mound 12
			08°56.15	84°18.73		
/4-112	BWS	25-Sep	08°55.74	84°18:81	1011	Mound 12
/4-119 (CTD 27)	CTD	25-Sep	08°55.64	84°18.47	1028 drift	Mound 12
/4-123 (CTD 28)	CTD	25-Sep	09°20.05	85°17.17	592	Rio Bongo Scarp
/4-124 (CTD 29)	CTD	26-Sep	08°57.50	84°38.99	1618	Parrita Scarp
/4-125 (CTD 30)	CTD	26-Sep	08°55.45	84°18.66	1041	Mound 12
/4-129	ADCP	26-Sep	08°55.65	84°18.82	1021	Mound 12
/4-131 (CTD 31)	CTD	27-Sep	08°55.33	84°18.22	1018	Mound 12

data – Subduction I – SONNE 163/2

Station CTD	Bottle	Depth [m]	Pressure [db]	Potential Temp. [°C]	Salinity	Density σ_θ	O_2-conc. [ml L^{-1}]	CH_4-conc. [nmol L^{-1}]	$\delta^{13}C$ [‰]
CTD 07	1	1867.0	1886.1	2.238	34.643	27.667	2.05	5.99	-48.60
	2	1859.3	1878.3	2.242	34.643	27.666	2.08	5.35	-49.68
	3	1850.4	1869.2	2.266	34.642	27.663	2.01	9.61	-48.23
	4	1838.6	1857.3	2.278	34.641	27.662	2.06	12.15	-47.54
	5	1829.9	1848.4	2.304	34.640	27.659	2.02	24.67	-49.09
	6	1819.6	1838.0	2.344	34.638	27.654	1.99	123.13	-52.46
	7	1809.5	1827.7	2.382	34.637	27.650	1.94	73.69	-48.67
	8	1799.8	1817.8	2.411	34.636	27.646	1.93	23.91	-42.71
	9	1780.5	1798.3	2.494	34.634	27.638	2.06	282.90	-50.21
	10	1759.5	1777.0	2.578	34.630	27.627	1.79	117.91	-51.92
	11	1740.5	1757.7	2.654	34.627	27.618	1.75	80.98	-55.81
	12	1720.2	1737.1	2.674	34.626	27.616	1.72	18.45	-54.11
	13	1700.0	1716.6	2.680	34.626	27.616	1.74	7.43	-52.29
	14	1659.3	1675.4	2.726	34.625	27.610	1.71	19.63	-53.09
	15	1619.6	1635.1	2.781	34.623	27.604	1.67	8.71	-57.49
	16	1579.6	1594.6	2.869	34.621	27.594	1.64	0.87	-47.78
	17	1538.5	1553.0	2.902	34.619	27.590	1.62		
	18	1496.9	1510.8	2.948	34.617	27.584	1.57		
	19	1447.2	1460.5	2.979	34.617	27.581	1.55	2.14	-54.91
	20	1397.0	1409.6	3.074	34.614	27.570	1.48	2.47	-54.75
	21	1346.6	1358.6	3.248	34.608	27.549	1.39	1.40	-48.11
	22	1300.7	1312.2	3.374	34.604	27.534	1.31	1.68	-52.22
	23	1197.4	1207.7	3.760	34.594	27.488	1.13	1.08	-37.51
	24	399.8	402.5	10.162	34.710	26.698	0.12	7.53	-34.74
CTD 08	1	1403.3	1416.0	3.190	34.610	27.556	1.42	2.93	-60.36
	2	1393.0	1405.6	3.194	34.609	27.555	1.30	2.78	-62.01
	3	1379.3	1391.8	3.219	34.608	27.552	1.36	2.77	-59.33
	4	1368.8	1381.1	3.235	34.608	27.550	1.37	2.40	-57.97
	5	1358.7	1370.9	3.253	34.607	27.548	1.38	2.10	-57.00
	6	1348.7	1360.8	3.266	34.607	27.546	1.34	1.56	
	7	1328.7	1340.5	3.402	34.602	27.530	1.39	2.28	-57.69
	8	1308.3	1319.9	3.460	34.600	27.523	1.29	1.54	-50.28
	9	1288.5	1299.8	3.473	34.600	27.521	1.21	1.31	-46.98
	10	1270.3	1281.4	3.532	34.598	27.514	1.17	1.68	-45.11
	11	1250.4	1261.3	3.606	34.597	27.505	1.16	1.29	-44.94
	12	1210.1	1220.5	3.750	34.594	27.489	1.10	1.61	-49.57
	13	1170.7	1180.7	3.883	34.591	27.473	1.06	1.95	-51.31
	14	1130.4	1139.9	4.180	34.586	27.438	0.96	2.30	-53.22
	15	1090.7	1099.8	4.544	34.579	27.393	0.78		
	16	1050.8	1059.5	4.768	34.577	27.367	0.67	1.72	-45.94
	17	1011.0	1019.2	4.935	34.577	27.347	0.67	1.62	-40.79
	18	970.8	978.6	5.059	34.576	27.333	0.63	2.07	-51.17
	19	931.1	938.4	5.254	34.576	27.310	0.61	1.27	-38.46
	20	889.8	896.8	5.601	34.579	27.270	0.57	1.78	-46.84
	21	850.2	856.8	5.770	34.579	27.249	0.47	2.13	
	22	799.8	805.9	5.999	34.581	27.221	0.39	1.46	-47.76
	23	750.1	755.7	6.156	34.583	27.203	0.34	1.18	-45.27
	24	399.6	402.3	10.184	34.711	26.695	0.08	6.19	-35.10
CTD 09	1	945.5	953.0	4.907	34.579	27.353	0.66	2.71	-54.65
	2	936.1	943.5	5.029	34.578	27.337	0.62	2.46	-53.58
	3	924.2	931.5	5.201	34.578	27.317	0.59	2.09	-51.96
	4	914.5	921.7	5.266	34.578	27.310	0.56	2.13	-51.67
	5	904.0	911.1	5.311	34.578	27.305	0.55	2.20	-51.64
	6	894.7	901.7	5.468	34.578	27.285	0.53	2.24	-51.81
	7	874.4	881.2	5.502	34.579	27.282	0.52	2.24	-50.65

Station CTD	Bottle	Depth	Pressure	Potential Temp.	Salinity	Density σ_θ	O_2-conc.	CH_4-conc.	$\delta^{13}C$
		[m]	[db]	[°C]			[ml L^{-1}]	[nmol L^{-1}]	[‰]
	8	854.6	861.2	5.577	34.579	27.273	0.49	2.02	-50.35
	9	834.0	840.4	5.624	34.579	27.267	0.50	2.43	-52.12
	10	814.6	820.9	5.698	34.580	27.259	0.45	3.04	-54.62
	11	794.1	800.1	5.786	34.580	27.248	0.43	3.45	-58.08
	12	753.8	759.4	5.873	34.581	27.238	0.43	3.21	-58.13
	13	713.0	718.3	6.105	34.583	27.209	0.35	3.26	-58.04
	14	673.2	678.1	6.310	34.585	27.185	0.32	3.01	-58.47
	15	633.5	638.0	6.648	34.592	27.146	0.30	3.88	-38.51
	16	593.1	597.3	7.013	34.603	27.104	0.19	3.98	-37.77
	17	547.4	551.2	7.587	34.616	27.033	0.14	3.25	-39.87
	18	498.2	501.6	8.092	34.626	26.966	0.08	4.54	-25.02
	19	448.3	451.3	8.749	34.648	26.882	0.07	7.82	-31.64
	20	399.6	402.2	9.675	34.689	26.764	0.07	7.78	-35.02
	21	350.0	352.3	11.082	34.756	26.570	0.15	2.55	-26.68
	22	299.7	301.6	11.981	34.809	26.444	0.54	1.83	-39.10
	23	31.8	32.0	20.238	34.726	24.490	2.62		
	24	4.1	4.1	29.342	34.440	21.529	4.90	2.22	-43.13
CTD 21	1	2235.1	2259.9	1.928	34.665	27.696	2.24	2.99	
	2	2226.2	2250.8	1.932	34.664	27.695	2.25	3.08	-48.45
	3	2213.6	2238.0	1.936	34.664	27.695	2.23	3.16	-48.38
	4	2195.2	2219.3	1.953	34.663	27.693	2.22	3.06	-47.12
	5	2170.0	2193.7	2.015	34.660	27.686	2.17	3.52	-46.64
	6	2140.5	2163.7	2.076	34.658	27.679	2.13	3.61	-45.99
	7	2109.8	2132.5	2.108	34.656	27.675	2.10	3.44	-45.76
	8	2080.3	2102.6	2.144	34.655	27.671	2.08	4.13	
	9	2050.1	2071.9	2.186	34.653	27.667	2.04	11.15	-52.80
	10	2020.1	2041.4	2.241	34.651	27.660	1.90	14.38	-53.53
	11	1990.4	2011.3	2.244	34.651	27.660	1.98	10.06	-52.77
	12	1960.2	1980.6	2.284	34.649	27.656	1.97	8.95	-50.95
	13	1930.2	1950.2	2.343	34.646	27.648	1.93	104.13	-55.73
	14	1900.4	1919.9	2.366	34.646	27.647	1.87	44.01	-51.98
	15	1870.6	1889.7	2.391	34.645	27.644	1.90	14.41	-46.79
	16	1840.2	1858.9	2.403	34.644	27.642	1.88	7.40	-42.91
	17	1810.7	1828.9	2.424	34.644	27.641	2.07	5.88	
	18	1780.3	1798.1	2.460	34.642	27.636	1.84	12.97	-43.61
	19	1749.9	1767.2	2.527	34.640	27.629	1.80	3.49	-46.41
	20	1719.5	1736.5	2.593	34.638	27.622	1.74	18.02	-50.15
	21	1690.2	1706.7	2.617	34.637	27.619	1.75	17.22	-52.78
	22	1658.8	1674.9	2.664	34.635	27.613	1.72	14.50	-54.97
	23	1630.2	1645.9	2.713	34.634	27.608	1.69	10.54	-56.68
	24	1599.6	1614.8	2.725	34.633	27.607	1.69	7.60	-57.13
CTD 22	1	1492.9	1506.9	2.892	34.619	27.581	1.46	23.76	-45.86
	2	1488.6	1502.4	2.903	34.619	27.580	1.44	21.57	-48.77
	3	1484.1	1497.9	2.934	34.617	27.576	1.39	8.71	-46.79
	4	1479.0	1492.8	2.968	34.616	27.572	1.39	5.31	-45.83
	5	1476.0	1489.7	2.971	34.616	27.572	1.38	5.11	-45.52
	6	1469.1	1482.7	2.976	34.616	27.571	1.38	5.51	-46.06
	7	1463.3	1476.9	3.006	34.614	27.567	1.34	2.44	-41.60
	8	1459.3	1472.8	3.032	34.613	27.564	1.34	2.16	-43.38
	9	1453.4	1466.8	3.045	34.613	27.562	1.31	1.47	
	10	1450.1	1463.5	3.065	34.613	27.560	1.26	1.34	-36.44
	11	1445.5	1458.8	3.098	34.611	27.556	1.29	0.88	-30.20
	12	1439.0	1452.3	3.128	34.610	27.552	1.30	0.94	-30.23
	13	1434.3	1447.4	3.135	34.610	27.552	1.30	1.01	-31.10
	14	1429.1	1442.2	3.140	34.610	27.551	1.28	1.00	-29.63
	15	1424.3	1437.3	3.149	34.610	27.550	1.28	1.03	-32.10
	16	1418.8	1431.8	3.192	34.608	27.545	1.44	0.74	-34.80
	17	1414.7	1427.6	3.197	34.608	27.544	1.25	0.69	-32.62
	18	1409.8	1422.6	3.224	34.607	27.541	1.26	0.69	-31.79

Station CTD	Bottle	Depth	Pressure	Potential Temp.	Salinity	Density σ_θ	O_2-conc.	CH_4-conc.	$\delta^{13}C$
		[m]	[db]	[°C]			[ml L^{-1}]	[nmol L^{-1}]	[‰]
	19	1399.5	1412.3	3.265	34.606	27.536	1.26	0.68	-31.29
	20	1388.9	1401.5	3.291	34.604	27.532	1.24	0.77	
	21	1378.4	1390.8	3.331	34.603	27.527	1.15	1.15	-32.78
	22	1370.4	1382.8	3.350	34.602	27.525	1.14	1.63	-31.17
	23	1348.7	1360.8	3.367	34.602	27.523	1.13	1.52	-32.49
	24	1329.6	1341.5	3.401	34.600	27.519	1.11	1.48	-34.99
CTD 23	1	1625.1	1640.8	2.774	34.628	27.598	1.61	3.10	-41.01
	2	1618.9	1634.5	2.776	34.628	27.598	1.61	2.98	-39.82
	3	1614.1	1629.6	2.782	34.628	27.597	1.59	3.15	-41.07
	4	1608.9	1624.4	2.782	34.628	27.597	1.60	3.14	-40.85
	5	1594.3	1609.5	2.793	34.627	27.596	1.58	5.56	-45.59
	6	1588.1	1603.3	2.799	34.627	27.595	1.59	6.23	-46.27
	7	1580.2	1595.3	2.815	34.626	27.593	1.59	9.14	-47.71
	8	1569.0	1583.9	2.846	34.625	27.589	1.55	15.94	-48.36
	9	1559.4	1574.2	2.856	34.624	27.588	1.52	14.97	-47.71
	10	1549.6	1564.2	2.895	34.623	27.583	1.25	12.75	-47.95
	11	1540.2	1554.7	2.924	34.621	27.579	1.46	11.21	-47.40
	12	1528.9	1543.3	2.947	34.621	27.577	1.44	9.37	-47.91
	13	1520.1	1534.4	2.965	34.620	27.575	1.51	7.05	-47.17
	14	1508.7	1522.8	2.969	34.620	27.574	1.40	5.42	-45.81
	15	1500.2	1514.2	2.974	34.619	27.573	1.41	4.39	-45.09
	16	1494.9	1508.9	2.980	34.615	27.570	1.41	2.20	-44.27
	17	1489.2	1503.1	3.020	34.613	27.564	1.37	1.16	-36.82
	18	1484.1	1497.9	3.044	34.613	27.562	1.55	0.93	-36.37
	19	1479.3	1493.1	3.063	34.612	27.560	1.34	0.79	-30.99
	20	1461.2	1474.7	3.121	34.611	27.553	1.34	0.99	-30.53
	21	1450.5	1463.9	3.139	34.610	27.551	1.35	0.99	-35.40
	22	1442.1	1455.4	3.174	34.608	27.546	1.32	0.72	-28.98
	23	1418.2	1431.2	3.263	34.605	27.535	1.21	0.75	
	24	1399.4	1412.1	3.312	34.603	27.529	1.15	0.73	-32.75
CTD 24	1	2391.6	2419.0	1.796	34.665	27.706	2.40	2.65	-53.06
	2	2381.0	2408.2	1.796	34.665	27.706	2.39	2.59	-54.33
	3	2349.8	2376.5	1.806	34.665	27.705	2.40	2.59	-54.18
	4	2300.0	2325.8	1.845	34.663	27.701	2.34	2.78	-51.66
	5	2250.7	2275.7	1.886	34.661	27.696	2.34	2.66	-45.23
	6	2195.1	2219.2	1.953	34.658	27.689	2.25	7.93	-54.51
	7	2145.0	2168.3	2.040	34.654	27.679	2.20	3.72	-45.65
	8	2095.6	2118.1	2.106	34.651	27.671	2.14	3.92	-46.80
	9	2036.4	2058.0	2.134	34.650	27.669	2.10	4.49	-47.74
	10	1974.3	1995.0	2.220	34.647	27.659	1.83	3.29	-46.92
	11	1925.8	1945.7	2.278	34.645	27.653	2.03	8.14	-50.07
	12	1885.2	1904.5	2.319	34.643	27.648	2.01	6.86	-50.18
	13	1845.9	1864.6	2.364	34.641	27.643	1.95	10.27	-45.18
	14	1804.8	1822.9	2.436	34.638	27.635	1.90	18.44	-42.33
	15	1765.5	1783.1	2.472	34.637	27.631	1.87	17.45	-43.33
	16	1726.0	1743.0	2.612	34.632	27.615	1.79	31.15	-51.12
	17	1686.3	1702.7	2.675	34.630	27.608	1.76	2.08	-54.13
	18	1645.7	1661.6	2.720	34.629	27.604	1.72	0.88	-56.20
	19	1606.3	1621.7	2.765	34.627	27.598	1.68	1.51	-55.79
	20	1559.8	1574.5	2.855	34.623	27.587	1.81	0.66	-39.29
	21	1522.3	1536.5	2.896	34.622	27.583	1.62	0.98	-44.46
	22	1483.9	1497.6	2.976	34.615	27.570	1.53	1.82	-47.77
	23	1435.4	1448.6	3.061	34.613	27.561	1.53	1.99	-50.06
	24	1383.5	1396.0	3.177	34.609	27.547	1.41	1.47	-43.22

data – Fluids and Subduction Costa Rica 2002 – METEOR 54/2+3

Station CTD	Bottle	Depth [m]	Pressure [db]	Potential Temp. [°C]	Salinity	Density σ_θ	O_2-conc. [ml/L]	CH_4-conc. [nmol/L]	$\delta^{13}C$ [‰]
M54/2	1	1616.2	1631.7	2.872	34.624	27.597	1.43	35.15	-44.90
19 (CTD 05)	2	1610.6	1626.1	2.885	34.624	27.595	1.43	40.18	-44.09
	3	1614.0	1629.5	2.881	34.623	27.595	1.43	40.23	-45.28
	4	1609.5	1625.0	2.883	34.623	27.595	1.43	39.38	-45.17
	5	1598.7	1614.0	2.902	34.622	27.592	1.43	42.31	-45.37
	6	1588.6	1603.8	2.919	34.622	27.591	1.24	39.05	-45.56
	7	1578.7	1593.7	2.939	34.623	27.589	1.24	34.81	-45.11
	8	1568.9	1583.8	2.950	34.619	27.585	1.24	26.59	
	9	1558.0	1572.8	3.053	34.616	27.574	1.24	31.96	
	10	1549.3	1564.0	3.136	34.614	27.564	1.24	17.11	-48.02
	11	1539.5	1554.0	3.161	34.614	27.562	1.07	11.80	
	12	1529.6	1544.0	3.180	34.613	27.560	1.07	11.16	-46.52
	13	1518.6	1532.9	3.224	34.610	27.553	1.07	12.42	
	14	1497.6	1511.6	3.245	34.610	27.551	1.07	14.32	-45.42
	15	1477.8	1491.5	3.295	34.609	27.545	1.07	13.49	-46.42
	16	1458.2	1471.7	3.304	34.608	27.544	1.07	12.28	-46.43
	17	1438.3	1451.5	3.405	34.607	27.533	0.90		
	18	1419.5	1432.5	3.423	34.605	27.530	0.90	6.28	-45.68
	19	1398.6	1411.3	3.446	34.603	27.526	0.90	4.44	-45.01
	20	1378.9	1391.4	3.495	34.602	27.521	0.90	3.02	-45.12
	21	1360.4	1372.6	3.531	34.600	27.516	0.90	1.88	-45.07
	22	1340.7	1352.7	3.607	34.599	27.507	0.90	2.52	-40.71
M54/2	1	1526.3	1540.7	3.034	34.615	27.574	1.24	24.17	-46.67
25 (CTD 06)	2	1524.2	1538.5	3.036	34.615	27.575	1.24	23.83	-44.96
	3	1522.0	1536.3	3.038	34.616	27.575	1.24	20.80	-45.71
	4	1519.8	1534.1	3.045	34.615	27.574	1.24	17.92	-45.08
	5	1510.0	1524.1	3.054	34.614	27.572	1.24	19.75	-45.38
	6	1500.2	1514.2	3.069	34.615	27.571	1.24	21.39	-46.49
	7	1490.4	1504.3	3.109	34.613	27.566	1.24	15.40	-45.25
	8	1480.6	1494.4	3.164	34.611	27.560	1.07	14.68	-45.72
	9	1469.8	1483.4	3.216	34.610	27.554	1.07	14.45	-45.61
	10	1459.9	1473.4	3.237	34.609	27.551	1.07	13.24	-45.06
	11	1448.9	1462.3	3.315	34.605	27.541	1.07	10.55	-45.55
	12	1439.0	1452.2	3.343	34.605	27.537	1.07	9.35	-45.23
	13	1428.9	1442.0	3.365	34.605	27.536	0.90	7.55	-43.88
	14	1419.1	1432.1	3.404	34.604	27.531	0.90	6.47	-43.62
	15	1410.4	1423.3	3.409	34.602	27.529	0.90	4.18	-43.97
	16	1400.5	1413.2	3.429	34.605	27.530	0.90	3.31	-44.33
	17	1390.5	1403.1	3.498	34.602	27.520	0.90	2.40	-42.99
	18	1379.2	1391.7	3.514	34.599	27.517	0.90	2.02	-42.30
	19	1358.4	1370.6	3.528	34.600	27.516	0.90	0.57	-39.13
	20	1339.8	1351.8	3.576	34.599	27.510	0.90	0.61	
	21	1321.0	1332.8	3.616	34.598	27.506	0.90		
	22	1300.3	1311.8	3.675	34.596	27.498	0.90		
M54/2	1	1506.8	1520.9	3.141	34.610	27.561	1.24	22.77	
28 (CTD 07)	2	1505.7	1519.8	3.140	34.610	27.561	1.07	20.53	-46.48
	3	1504.6	1518.7	3.138	34.610	27.561	1.24	16.94	-46.09
	4	1503.5	1517.6	3.140	34.611	27.561	1.24	20.81	-46.81

Station CTD	Bottle	Depth [m]	Pressure [db]	Potential Temp. [°C]	Salinity	Density σ_θ	O_2-conc. [ml/L]	CH_4-conc. [nmol/L]	$\delta^{13}C$ [‰]
	5	1493.8	1507.7	3.164	34.611	27.559	1.07	12.16	
	6	1483.9	1497.7	3.195	34.609	27.555	1.07	9.39	-43.74
	7	1474.0	1487.7	3.224	34.608	27.551	1.07	14.31	-46.30
	8	1464.2	1477.7	3.234	34.608	27.550	1.07	10.46	
	9	1455.5	1468.9	3.237	34.608	27.550	1.07	9.46	-44.28
	10	1444.5	1457.8	3.250	34.607	27.548	1.07	8.90	-44.17
	11	1434.6	1447.8	3.266	34.607	27.547	1.07	9.83	-44.30
	12	1424.9	1437.9	3.267	34.607	27.547	1.07	11.31	
	13	1414.0	1426.9	3.301	34.606	27.542	1.07	11.54	-45.88
	14	1404.2	1417.0	3.305	34.606	27.542	1.07	11.85	-45.70
	15	1395.4	1408.1	3.333	34.606	27.539	1.07	10.56	-45.68
	16	1385.6	1398.2	3.384	34.603	27.532	1.07	9.31	-44.81
	17	1374.6	1387.0	3.394	34.604	27.532	0.90	8.78	-44.58
	18	1363.6	1375.9	3.457	34.602	27.524	0.90	5.61	-43.83
	19	1345.1	1357.2	3.536	34.599	27.514	0.90	3.80	-43.42
	20	1325.5	1337.3	3.604	34.597	27.506	0.90	1.90	
	21	1303.6	1315.2	3.657	34.598	27.501	0.90	0.47	-38.22
	22	1283.9	1295.2	3.766	34.593	27.487	0.75		
M54/2	1	1777.3	1795.0	2.566	34.642	27.638	1.50	281.12	-55.18
47 (CTD 08)	2	1775.1	1792.8	2.566	34.642	27.638	1.44	249.23	-56.13
	3	1772.9	1790.6	2.571	34.641	27.637	1.46	242.79	-55.32
	4	1763.0	1780.5	2.617	34.641	27.633	1.43	189.10	-54.51
	5	1751.9	1769.3	2.640	34.639	27.629	1.41	182.74	-54.57
	6	1721.2	1738.1	2.683	34.638	27.624	1.39	118.73	-52.42
	7	1692.8	1709.3	2.722	34.636	27.620	1.37	358.50	-56.01
	8	1663.2	1679.3	2.773	34.636	27.615	1.33	202.58	-55.88
	9	1633.4	1649.1	2.803	34.634	27.611	1.33	82.89	-55.43
	10	1604.7	1620.0	2.828	34.634	27.608	1.32	12.71	
	10	1604.7	1620.0	2.828	34.634	27.608	1.32	12.23	
	11	1573.9	1588.8	2.891	34.631	27.601	1.26	142.99	-54.29
	12	1544.3	1558.8	3.010	34.627	27.587	1.21	8.22	
	13	1515.6	1529.8	3.062	34.625	27.580	1.16	4.94	-52.01
	14	1485.2	1499.0	3.181	34.622	27.566	1.12	2.29	-57.64
	15	1455.7	1469.1	3.293	34.620	27.554	1.07	2.87	-55.24
	16	1424.9	1437.9	3.353	34.617	27.546	1.05	2.26	-47.03
	17	1395.1	1407.7	3.369	34.617	27.545	1.04	1.57	-42.59
	18	1344.6	1356.6	3.463	34.615	27.534	1.04	1.30	-42.88
	19	1295.2	1306.6	3.592	34.612	27.519	0.99	1.31	-43.56
	20	1246.8	1257.6	3.673	34.608	27.507	0.89	1.34	-48.00
	21	1197.1	1207.4	4.030	34.595	27.461	0.79	2.11	
	22	1146.7	1156.4	4.289	34.598	27.436	0.81	2.08	
M54/2	1	1883.7	1903.0	2.386	34.639	27.651	2.08	108.18	-52.63
50 (CTD 09)	2	1881.5	1900.7	2.397	34.639	27.650	2.18	115.92	
	3	1879.3	1898.5	2.404	34.639	27.649	2.19	144.77	-52.72
	4	1869.3	1888.4	2.445	34.637	27.645	2.15	178.52	-52.94
	5	1859.6	1878.5	2.465	34.638	27.643	2.15	151.12	-52.06
	6	1829.1	1847.6	2.484	34.637	27.641	1.94	113.41	
	7	1799.8	1817.8	2.554	34.635	27.633	1.92	42.72	-52.02
	8	1769.2	1786.8	2.607	34.631	27.626	1.85	47.42	-52.51
	9	1759.2	1776.7	2.614	34.632	27.626	1.02	24.30	-49.34
	10	1749.4	1766.7	2.628	34.634	27.626	1.89	19.22	

Station CTD	Bottle	Depth [m]	Pressure [db]	Potential Temp. [°C]	Salinity	Density σ_θ	O_2-conc. [ml/L]	CH_4-conc. [nmol/L]	$\delta^{13}C$ [‰]
	11	1739.4	1756.6	2.631	34.633	27.625	1.84	51.03	-52.82
	12	1709.5	1726.3	2.728	34.629	27.614	1.79	88.71	
	13	1678.4	1694.7	2.798	34.627	27.606	1.71	8.41	-47.27
	14	1647.5	1663.4	2.845	34.624	27.599	1.77	4.64	-45.00
	15	1619.0	1634.5	2.864	34.623	27.597	1.75	10.90	-53.69
	16	1588.2	1603.3	2.917	34.623	27.592	1.62	38.53	
	17	1559.8	1574.5	2.983	34.620	27.583	1.63		
	18	1509.9	1524.0	3.060	34.620	27.576	1.51	3.69	-53.20
	19	1458.0	1471.4	3.232	34.612	27.554	1.44	2.58	
	20	1408.5	1421.3	3.429	34.606	27.530	1.46	1.33	
	21	1359.1	1371.3	3.531	34.604	27.519	1.27	1.60	-50.13
	22	1310.6	1322.2	3.625	34.600	27.506	1.30	1.13	
M54/2	1	1960.0	1980.4	2.335	34.644	27.660	1.46	19.77	-27.30
53 (CTD 10)	2	1958.0	1978.7	2.335	34.645	27.660	1.46	17.43	
	3	1948.0	1968.4	2.340	34.645	27.659	1.44	19.37	-26.70
	4	1938.0	1958.4	2.360	34.644	27.657	1.43	25.21	-27.55
	5	1908.0	1927.6	2.472	34.640	27.644	1.37	50.92	-38.58
	6	1878.0	1897.7	2.557	34.636	27.634	1.30	30.11	-44.42
	7	1868.0	1887.4	2.577	34.635	27.632	1.30	32.13	
	8	1858.0	1877.4	2.597	34.635	27.630	1.28	32.23	-43.96
	9	1848.0	1866.9	2.611	34.635	27.628	1.26	41.01	-47.61
	10	1838.0	1856.5	2.624	34.634	27.627	1.28	27.98	-44.48
	11	1807.0	1826.4	2.670	34.632	27.621	1.24	24.00	-43.19
	12	1778.0	1796.9	2.678	34.633	27.621	1.24	20.32	-42.56
	13	1748.0	1766.0	2.716	34.631	27.616	1.23	17.56	-47.83
	14	1718.0	1736.2	2.791	34.628	27.607	1.19		
	15	1689.0	1706.0	2.808	34.628	27.605	1.17	16.86	-48.23
	16	1660.0	1676.1	2.848	34.627	27.601	1.14		
	17	1610.0	1625.6	2.962	34.623	27.587	1.09	5.13	-53.87
	18	1559.0	1572.9	3.080	34.619	27.573	1.05	5.67	-55.46
	19	1509.0	1524.3	3.106	34.618	27.571	1.04	1.35	-44.99
	20	1460.0	1474.4	3.146	34.618	27.567	1.04		
	21	1411.0	1424.6	3.267	34.614	27.552	0.99	1.26	-43.44
	22	1361.0	1374.4	3.451	34.607	27.529	0.87	1.18	-43.45
M54/2	1	747.0	753.4	6.114	34.586	27.211	0.27	4.19	
58/1 (CTD 11)	2	746.0	752.9	6.111	34.587	27.212	0.24	4.14	
	3	744.0	750.3	6.115	34.587	27.212	0.24	4.69	
	4	734.0	741.2	6.232	34.589	27.198	0.22	5.16	
	5	725.0	731.4	6.400	34.592	27.178	0.20	4.07	
	6	715.0	721.1	6.565	34.595	27.159	0.19	4.14	
	7	705.0	710.7	6.687	34.596	27.144	0.17	4.05	
	8	696.0	701.4	6.966	34.600	27.109	0.12	3.38	
	9	685.0	690.3	7.023	34.601	27.102	0.12	0.96	
	10	656.0	661.1	7.329	34.611	27.066	0.11	1.19	
	11	626.0	631.7	7.759	34.623	27.014	0.10	3.23	
	12	594.0	598.6	7.918	34.626	26.993	0.09	2.04	
	13	565.0	570.2	8.027	34.626	26.976	0.09	3.18	
	14	537.0	541.4	8.380	34.639	26.933	0.09	3.68	
	15	507.0	511.0	8.653	34.646	26.896	0.09	7.02	
	16	477.0	480.7	9.154	34.670	26.835	0.09	4.54	

Station CTD	Bottle	Depth [m]	Pressure [db]	Potential Temp. [°C]	Salinity	Density σ_θ	O_2-conc. [ml/L]	CH_4-conc. [nmol/L]	$\delta^{13}C$ [‰]
	17	446.0	449.0	9.762	34.691	26.752	0.09	10.79	
	18	414.0	417.1	10.695	34.736	26.625	0.12	5.49	
	19	383.0	386.2	11.105	34.760	26.570	0.17	4.71	
	20	356.0	358.6	11.322	34.770	26.538	0.21	1.59	
	21	326.0	328.3	12.029	34.820	26.445	0.11	2.02	
	22	294.0	296.1	12.689	34.866	26.351	0.20		
M54/2	1	829.0	836.0	5.913	34.578	27.231	0.35	1.63	
62/1 (CTD 12)	2	827.0	832.8	5.933	34.579	27.229	0.32	1.65	
	3	824.0	830.3	5.891	34.579	27.234	0.32	1.78	
	4	814.0	820.5	5.880	34.580	27.236	0.32	2.29	
	5	803.0	808.9	5.930	34.580	27.230	0.30	2.01	
	6	791.0	797.4	6.008	34.581	27.221	0.28	1.66	
	7	781.0	787.4	6.004	34.581	27.221	0.28	1.87	
	8	771.0	777.6	6.070	34.582	27.213	0.27	1.85	
	9	738.0	744.1	6.274	34.585	27.189	0.23	1.51	
	10	709.0	715.1	6.625	34.592	27.149	0.23	0.80	
	11	681.0	686.7	6.824	34.593	27.122	0.19	0.73	
	12	650.0	654.9	7.181	34.605	27.083	0.17	0.93	
	13	620.0	625.0	7.412	34.612	27.055	0.15	0.81	
	14	591.0	595.6	7.643	34.617	27.026	0.13	1.83	
	15	560.0	564.7	7.939	34.625	26.989	0.13	2.16	
	16	531.0	535.8	8.244	34.631	26.948	0.12	2.79	
	16	531.0	535.8	8.244	34.631	26.948	0.12	2.76	
	17	503.0	506.7	8.621	34.643	26.899	0.12	5.71	
	18	471.0	474.2	9.594	34.683	26.773	0.12	8.96	
	19	439.0	442.1	10.131	34.706	26.700	0.13	8.38	
	20	407.0	410.2	10.307	34.715	26.677	0.13	7.49	
	21	377.0	379.2	10.963	34.747	26.585	0.16	3.75	
	22	347.0	349.4	11.764	34.799	26.478	0.27	1.69	
M54/2	1	1904.0	1923.8	2.550	34.636	27.635	0.97	6.93	-31.21
66 (CTD 13)	2	1902.0	1921.1	2.550	34.636	27.635	0.95	6.62	-32.62
	3	1892.0	1910.8	2.558	34.636	27.634	0.97	5.80	-28.85
	4	1882.0	1901.3	2.560	34.637	27.634	0.95	6.51	-29.05
	5	1872.0	1891.2	2.560	34.636	27.634	0.95	6.20	-29.77
	6	1862.0	1880.4	2.561	34.636	27.634	0.95	6.06	-29.49
	7	1852.0	1870.7	2.564	34.637	27.634	0.95	5.68	-28.57
	8	1822.0	1840.9	2.589	34.635	27.631	0.95	5.94	-33.35
	9	1792.0	1809.7	2.655	34.633	27.623	0.90	4.93	-38.11
	10	1762.0	1779.8	2.690	34.632	27.619	0.90	10.42	-45.11
	11	1732.0	1750.1	2.741	34.630	27.613	0.87	84.18	-49.94
	12	1703.0	1720.1	2.812	34.628	27.605	0.86	99.34	-50.22
	13	1692.0	1708.7	2.834	34.627	27.602	0.86	16.87	-49.92
	14	1683.0	1699.3	2.869	34.626	27.599	0.82	18.90	-49.60
	15	1673.0	1689.3	2.874	34.626	27.598	0.82	4.92	-45.80
	16	1623.0	1639.2	2.976	34.623	27.586	0.79	2.66	-44.74
	16	1623.0	1639.2	2.976	34.623	27.586	0.79	2.76	
	17	1573.0	1589.0	3.073	34.620	27.575	0.78		
	18	1524.0	1538.8	3.115	34.618	27.570	0.75	3.81	-53.20
	19	1474.0	1488.5	3.270	34.613	27.551	0.72	2.01	-50.61
	20	1425.0	1438.3	3.398	34.609	27.536	0.66	1.34	-45.72

Station CTD	Bottle	Depth [m]	Pressure [db]	Potential Temp. [°C]	Salinity	Density σ_θ	O_2-conc. [ml/L]	CH_4-conc. [nmol/L]	$\delta^{13}C$ [‰]
	21	1375.0	1387.1	3.505	34.606	27.523	0.63	1.19	-44.10
	22	1326.0	1338.2	3.556	34.604	27.516	0.58	1.06	-39.60
M54/2	1	987.0	995.8	5.109	34.579	27.329	0.50	19.49	-62.15
86 (CTD 17)	2	985.0	993.4	5.118	34.579	27.328	0.49	22.38	-62.55
	3	983.0	991.3	5.131	34.580	27.327	0.47	16.23	-62.60
	4	981.0	989.2	5.149	34.580	27.325	0.47	11.72	-60.90
	5	971.0	979.2	5.216	34.580	27.317	0.45	8.99	-57.25
	6	960.0	968.6	5.259	34.580	27.312	0.45	6.18	-57.78
	7	951.0	958.9	5.267	34.580	27.311	0.43	4.89	-55.65
	8	941.0	948.6	5.282	34.580	27.309	0.42	5.85	-55.97
	9	931.0	938.5	5.295	34.581	27.308	0.42	2.12	-49.09
	10	901.0	908.4	5.494	34.580	27.284	0.40	3.46	-47.70
	11	871.0	878.2	5.658	34.582	27.265	0.36	3.15	-48.34
	12	841.0	848.3	5.719	34.583	27.259	0.33	2.69	-45.48
	13	811.0	818.0	5.792	34.583	27.250	0.32	4.72	
	14	781.0	787.8	6.023	34.586	27.223	0.29	8.80	-37.64
	15	751.0	757.7	6.328	34.590	27.186	0.24	8.14	-28.85
	16	722.0	727.5	6.592	34.594	27.155	0.21	6.03	-36.00
	17	672.0	677.3	6.975	34.601	27.108	0.17	0.72	
	18	622.0	627.2	7.308	34.609	27.067	0.15	2.68	-16.60
	19	572.0	577.1	7.686	34.610	27.014	0.12	1.09	
	20	523.0	527.1	8.356	34.647	26.943	0.12	3.35	-26.64
	21	473.0	476.6	9.030	34.668	26.853	0.12	9.48	-41.60
	22	423.0	426.3	9.776	34.693	26.751	0.13	9.19	-43.72
M54/2	1	993.0	1001.4	5.215	34.580	27.317	0.51	2.25	
93 (CTD 18)	2	991.0	999.6	5.207	34.580	27.318	0.51	2.51	-43.90
	3	989.0	997.1	5.229	34.581	27.316	0.50	2.21	-44.67
	4	987.0	995.1	5.228	34.581	27.317	0.50	2.36	
	5	977.0	985.0	5.274	34.581	27.311	0.49	2.39	-43.39
	6	967.0	975.4	5.282	34.582	27.311	0.49	2.42	
	7	957.0	965.1	5.299	34.581	27.308	0.47	2.70	-42.39
	8	947.0	954.7	5.322	34.581	27.306	0.46	2.71	
	9	937.0	944.9	5.344	34.581	27.303	0.45	3.36	-40.71
	10	907.0	914.7	5.436	34.582	27.292	0.42	2.48	
	11	877.0	884.5	5.560	34.582	27.278	0.41	1.23	-42.64
	12	847.0	854.2	5.669	34.584	27.266	0.40	4.62	-49.49
	13	817.0	823.8	5.782	34.585	27.252	0.33	4.23	
	14	787.0	793.7	5.886	34.586	27.240	0.30	6.61	-32.42
	15	757.0	763.8	6.215	34.590	27.202	0.24	6.22	
	15	757.0	763.8	6.215	34.590	27.202	0.24	6.25	-21.34
	16	727.0	733.5	6.489	34.595	27.169	0.20	7.77	-17.78
	17	678.0	683.5	7.006	34.605	27.107	0.13	2.12	-19.72
	18	628.0	633.1	7.388	34.611	27.058	0.10	1.35	-28.00
	19	578.0	583.0	7.894	34.623	26.994	0.07	7.11	
	20	529.0	533.0	8.401	34.650	26.939	0.07	6.14	-33.47
	21	479.0	482.5	8.809	34.666	26.887	0.07	6.28	-32.53
	22	429.0	432.5	9.215	34.672	26.827	0.07	7.06	-32.89
M54/2	1	968.0	976.3	5.141	34.578	27.324	0.51	15.76	
96 (CTD 19)	2	966.0	973.4	5.155	34.578	27.322	0.50	15.18	
	3	963.0	970.6	5.195	34.578	27.318	0.49	14.86	-63.07

Station CTD	Bottle	Depth [m]	Pressure [db]	Potential Temp. [°C]	Salinity	Density σ_θ	O_2-conc. [ml/L]	CH_4-conc. [nmol/L]	$\delta^{13}C$ [‰]
	4	960.0	968.0	5.210	34.579	27.317	0.47	7.65	
	5	950.0	958.0	5.266	34.578	27.310	0.47	4.36	
	6	940.0	947.4	5.317	34.578	27.304	0.43	2.70	
	7	930.0	938.0	5.384	34.578	27.296	0.42	2.14	-44.08
	8	920.0	927.4	5.430	34.579	27.291	0.41	2.55	
	9	909.0	916.4	5.465	34.579	27.287	0.40	2.32	-45.72
	10	880.0	887.2	5.503	34.580	27.282	0.38	1.63	
	11	850.0	857.4	5.588	34.580	27.272	0.38	1.83	
	12	820.0	826.9	5.652	34.581	27.265	0.37	1.37	-41.31
	13	791.0	797.4	5.811	34.582	27.246	0.32	3.08	-42.20
	14	761.0	767.1	5.960	34.584	27.229	0.28	5.07	
	15	731.0	737.3	6.453	34.590	27.170	0.19	4.91	-18.44
	16	701.0	706.8	6.767	34.597	27.133	0.15	6.17	
	17	651.0	656.3	7.072	34.603	27.096	0.12	2.88	
	18	601.0	605.9	7.340	34.609	27.063	0.09	1.24	
	19	552.0	556.5	7.808	34.620	27.004	0.07	1.42	-22.84
	20	502.0	505.4	8.437	34.649	26.932	0.07	1.68	
	21	452.0	455.5	8.797	34.665	26.889	0.07	1.66	-30.99
	22	402.0	405.3	9.554	34.685	26.782	0.07	3.33	
M54/2	1	979.0	988.2	5.134	34.581	27.328	0.47	17.91	-61.50
99 (CTD 20)	2	978.0	986.4	5.143	34.581	27.327	0.47	20.92	-62.46
	3	976.0	984.0	5.152	34.581	27.326	0.46	21.87	-62.05
	4	974.0	981.8	5.158	34.582	27.325	0.45	23.37	
	5	964.0	972.0	5.187	34.582	27.322	0.45	13.07	
	6	954.0	962.1	5.284	34.582	27.311	0.42	7.06	-57.92
	7	944.0	951.8	5.341	34.582	27.304	0.41	4.73	-54.68
	8	934.0	942.0	5.346	34.582	27.303	0.40	3.31	-47.97
	9	923.0	930.9	5.352	34.582	27.303	0.38	2.69	-46.25
	10	894.0	901.7	5.531	34.583	27.282	0.36	1.05	-41.48
	11	864.0	870.9	5.683	34.584	27.264	0.33	2.00	-41.68
	12	834.0	841.4	5.747	34.585	27.256	0.32	5.50	-37.03
	13	804.0	810.7	5.839	34.585	27.245	0.29	9.58	-32.25
	14	774.0	780.7	6.069	34.588	27.219	0.24	9.21	-27.07
	15	744.0	750.1	6.425	34.594	27.177	0.19	7.10	-21.35
	16	714.0	720.3	6.527	34.595	27.164	0.17	1.22	-18.03
	17	665.0	670.3	6.858	34.601	27.124	0.13	1.41	-18.60
	18	615.0	620.2	7.403	34.613	27.057	0.08	1.58	-22.60
	19	565.0	569.5	7.867	34.624	26.999	0.06	8.32	-34.03
	20	515.0	519.5	8.432	34.651	26.934	0.07	8.48	-35.22
	21	466.0	469.6	8.822	34.668	26.887	0.06	7.73	-34.79
	22	416.0	418.9	9.380	34.679	26.805	0.06	8.09	-34.92
M54/3a	1	1489.0	1503.9	3.024	34.617	27.577	1.56	7.49	
114 (CTD 01)	2	1489.0	1503.9	3.024	34.617	27.577	1.56		
	3	1489.0	1503.9	3.024	34.617	27.577	1.56		
	4	1487.0	1501.4	3.026	34.617	27.577	1.52	6.97	
	5	1483.0	1496.3	3.043	34.617	27.576	1.52	5.34	
	6	1476.0	1488.8	3.048	34.618	27.575	1.52	5.46	
	7	1464.0	1478.5	3.054	34.617	27.575	1.50	5.89	
	8	1455.0	1468.3	3.106	34.615	27.568	1.48	2.13	
	9	1446.0	1460.5	3.127	34.615	27.566	1.43	1.67	

Station CTD	Bottle	Depth [m]	Pressure [db]	Potential Temp. [°C]	Salinity	Density σ_θ	O_2-conc. [ml/L]	CH_4-conc. [nmol/L]	$\delta^{13}C$ [‰]
	10	1436.0	1449.2	3.144	34.615	27.564	1.41	3.63	
	11	1436.0	1448.5	3.143	34.613	27.563	1.41		
	12	1425.0	1437.4	3.181	34.613	27.560	1.37	6.46	
	13	1414.0	1426.8	3.229	34.612	27.554	1.30	7.59	
	14	1400.0	1412.8	3.247	34.611	27.552	1.30	7.37	
	15	1378.0	1390.6	3.262	34.610	27.549	1.28	7.66	
	16	1358.0	1370.3	3.311	34.609	27.544	1.24	5.77	
	17	1339.0	1352.2	3.349	34.609	27.541	1.30		
	18	1320.0	1331.3	3.383	34.607	27.535	1.19	0.93	
	19	1300.0	1311.9	3.429	34.605	27.530	1.14	0.83	
	20	1278.0	1289.5	3.523	34.602	27.518	1.07	0.86	
	21	1198.0	1208.7	3.810	34.594	27.482	0.84	1.44	
	22	1198.0	1208.7	3.810	34.594	27.482	0.84		
M54/3a	1	1650.0	1665.0	2.582	34.634	27.630	1.92	1.43	-31.65
118 (CTD 02)	2	1648.0	1665.5	2.582	34.635	27.631	1.80	1.45	-36.66
	3	1648.0	1664.5	2.581	34.634	27.631	1.82	1.47	-35.09
	4	1644.0	1660.8	2.583	34.634	27.630	1.83	1.42	-32.05
	5	1640.0	1656.2	2.595	34.634	27.629	1.80	1.36	-31.61
	6	1628.0	1643.6	2.635	34.634	27.626	1.75	1.95	-30.13
	7	1616.0	1631.6	2.647	34.633	27.624	1.82	1.96	-31.46
	8	1598.0	1613.7	2.672	34.633	27.621	1.68	2.16	
	9	1580.0	1574.7	2.739	34.630	27.613	1.68	2.75	-31.07
	10	1560.0	1574.6	2.758	34.630	27.611	1.66	4.01	-30.04
	11	1540.0	1554.2	2.752	34.629	27.611	1.44	4.55	-32.08
	12	1520.0	1534.1	2.819	34.626	27.603	1.60	5.36	-31.68
	13	1500.0	1512.3	2.903	34.623	27.593	1.54	6.56	-30.21
	14	1475.0	1488.3	2.934	34.622	27.590	1.49	3.38	-32.16
	15	1455.0	1467.7	2.997	34.620	27.582	1.48	2.01	-36.96
	16	1434.0	1447.4	3.041	34.619	27.577	1.41	6.20	-39.08
	17	1417.0	1430.3	3.087	34.617	27.571			
	18	1400.0	1412.7	3.127	34.615	27.566	1.33	8.33	-39.72
	19	1375.0	1387.1	3.226	34.612	27.554	1.25	3.09	-41.33
	20	1350.0	1362.4	3.275	34.610	27.548	1.20	0.62	-33.58
	21	1326.0	1337.8	3.356	34.606	27.538	1.10	0.70	-34.61
	22	1302.0	1313.1	3.436	34.604	27.528	1.08	0.76	-28.73
M54/3a	1	2248.0	2273.0	1.916	34.662	27.708	2.48	19.16	-55.04
125 (CTD 03)	2	2248.0	2273.0	1.916	34.662	27.708			
	3	2243.0	2268.0	1.921	34.665	27.710	2.32	11.39	-55.45
	4	2243.0	2268.0	1.921	34.665	27.710			
	5	2238.6	2263.5	1.955	34.662	27.704	2.49	5.36	
	6	2238.6	2263.5	1.955	34.662	27.704			
	7	2234.3	2259.1	1.956	34.662	27.705	2.34	2.19	-48.07
	8	2234.3	2259.1	1.956	34.662	27.705			
	9	2227.7	2252.4	1.971	34.662	27.703	2.26	2.12	-50.16
	10	2222.2	2246.8	1.990	34.662	27.701	2.30	2.10	-50.32
	11	2216.8	2241.3	1.999	34.660	27.699	2.32	1.93	-48.45
	12	2213.5	2238.0	2.007	34.662	27.700	2.28	1.76	-49.04
	13	2201.6	2225.9	2.027	34.658	27.696	2.27	1.82	-48.01
	14	2190.7	2214.8	2.037	34.661	27.697	2.33	1.81	-49.87
	15	2183.0	2207.0	2.061	34.659	27.694	2.28	1.80	

Station CTD	Bottle	Depth [m]	Pressure [db]	Potential Temp. [°C]	Salinity	Density σ_θ	O_2-conc. [ml/L]	CH_4-conc. [nmol/L]	$\delta^{13}C$ [‰]
	16	2173.2	2197.0	2.072	34.659	27.692	2.25	1.73	
	17	2164.6	2188.3	2.077	34.658	27.692	2.24	1.74	-49.07
	18	2152.7	2176.2	2.080	34.658	27.692	2.23	1.71	-50.26
	19	2133.7	2156.9	2.093	34.658	27.690	2.23	1.61	-47.73
	20	2111.5	2134.3	2.124	34.656	27.686	2.21	1.34	
	21	2092.9	2115.4	2.136	34.655	27.685	2.26	1.61	-46.05
	22	2040.7	2062.4	2.198	34.654	27.678	2.17	3.50	-51.14
M54/3a	1	2343.0	2368.6	1.815	34.668	27.720	2.48	1.53	-50.96
127 (CTD 04)	2	2336.0	2363.0	1.843	34.667	27.717	2.48	3.24	-54.01
	3	2325.0	2350.6	1.868	34.666	27.714	2.49	5.44	
	4	2317.0	2343.3	1.867	34.666	27.715	2.73	7.27	-54.38
	5	2308.0	2333.5	1.876	34.666	27.714	2.40	5.45	-54.72
	6	2299.0	2324.2	1.893	34.665	27.711	2.38	8.64	-55.63
	7	2289.0	2313.7	1.891	34.665	27.712	2.38	12.84	-55.04
	8	2278.0	2303.6	1.895	34.665	27.711	2.32	13.74	-55.32
	9	2268.0	2292.7	1.907	34.664	27.710	2.37	11.75	-54.90
	10	2258.0	2283.2	1.926	34.664	27.708	2.35	10.90	-54.58
	11	2248.0	2273.0	1.950	34.662	27.705	2.33	8.78	-52.29
	12	2239.0	2264.2	1.970	34.662	27.703	2.35	5.08	-52.56
	13	2229.0	2253.4	2.013	34.660	27.698	2.27	3.19	-50.69
	14	2200.0	2223.8	2.060	34.658	27.693	2.26	1.88	-48.70
	15	2150.0	2172.5	2.135	34.655	27.684	2.19	2.02	-49.91
	16	2100.0	2121.8	2.181	34.652	27.679	2.16	2.83	-48.69
	17	2050.0	2071.3	2.234	34.651	27.673	2.11	5.45	-50.60
	18	1990.0	2013.0	2.298	34.648	27.666	2.07	4.68	-51.50
	19	1962.0	1982.1	2.318	34.647	27.663	2.04	4.02	-50.33
	20	1932.0	1951.0	2.335	34.646	27.661	2.06	3.13	-49.10
	21	1900.0	1918.7	2.348	34.646	27.660	2.03	1.93	
	22	1870.0	1890.9	2.388	34.644	27.655	2.04	1.83	
M54/3a	1	1537.9	1554.0	3.161	34.614	27.562	1.44	30.29	-43.61
128	3	1537.6	1554.0	3.161	34.614	27.562	1.44	29.89	-40.68
	4	1537.4	1554.0	3.161	34.614	27.562	1.44	29.00	-43.10
			Ref.: M54/2-19						
M54/3a	2	1535.0	1554.0	3.161	34.614	27.562	1.44	27.99	-46.32
131	3	1535.0	1554.0	3.161	34.614	27.562	1.44	30.23	
	4	1535.0	1554.0	3.161	34.614	27.562	1.44	34.17	-46.10
			Ref.: M54/2-19						
M54/3a	1	1004.0	1013.0	4.416	34.583	27.411	0.82	4.19	
135 (CTD 05)	2	1004.0	1013.0	4.416	34.583	27.411			
	3	1004.0	1013.0	4.416	34.583	27.411			
	4	1001.0	1009.9	4.404	34.584	27.413	0.82	4.12	
	5	1001.0	1009.9	4.404	34.584	27.413			
	6	997.0	1004.6	4.429	34.583	27.409	0.76	4.01	
	7	997.0	1004.6	4.429	34.583	27.409			
	8	991.0	998.8	4.447	34.583	27.407	0.78	4.09	
	9	986.0	993.6	4.478	34.583	27.404	0.78	4.37	
	10	975.0	982.9	4.543	34.583	27.396	0.77	4.56	
	11	965.0	973.0	4.605	34.582	27.389	0.75	3.35	

Station CTD	Bottle	Depth [m]	Pressure [db]	Potential Temp. [°C]	Salinity	Density σ_θ	O_2-conc. [ml/L]	CH_4-conc. [nmol/L]	$\delta^{13}C$ [‰]
	12	950.0	958.4	4.669	34.582	27.381	0.75	2.55	
	13	930.0	937.8	4.804	34.581	27.365	0.71	1.81	
	14	910.0	917.2	4.963	34.581	27.347	0.66	1.72	
	15	880.0	887.4	5.254	34.581	27.313	0.57	2.39	
	16	850.0	857.5	5.373	34.582	27.300	0.55	3.47	
	17	820.0	827.1	5.512	34.582	27.283	0.54	3.86	
	18	790.0	797.4	5.669	34.583	27.265	0.48	2.96	
	19	760.0	766.5	5.785	34.584	27.251	0.44	3.55	
	20	730.0	736.5	6.052	34.586	27.219	0.36	2.45	
	21	700.0	705.8	6.431	34.593	27.175	0.28	8.52	
	22	670.0	676.2	6.793	34.597	27.130	0.17	0.65	
M54/3a	1	1907.0	1927.1	2.422	34.643	27.651	1.95	38.30	-49.20
141 (CTD 06)	2	1904.0	1924.7	2.419	34.644	27.652	1.97	35.18	-49.19
	3	1900.0	1919.6	2.425	34.643	27.651	1.89	40.23	-48.88
	4	1880.0	1899.3	2.429	34.643	27.651	1.94	46.77	-49.72
	5	1860.0	1879.3	2.451	34.642	27.648	1.91	55.45	
	6	1840.0	1859.0	2.471	34.642	27.646	1.90	68.76	-45.63
	7	1820.0	1838.9	2.483	34.641	27.645	1.90	73.60	-44.08
	8	1800.0	1818.2	2.511	34.641	27.642	1.89	61.64	-39.57
	9	1780.0	1798.5	2.524	34.640	27.640	1.86	51.56	-35.16
	10	1760.0	1778.3	2.535	34.640	27.639	1.89	44.43	
	11	1740.0	1758.1	2.539	34.640	27.639	1.86	47.60	-31.45
	12	1720.0	1737.7	2.569	34.638	27.635	1.78	28.08	-33.64
	13	1710.0	1728.1	2.579	34.638	27.634	1.80	16.58	
	14	1700.0	1717.8	2.582	34.638	27.633	1.86	14.23	-39.91
	15	1690.0	1707.8	2.585	34.638	27.633	1.81	10.20	-41.50
	16	1680.0	1697.8	2.602	34.637	27.631	1.91	7.39	-43.94
	17	1651.0	1667.6	2.630	34.637	27.628	1.79	5.50	-49.64
	18	1621.0	1637.6	2.676	34.635	27.623	1.75	4.27	-44.36
	19	1591.0	1607.1	2.724	34.633	27.617	1.72	8.45	-43.73
	20	1562.0	1577.4	2.782	34.630	27.609	1.62	4.51	-43.51
	21	1532.0	1547.2	2.841	34.629	27.603	1.64	1.95	-41.86
	22	1502.0	1517.1	2.884	34.627	27.598	1.68	1.85	-36.85
M54/3a	1	1019.9	1013.0	4.416	34.583	27.411	0.81	16.88	-46.43
142/1	3	1019.6	1013.0	4.416	34.583	27.411	0.81	9.34	-46.38
	5	1018.8	1013.0	4.416	34.583	27.411	0.81	8.74	-46.21
			Ref.: M54/3a-135						
M54/3a	1	1000.0	1007.9	4.293	34.583	27.423	0.84	3.68	-47.07
142/2 (CTD 07)	2	997.0	1004.4	4.310	34.583	27.422	0.83	5.29	-45.55
	3	992.0	1000.0	4.321	34.583	27.421	0.81	5.34	-47.46
	4	987.0	994.6	4.346	34.583	27.418	0.81	4.48	-49.18
	5	982.0	989.7	4.380	34.582	27.414	0.81	4.80	-48.18
	6	971.0	979.1	4.435	34.581	27.407	0.79	4.29	-50.46
	7	961.0	969.1	4.568	34.579	27.390	0.71	2.73	
	8	952.0	959.2	4.645	34.579	27.382	0.70	1.84	-45.52
	9	930.0	939.0	4.738	34.579	27.372	0.70		
	10	930.0	938.8	4.757	34.580	27.370	0.69	2.02	-47.54
	11	910.0	918.5	4.770	34.580	27.368	0.69	1.92	-45.02
	12	881.0	888.4	5.048	34.579	27.336	0.60	1.68	-41.69

Station CTD	Bottle	Depth [m]	Pressure [db]	Potential Temp. [°C]	Salinity	Density σ_θ	O_2-conc. [ml/L]	CH_4-conc. [nmol/L]	$\delta^{13}C$ [‰]
	13	850.0	857.1	5.260	34.580	27.312	0.60	3.10	
	14	820.0	827.8	5.352	34.580	27.301	0.58	5.41	-50.21
	15	800.0	807.4	5.447	34.580	27.289	0.54	3.17	
	16	780.0	787.4	5.570	34.579	27.274	0.48	2.31	-45.92
	17	761.0	766.8	5.747	34.580	27.253	0.39	2.38	-47.83
	18	741.0	746.9	5.798	34.581	27.247	0.37	3.89	-56.00
	19	722.0	727.0	6.024	34.583	27.220	0.35	2.05	-42.32
	20	681.0	686.5	6.151	34.586	27.206	0.34	2.41	-37.07
	21	632.0	636.9	6.691	34.592	27.140	0.19	0.90	-34.36
	22	402.0	405.7	9.380	34.673	26.801	0.26	9.81	-35.33
M54/3a	1	989.0	997.0	4.622	34.580	27.385	0.77	125.15	-66.11
150 (CTD 08)	2	986.0	993.8	4.622	34.580	27.385	0.74	63.90	-63.09
	3	981.0	988.6	4.627	34.580	27.385	0.75	72.47	-65.25
	4	975.0	982.2	4.649	34.580	27.382	0.77	21.16	
	5	970.0	977.8	4.717	34.578	27.373	0.70	5.20	-59.66
	6	964.0	971.5	4.717	34.578	27.373	0.71	2.10	-47.93
	7	954.0	960.6	4.724	34.578	27.373	0.70	1.81	-46.87
	8	943.0	951.4	4.814	34.578	27.362	0.73	2.30	-51.23
	9	934.0	941.6	4.835	34.579	27.361	0.70	1.75	
	10	914.0	921.3	4.962	34.579	27.346	0.70	2.93	
	11	888.0	895.2	5.027	34.577	27.337	0.63	2.00	-45.54
	12	860.0	866.5	5.172	34.577	27.320	0.59		
	13	830.0	836.8	5.373	34.577	27.296	0.51	2.03	
	14	801.0	806.8	5.495	34.577	27.282	0.45	2.07	-46.84
	15	781.0	787.0	5.605	34.577	27.268	0.40	1.24	
	16	761.0	766.3	5.773	34.580	27.250	0.38	2.16	-43.00
	17	740.0	746.8	5.895	34.582	27.236	0.36	2.12	-40.71
	18	720.0	726.3	6.098	34.583	27.211	0.29	3.30	-48.78
	19	700.0	706.2	6.354	34.585	27.179	0.21	0.87	
	20	651.0	656.1	6.891	34.597	27.116	0.15	0.93	-22.70
	21	601.0	605.7	7.203	34.603	27.078	0.11	0.73	-21.75
	22	402.0	405.3	9.200	34.667	26.826	0.09	9.38	-35.23
M54/3a	1	1747.0	1763.9	2.514	34.639	27.640	2.14	1162.14	-55.00
151 (CTD 09)	2	1742.0	1758.4	2.512	34.637	27.639	2.14	524.31	-49.82
	3-20	1700.0	1715.7	2.550	34.638	27.636	1.88	304.42	-43.99
	21-22	1450.0	1460.1	3.031	34.621	27.580	1.53		
M54/3a	1	2388.0	2416.1	1.857	34.668	27.717	2.50	2.79	-52.92
152 (CTD 10)	2	2385.0	2411.8	1.856	34.668	27.717	2.49	3.17	-54.77
	3	2370.0	2397.2	1.859	34.667	27.716	2.40	2.56	-56.42
	4	2340.0	2366.5	1.880	34.667	27.714	2.45	2.37	-52.32
	5	2300.0	2325.9	1.886	34.666	27.713	2.46		
	6	2200.0	2224.6	1.934	34.664	27.707	2.44	2.02	-49.40
	7	2100.0	2123.0	2.069	34.657	27.692	2.33	1.79	-45.13
	8	2002.0	2023.2	2.267	34.649	27.669	2.14	3.08	-45.80
	9	1920.0	1939.3	2.337	34.646	27.661	2.07	6.90	-47.39
	10	1890.0	1908.3	2.363	34.645	27.657	2.12	2.65	-43.59
	11	1860.0	1877.7	2.388	34.644	27.655	2.05	6.91	-47.27
	12	1830.0	1848.7	2.417	34.643	27.651	2.01	7.25	
	13	1800.0	1817.7	2.460	34.641	27.646	1.93	2.13	-39.87

Station CTD	Bottle	Depth [m]	Pressure [db]	Potential Temp. [°C]	Salinity	Density σ_θ	O_2-conc. [ml/L]	CH_4-conc. [nmol/L]	$\delta^{13}C$ [‰]
	14	1770.0	1788.1	2.485	34.640	27.643	1.99	2.10	-41.59
	15	1740.0	1758.0	2.533	34.638	27.637	1.94	1.91	-43.16
	16	1711.0	1728.2	2.566	34.637	27.634	1.88	1.93	-45.60
	17	1701.0	1717.7	2.570	34.636	27.633	1.88	1.84	-47.33
	18	1690.0	1707.2	2.597	34.635	27.630	1.87	3.29	-51.23
	19	1650.0	1666.6	2.676	34.632	27.621	1.82	1.72	-43.62
	20	1601.0	1617.5	2.782	34.629	27.608	1.74	2.53	-47.13
	21	1550.0	1567.1	2.835	34.626	27.602	1.64	2.04	-47.95
	22	1502.0	1516.8	2.913	34.624	27.593	1.73	1.24	-45.27
M54/3a	1	997.0	1005.5	4.410	34.579	27.408	0.79	2.61	-50.87
162 (CTD 12)	1	997.0	1005.5	4.410	34.579	27.408	0.79	2.48	-49.35
	2	995.0	1002.5	4.408	34.579	27.408	0.80	2.89	-50.33
	2	995.0	1002.5	4.408	34.579	27.408	0.80	2.64	-50.16
	3	990.0	997.6	4.410	34.579	27.408	0.78	3.23	
	4	985.0	992.1	4.468	34.579	27.402	0.80	2.76	-49.58
	4	985.0	992.1	4.468	34.579	27.402	0.80	2.42	-47.57
	5	974.0	981.9	4.576	34.577	27.388	0.74	2.61	
	6	963.0	971.6	4.729	34.576	27.370	0.68	2.52	-48.36
	7	953.0	961.1	4.832	34.575	27.358	0.65	2.37	-48.53
	8	943.0	950.7	4.918	34.575	27.348	0.63	3.13	-47.72
	9	934.0	940.9	4.995	34.574	27.338	0.49	1.84	-46.60
	10	914.0	921.5	5.085	34.572	27.326	0.46	2.85	-55.07
	11	890.0	896.2	5.246	34.573	27.308	0.44	2.02	
	12	860.0	865.8	5.339	34.573	27.297	0.41	2.39	-51.44
	13	830.0	836.0	5.461	34.575	27.284	0.41	2.01	-43.40
	14	800.0	806.0	5.598	34.577	27.269	0.36	2.47	-44.68
	15	780.0	785.7	5.715	34.578	27.255	0.33	2.61	-45.76
	16	760.0	765.6	5.988	34.583	27.225	0.30	3.70	-49.87
	17	740.0	745.6	6.126	34.584	27.208			
	18	720.0	725.7	6.300	34.584	27.185	0.24	2.34	-46.24
	19	700.0	704.9	6.385	34.587	27.176	0.21	2.18	-33.49
	20	650.0	655.2	6.802	34.595	27.127	0.16	2.13	-39.39
	21	600.0	604.9	7.296	34.606	27.067	0.10	2.03	-36.80
	22	400.0	405.1	9.365	34.676	26.805	0.05	9.69	-52.75
M54/3a	1	1573.0	1588.6	2.941	34.622	27.589			
167 (CTD 13)	2	1563.0	1578.3	2.984	34.620	27.584			
	3	1543.0	1558.1	3.026	34.619	27.579			
	4	1504.0	1517.8	3.099	34.617	27.570			
	5	1444.0	1457.9	3.186	34.614	27.560			
	6	1345.0	1357.4	3.314	34.611	27.545			
	7	1200.0	1210.8	3.569	34.603	27.514			
	8	1002.0	1010.1	4.729	34.580	27.373			
	9	853.0	859.9	5.414	34.577	27.291			
	10	803.0	809.4	5.558	34.577	27.274	0.39	3.62	
	11	753.0	759.1	5.769	34.577	27.247	0.29	1.26	
	12	704.0	709.0	6.273	34.584	27.189	0.22	1.43	
	13	654.0	658.4	6.676	34.592	27.142	0.17	2.09	
	14	103.0	103.9	14.941	34.923	25.926	0.53	5.80	
	15	80.0	80.2	16.353	34.900	25.591	0.78	5.02	
	16	57.0	59.6	17.659	34.836	25.231	1.05	8.90	

Station CTD	Bottle	Depth [m]	Pressure [db]	Potential Temp. [°C]	Salinity	Density σ_θ	O_2-conc. [ml/L]	CH_4-conc. [nmol/L]	$\delta^{13}C$ [‰]
	17	48.0	48.9	18.591	34.782	24.959	1.28	9.71	
	18	38.0	38.4	19.671	34.704	24.624	1.49	10.28	
	19	28.0	27.7	21.826	34.507	23.893	1.89	11.46	
	20	17.0	17.2	25.254	33.535	22.159	3.78	6.01	
	21	10.0	9.1	28.102	31.751	19.922	4.68	2.58	
	22	5.0	4.0	28.126	31.716	19.889	4.65	2.38	
M54/3a	1	1017.9	1004.8	4.686	34.577	27.376	0.72	68.93	-71.78
168	2	1017.8	1004.8	4.686	34.577	27.376	0.71	50.13	-73.29
	3	1017.6	1004.8	4.686	34.577	27.376	0.77	45.08	-71.82
	4	1017.4	1004.8	4.686	34.577	27.376	0.76	34.74	-72.48
	5	1016.8	1004.8	4.686	34.577	27.376	0.79	17.38	-67.95
			Ref.: M54/3a-169						
M54/3a	1	996.0	1004.8	4.686	34.577	27.376	0.64	7.69	-46.66
169 (CTD 14)	2	994.0	1002.7	4.687	34.577	27.376	0.64	6.53	-46.43
	3	990.0	997.4	4.697	34.578	27.375	0.63	2.97	-47.39
	4	985.0	992.9	4.701	34.578	27.375	0.63	2.22	-47.71
	5	979.0	987.2	4.699	34.578	27.375	0.63	2.24	-47.60
	6	974.0	982.4	4.703	34.578	27.375	0.61	2.26	
	7	964.0	972.0	4.814	34.577	27.361	0.60	2.24	-47.12
	8	954.0	961.3	4.826	34.578	27.361	0.60	2.35	-47.27
	9	954.0	961.3	4.826	34.578	27.361	0.60	2.26	-47.27
	10	932.0	940.2	4.985	34.578	27.342	0.56	2.21	
	11	915.0	921.7	5.064	34.577	27.332	0.53	2.44	-50.32
	12	890.0	895.9	5.173	34.576	27.319	0.47	2.19	-46.95
	13	860.0	866.6	5.452	34.576	27.286	0.42	1.81	-45.89
	14	830.0	835.5	5.655	34.578	27.263	0.36	2.04	-44.21
	15	800.0	805.8	5.895	34.576	27.231	0.24	0.65	-38.16
	16	780.0	786.1	6.102	34.577	27.206	0.20	0.58	-35.31
	17	760.0	766.1	6.301	34.583	27.184	0.17	0.97	
	18	740.0	746.3	6.402	34.584	27.172	0.14	0.61	-31.06
	19	720.0	726.2	6.545	34.589	27.157	0.16	1.87	
	20	700.0	705.9	6.616	34.592	27.150	0.18	1.44	-39.12
	21	650.0	655.4	6.804	34.596	27.127	0.16	2.33	-38.89
	22	600.0	605.2	7.290	34.605	27.067	0.10	3.06	-31.77
M54/3a	1	1743.0	1758.4	2.512	34.637	27.639	3.79	407.44	-50.41
173/1	2	1749.0	1763.9	2.514	34.639	27.640	3.78	440.87	-50.85
	3	1764.0	1776.7	2.614	34.632	27.626	3.80	459.52	-50.76
	4	1776.0	1786.8	2.607	34.631	27.626	3.79	571.51	-51.31
	5	1782.0	1817.8	2.554	34.635	27.633	3.77	665.73	-52.41
			Ref.: 1-2: M54/3a-151, 3-5: M54/2-50						
M54/3a	2	1768.0	1776.7	2.614	34.632	27.626	3.55	1506.21	-55.18
173/2	1	1771.0	1786.8	2.607	34.631	27.626	3.65	555.20	
	3	1775.0	1786.8	2.607	34.631	27.626	3.51	1343.02	-54.61
	4	1778.0	1786.8	2.607	34.631	27.626	3.68		-54.30
	5	1812.0	1817.8	2.554	34.635	27.633	3.74	1499.59	-54.79
			Ref.: 1-5: M54/2-50						
M54/3a	1	2182.0	2206.5	1.995	34.666	27.705	1.91	16.03	-57.16

Station CTD	Bottle	Depth [m]	Pressure [db]	Potential Temp. [°C]	Salinity	Density σ_θ	O_2-conc. [ml/L]	CH_4-conc. [nmol/L]	$\delta^{13}C$ [‰]
180 (CTD 15)	2	2176.0	2200.2	1.994	34.666	27.705	1.91	15.96	-57.38
	3	2167.0	2190.1	2.020	34.665	27.702	1.89	20.02	-57.92
	4	2156.0	2180.1	2.030	34.665	27.701	1.89	20.65	-57.60
	5	2100.0	2121.5	2.101	34.662	27.693	1.85	12.69	-57.47
	6	2050.0	2071.3	2.189	34.658	27.683	1.81	9.82	-51.43
	7	2000.0	2021.0	2.270	34.655	27.673	1.75	14.92	-51.05
	8	1950.0	1970.7	2.319	34.652	27.667	1.73	9.82	-50.86
	9	1900.0	1919.2	2.379	34.650	27.660	1.69	7.03	-49.42
	10	1880.0	1900.2	2.399	34.649	27.658	1.67	10.17	-50.84
	11	1860.0	1880.2	2.408	34.649	27.657	1.67	4.97	-45.65
	12	1839.0	1858.4	2.440	34.647	27.653	1.65	5.58	-44.76
	13	1817.0	1837.0	2.460	34.647	27.651	1.65	12.03	-41.87
	14	1786.0	1814.5	2.494	34.645	27.647	1.62	2.78	-43.37
	15	1747.0	1763.9	2.547	34.643	27.640	1.58	3.05	-46.58
	16	1728.0	1744.1	2.587	34.641	27.636	1.56	18.34	-23.89
	16	1728.0	1744.1	2.587	34.641	27.636	1.56	18.34	-24.38
	17	1707.0	1723.9	2.622	34.640	27.632	1.52	5.27	-40.41
	18	1688.0	1703.9	2.642	34.640	27.629	1.52		
	19	1668.0	1683.8	2.679	34.638	27.625	1.50	2.67	-47.17
	20	1647.0	1663.6	2.733	34.637	27.619	1.46	5.51	-48.38
	21	1599.0	1613.6	2.836	34.633	27.607	1.39	1.98	-47.18
	22	1500.0	1513.3	3.042	34.626	27.582	1.28	1.02	-37.51
M54/3a	1	1008.9	997.0	4.622	34.580	27.385	1.50	15.64	-63.13
187	2	1008.8	997.0	4.622	34.580	27.385	1.57	14.95	-62.81
	3	1008.6	997.0	4.622	34.580	27.385	1.65	14.98	-61.48
	4	1008.4	997.0	4.622	34.580	27.385	1.65	13.92	-61.26
	5	1007.8	997.0	4.622	34.580	27.385	1.68	12.95	-61.38

Ref.: M54/3a-150

data – Subduction II – SONNE 173/3+4

Station CTD	Bottle	Depth [m]	Pressure [db]	Potential Temp. [°C]	Salinity	Density σ_θ	O_2-conc. [ml/L]	CH_4-conc. [nmol/L]	$\delta^{13}C$ [‰]
SO173/4	1	1900.5	1920.1	2.176	34.647	27.674	2.03	29.34	-54.20
76 (CTD 18)	2	1895.8	1915.2	2.180	34.646	27.674	2.01	42.11	-54.47
	3	1894.1	1913.5	2.186	34.646	27.673	0.27	39.71	
	4	1885.1	1904.4	2.211	34.645	27.670	2.02	40.21	-53.31
	5	1876.1	1895.2	2.215	34.645	27.670	0.24	27.62	-53.34
	6	1865.5	1884.6	2.211	34.645	27.670	2.00	46.46	-53.50
	7	1835.5	1854.0	2.369	34.638	27.652	1.89	63.98	-54.03
	8	1805.0	1823.2	2.410	34.637	27.647	1.86	17.71	-47.64
	9	1775.1	1792.8	2.437	34.636	27.644	1.84	39.00	-47.85
	10	1745.1	1762.4	2.496	34.633	27.637	1.72	23.25	-43.65
	11	1734.0	1751.1	2.576	34.631	27.628	1.75	22.12	-42.66
	12	1724.3	1741.3	2.624	34.628	27.622	1.71	101.76	-48.16
	13	1713.8	1730.7	2.667	34.628	27.618	1.66	35.68	-44.99
	14	1704.7	1721.4	2.694	34.627	27.615	1.65	26.13	-44.20
	15	1694.3	1710.9	2.711	34.627	27.613	1.64	96.14	-46.61
	16	1664.9	1681.1	2.813	34.623	27.601	1.62	25.96	-49.41
	17	1633.7	1649.4	2.896	34.621	27.592	1.56	19.82	-53.17
	18	1603.0	1618.3	2.937	34.620	27.587			
	19	1572.7	1587.6	2.966	34.619	27.584	1.50	2.53	-48.87
	20	1523.3	1537.6	3.016	34.617	27.578	1.50	3.26	-52.99
	21	1475.1	1488.7	3.092	34.615	27.569	1.47	2.77	-52.84
	22	1425.5	1438.5	3.187	34.613	27.559	1.40	1.52	
	23	1376.5	1388.9	3.365	34.606	27.536	1.26	1.20	-45.43
	24	1326.6	1338.4	3.494	34.603	27.521	1.22	1.36	-50.43
SO173/4	1	1506.1	1520.2	3.074	34.613	27.569	1.31	2.03	-41.62
86 (CTD 21)	2	1505.3	1519.3	3.064	34.614	27.571	1.31	4.04	-44.37
	3	1500.5	1514.5	3.070	34.613	27.570	1.31	3.05	-43.09
	4	1493.2	1507.1	3.078	34.613	27.569	1.30	2.95	-43.52
	5	1485.3	1499.1	3.092	34.612	27.567	1.29	1.95	-41.90
	6	1474.4	1488.1	3.123	34.611	27.563	1.25	2.70	-42.00
	7	1463.8	1477.3	3.157	34.610	27.559	1.23	2.56	-42.29
	8	1454.2	1467.6	3.162	34.610	27.558	1.21	2.88	-42.36
	9	1445.6	1458.9	3.169	34.609	27.558	1.21	2.66	-41.26
	10	1435.1	1448.3	3.181	34.609	27.556	1.20	2.30	-40.21
	11	1425.3	1438.3	3.210	34.609	27.553	1.19	1.50	-39.26
	12	1414.6	1427.5	3.228	34.608	27.551	1.18	1.38	-38.11
	13	1405.0	1417.8	3.248	34.607	27.549	1.18	0.90	-34.44
	14	1395.4	1408.1	3.283	34.607	27.545	1.18	0.59	-37.56
	15	1384.9	1397.4	3.304	34.606	27.542	1.17	0.59	-37.13
	16	1375.4	1387.8	3.327	34.605	27.539	1.15	1.29	-38.23
	17	1365.0	1377.3	3.342	34.605	27.538	1.14		
	18	1354.0	1366.1	3.367	34.604	27.534	1.11	1.64	-37.81
	19	1343.6	1355.6	3.372	34.604	27.534	1.11	1.75	-37.65
	20	1334.5	1346.4	3.399	34.603	27.530	1.08	1.76	-38.60
	21	1314.9	1326.5	3.435	34.602	27.526	1.05	1.74	-37.87
	22	1294.7	1306.1	3.457	34.602	27.524	1.06	1.10	-39.74
	23	1275.0	1286.2	3.521	34.601	27.517	1.08	0.73	-39.24
	24	1256.1	1267.0	3.610	34.596	27.504	0.97	0.47	-39.18

Station CTD	Bottle	Depth [m]	Pressure [db]	Potential Temp. [°C]	Salinity	Density σ_θ	O_2-conc. [ml/L]	CH_4-conc. [nmol/L]	$\delta^{13}C$ [‰]
SO173/4	1	2255.2	2280.3	1.818	34.663	27.716	2.24	4.67	
92 (CTD 22)	2	2251.8	2276.9	1.817	34.663	27.716	2.26	5.48	
	3	2248.8	2273.8	1.818	34.663	27.716	2.28	5.71	
	4	2247.1	2272.1	1.819	34.663	27.716	2.24	5.34	
	5	2243.0	2267.9	1.825	34.663	27.715	2.24	4.20	
	6	2237.7	2262.5	1.831	34.663	27.715	2.53	3.43	
	7	2232.4	2257.1	1.835	34.662	27.714	2.23	2.93	
	8	2224.0	2248.6	1.845	34.662	27.713	2.24	3.15	
	9	2211.7	2236.0	1.856	34.661	27.712	2.22	1.87	
	10	2202.8	2227.0	1.883	34.660	27.708	2.09	1.66	
	11	2190.7	2214.7	1.897	34.659	27.707	2.22	1.65	
	12	2181.0	2204.9	1.902	34.659	27.706	2.18		
	13	2170.4	2194.1	1.909	34.659	27.706	2.17	1.61	
	14	2163.1	2186.6	1.910	34.659	27.705	2.19	1.63	
	15	2151.0	2174.3	1.911	34.659	27.705	2.16	1.63	
	16	2131.5	2154.6	1.922	34.658	27.704	2.17	1.48	
	17	2111.3	2134.1	1.933	34.658	27.703	2.15	1.56	
	18	2091.5	2114.0	1.956	34.656	27.700	2.14	1.51	
	19	2072.1	2094.2	1.968	34.656	27.699	2.11	1.49	
	20	2050.6	2072.4	1.995	34.655	27.695	2.11	1.39	
	21	2031.9	2053.4	2.013	34.654	27.693	2.12	1.37	
	22	2012.7	2034.0	2.031	34.653	27.691	2.11	1.38	
	23	1991.3	2012.2	2.053	34.652	27.689	2.09	0.78	
	24	1940.6	1960.7	2.128	34.649	27.680	2.02	0.75	
SO173/4	1	1626.7	1642.3	2.879	34.620	27.593	1.48	1.91	
93 (CTD 23)	2	1626.5	1642.1	2.871	34.620	27.594	1.48	1.94	
	3	1623.0	1638.5	2.872	34.621	27.594	1.48	2.11	
	4	1620.2	1635.8	2.875	34.620	27.593	1.48	2.03	
	5	1610.6	1626.0	2.892	34.620	27.591	1.46	1.95	
	6	1602.0	1617.3	2.897	34.620	27.591	1.46	1.95	
	7	1591.7	1606.8	2.902	34.619	27.590	1.46	2.25	
	8	1581.5	1596.6	2.916	34.619	27.588	1.45	2.30	
	9	1571.4	1586.3	2.928	34.618	27.587	1.44	2.41	
	10	1561.3	1576.1	2.947	34.618	27.585	1.42	2.50	
	11	1552.8	1567.4	2.955	34.618	27.584	1.39	2.61	
	12	1540.6	1555.1	2.980	34.616	27.581	1.39		
	13	1530.1	1544.4	2.991	34.616	27.579	1.38	2.29	
	14	1509.2	1523.3	3.054	34.613	27.571	1.37	1.14	
	15	1501.2	1515.2	3.089	34.612	27.567	1.32	0.97	
	16	1469.8	1483.4	3.148	34.610	27.560	1.25	1.16	
	17	1449.9	1463.2	3.209	34.608	27.553	1.20	1.22	
	18	1429.8	1442.9	3.261	34.607	27.547	1.18	1.15	
	19	1410.7	1423.6	3.294	34.606	27.543	1.17	1.08	
	20	1391.0	1403.6	3.325	34.605	27.539	1.14	1.30	
	21	1370.6	1383.0	3.353	34.604	27.536	1.12	1.50	
	22	1350.5	1362.6	3.390	34.604	27.532	1.12	1.30	
	23	1331.0	1342.9	3.421	34.603	27.528	1.10	1.56	
	24	1310.9	1322.5	3.498	34.601	27.519	1.09	0.79	
SO173/4	1	1924.4	1944.3	2.239	34.645	27.668	1.98	27.44	-53.97
99 (CTD 24)	2	1921.0	1940.8	2.237	34.645	27.668	1.98	29.68	-54.25
	3	1911.3	1931.0	2.240	34.645	27.668	1.93	25.71	-53.85

Station CTD	Bottle	Depth [m]	Pressure [db]	Potential Temp. [°C]	Salinity	Density σ_θ	O_2-conc. [ml/L]	CH_4-conc. [nmol/L]	$\delta^{13}C$ [‰]
	4	1900.9	1920.4	2.253	34.645	27.667	1.95	18.81	-52.37
	5	1891.5	1910.9	2.257	34.645	27.666	1.95	18.39	-52.57
	6	1861.0	1879.9	2.315	34.642	27.659	2.13	16.06	-51.30
	7	1831.3	1849.8	2.386	34.639	27.651	1.86	17.35	-48.65
	8	1801.8	1819.9	2.420	34.638	27.647	1.86	48.03	-49.83
	9	1771.2	1788.8	2.458	34.636	27.643	1.85	25.52	-49.58
	10	1760.4	1777.9	2.466	34.636	27.642	1.72	29.51	-50.69
	11	1752.2	1769.6	2.470	34.636	27.641	1.80	60.51	-51.76
	12	1742.0	1759.2	2.477	34.636	27.641	1.81	68.80	-52.77
	13	1730.7	1747.8	2.498	34.635	27.638	1.77	48.33	-51.94
	14	1720.7	1737.6	2.531	34.634	27.634	1.77	39.30	-50.68
	15	1711.5	1728.3	2.558	34.633	27.631	1.72	30.45	-49.25
	16	1701.0	1717.6	2.562	34.633	27.631	1.77	28.08	-48.84
	17	1691.2	1707.8	2.590	34.632	27.628	1.70	7.48	-44.39
	18	1680.1	1696.5	2.614	34.631	27.625	1.72	4.45	-40.02
	19	1633.4	1649.2	2.629	34.631	27.624	1.72	6.30	-42.09
	20	1583.0	1598.1	2.770	34.627	27.608	1.63	5.43	-43.81
	21	1533.2	1547.6	2.898	34.623	27.593	1.54	5.56	-48.50
	22	1482.8	1496.5	3.001	34.619	27.581	1.48	3.21	-51.89
	23	1433.0	1446.1	3.122	34.615	27.567	1.39	1.33	-44.35
	24	397.7	400.4	10.110	34.701	26.700	1.77	16.37	
SO173/4	1	980.1	988.0	4.444	34.586	27.410	0.83	9.32	-57.56
106 (CTD 25)	2	979.3	987.2	4.462	34.586	27.407	0.82	8.10	-57.00
	3	977.0	984.8	4.477	34.585	27.405	0.94	10.43	-55.61
	4	975.1	982.9	4.500	34.585	27.402	0.80	11.74	-59.10
	5	964.6	972.3	4.674	34.582	27.381	0.72	10.09	-58.55
	6	953.8	961.4	4.694	34.582	27.379	0.80	4.78	-50.59
	7	944.0	951.5	4.767	34.581	27.370	0.68	3.78	-48.18
	8	935.3	942.7	4.875	34.581	27.358	0.68	3.22	-48.70
	9	924.8	932.1	4.933	34.581	27.351	0.71	2.50	-45.82
	10	893.8	900.8	5.024	34.581	27.340	0.66	2.79	-46.11
	11	864.3	871.0	5.165	34.580	27.323	0.56	3.65	-49.60
	12	834.9	841.3	5.334	34.578	27.302	0.47	5.16	-46.60
	13	990.7	998.7	4.406	34.587	27.415	0.82	7.87	-54.77
	14	988.0	996.0	4.393	34.586	27.415	0.83	7.04	-55.33
	15	982.7	990.6	4.428	34.586	27.411	0.84	7.17	-54.59
	16	978.3	986.1	4.444	34.586	27.409	0.84	8.52	-55.44
	17	973.2	981.1	4.517	34.584	27.400	0.80	8.34	-54.51
	18	968.6	976.4	4.551	34.584	27.396	0.78	16.31	-60.84
	19	958.2	965.9	4.728	34.581	27.374	0.75	26.09	-60.90
	20	950.0	957.6	4.828	34.581	27.363	0.70	8.89	-59.51
	21	938.4	945.9	4.826	34.582	27.364	0.68	7.20	-57.69
	22	917.7	924.9	4.960	34.581	27.348	0.68	2.33	-44.54
	23	887.7	894.7	5.119	34.580	27.329	0.61	3.19	-44.66
	24	857.6	864.3	5.300	34.578	27.306	0.51	4.56	-47.11
SO173/4	1	1606.2	1621.5	2.754	34.627	27.610	1.60	19.72	
124 (CTD 29)	2	1604.2	1619.5	2.757	34.627	27.609	1.61	18.78	
	3	1593.6	1608.8	2.791	34.626	27.605	1.61	8.67	
	4	1585.0	1600.1	2.801	34.626	27.604	1.59	4.00	
	5	1572.6	1587.5	2.820	34.625	27.602	1.59	3.18	

Station CTD	Bottle	Depth [m]	Pressure [db]	Potential Temp. [°C]	Salinity	Density σ_θ	O_2-conc. [ml/L]	CH_4-conc. [nmol/L]	$\delta^{13}C$ [‰]
	6	1563.2	1578.0	2.824	34.625	27.602	1.63	3.72	
	7	1553.7	1568.4	2.828	34.625	27.601	1.62	3.26	
	8	1543.2	1557.7	2.847	34.624	27.599	1.60		
	9	1533.2	1547.6	2.879	34.623	27.595	1.54	4.29	
	10	1508.8	1522.9	3.021	34.619	27.579	1.39	1.77	
	11	1483.9	1497.6	3.049	34.618	27.576	1.45	0.81	
	12	1459.6	1473.0	3.074	34.618	27.573	1.46	0.83	
	13	1444.7	1458.0	3.121	34.616	27.567	1.58	1.44	
	14	1418.0	1431.0	3.173	34.615	27.561	1.44	0.76	
	15	1404.2	1417.0	3.186	34.614	27.560	1.42	0.75	
	16	1388.3	1400.8	3.211	34.613	27.557	1.46	0.76	
	17	1364.0	1376.2	3.238	34.612	27.553	1.39	0.69	
	18	1339.4	1351.3	3.278	34.610	27.548	1.32		
	19	1312.4	1324.0	3.406	34.608	27.534	1.31	0.94	
	20	1288.4	1299.7	3.470	34.606	27.526	1.34	1.12	
	21	1264.4	1275.4	3.553	34.604	27.517	1.30	1.21	
	22	1238.7	1249.4	3.672	34.601	27.503	1.17	1.40	
	23	1212.5	1222.9	3.801	34.599	27.487	1.16	0.95	
	24	1187.6	1197.8	3.899	34.595	27.475	1.08	0.87	

Station	Instrument	Depth Instr. [m]	Start measurement Date	Time [UTC]	End measurement Date	Time [UTC]	ave. Ensemple Interval	Area
M54/3a-130	ADCP 300 kHz	1541	15-Sep-02	20:02:26	27-Sep-02	9:32:26	10	Mound Culebra
M54/3a-146	ADCP 1200 kHz	1021	19-Sep-02	6:08:37	20-Sep-02	20:08:37	5	Mound 11
M54/3a-165	ADCP 1200 kHz	1018	23-Sep-02	5:59:52	24-Sep-02	15:59:52	5	Mound 12
SO173/4-100	RCM8	1870	16-Sep-03	12:50:00	23-Sep-03	13:51:00	1	Jaco Scarp
SO173/4-100	RCM8	1760	16-Sep-03	12:40:00	23-Sep-03	13:53:00	1	Jaco Scarp
SO173/4-101	RCM8	2030	16-Sep-03	14:01:00	23-Sep-03	11:38:00	1	Jaco Scarp

Station	Date	Depth [m]	Velocity E [m/d]	Velocity N [m/d]	Direction	Velocity [m/s]
M54/3a-130	16.-17.09.02	1533	-415	-786	SW	0.0104
		1528	1200	-731	SE	0.0164
		1523	1599	-915	SE	0.0215
		1518	1917	-1118	SE	0.0259
		1513	1814	-1602	SE	0.0282
	17.-18.09.02	1533	-1482	-1356	SW	0.0234
		1528	37	-1298	SE	0.0151
		1523	122	-1089	SE	0.0128
		1518	318	-1018	SE	0.0124
		1513	280	-1018	SE	0.0123
	18.-19.09.02	1533	-1389	-1096	SW	0.0206
		1528	113	-1284	SE	0.0150
		1523	-59	-1491	SW	0.0174
		1518	-9	-20	SW	0.0002
		1513	127	-1508	SE	0.0176
	19.-20.09.02	1533	-1185	-429	SW	0.0147
		1528	-307	-849	SW	0.0105
		1523	-377	-1054	SW	0.0130
		1518	-117	-1032	SW	0.0121
		1513	-9	-999	SW	0.0116
	20.-21.09.02	1533	-577	201	NW	0.0071
		1528	263	51	NE	0.0031
		1523	280	-16	SE	0.0033
		1518	548	-133	SE	0.0066
		1513	476	-373	SE	0.0070
	21.-22.09.02	1533	-1985	176	NW	0.0232
		1528	-920	550	NW	0.0125
		1523	-952	496	NW	0.0125
		1518	-795	361	NW	0.0102
		1513	-726	197	NW	0.0088
	22.-23.09.02	1533	-1030	1726	NW	0.0234
		1528	20	1770	NE	0.0206
		1523	466	1787	NE	0.0215
		1518	843	1537	NE	0.0204
		1513	878	1177	NE	0.0171
	23.-24.09.02	1533	-828	3204	NW	0.0386
		1528	-847	3219	NW	0.0388
		1523	-975	3145	NW	0.0384
		1518	-886	2808	NW	0.0343
		1513	-888	2169	NW	0.0273

Station	Date	Depth [m]	Velocity E [m/d]	Velocity N [m/d]	Direction	Velocity [m/s]
	24.-25.09.02	1533	-935	3925	NW	0.0470
		1528	-242	3936	NW	0.0460
		1523	-196	3582	NW	0.0418
		1518	-244	3204	NW	0.0374
		1513	-473	2792	NW	0.0330
	25.-26.09.02	1533	-1415	4180	NW	0.0514
		1528	-1223	4430	NW	0.0536
		1523	-1140	4366	NW	0.0526
		1518	-973	3887	NW	0.0467
		1513	-836	3501	NW	0.0420
	26.-27.09.02	1533	-67	3225	NW	0.0376
		1528	-371	3383	NW	0.0397
		1523	-399	3584	NW	0.0420
		1518	-392	3431	NW	0.0402
		1513	-352	3300	NW	0.0387
M54/3a-146	19.-20.09.02	1018	-694	604	NW	0.0106
		1014	-945	777	NW	0.0142
M54/3a-165	23.-24.09.02	1015	-2402	2716	NW	0.0420
		1010	-3625	3722	NW	0.0601
SO173/4-100	17.-18.09.03	1870	-382	312	NW	0.0057
		1760	416	-219	SE	0.0054
	18.-19.09.03	1870	-392	-829	SW	0.0106
		1760	-618	846	NW	0.0121
	19.-20.09.03	1870	-629	-641	SW	0.0104
		1760	129	713	NE	0.0084
	20.-21.09.03	1870	-599	-237	SW	0.0381
		1760	-1189	147	NW	0.0139
	21.-22.09.03	1870	417	977	NE	0.0123
		1760	-770	655	NW	0.0117
	22.-23.09.03	1870	1879	-978	SE	0.0245
		1760	128	402	NE	0.0049
SO173/4-101	17.-18.09.03	2030	-1249	-580	SW	0.0159
	18.-19.09.03	2030	-820	1271	NW	0.0175
	19.-20.09.03	2030	-232	1727	NW	0.0220
	20.-21.09.03	2030	-260	224	NW	0.0040
	21.-22.09.03	2030	-392	645	NW	0.0087
	22.-23.09.03	2030	-1287	608	NW	0.0165